Developing non-heat treated UHPC in South Africa

Jin Zang

Dissertation presented in partial fulfilment of the requirements for the degree of Doctor of Philosophy in Structural Engineering at the University of Stellenbosch

Supervisor: Prof. GPAG van Zijl
Department of Civil Engineering

March 2015

i

Declaration

By submitting this dissertation, I declare that the entirety of the work contained therein is my own, original work, that I am the sole author thereof (save to the extent explicitly otherwise stated), that reproduction and publication thereof by Stellenbosch University will not infringe any third party rights and that I have not previously in its entirety or in part submitted it for obtaining any qualification.

Signature: ....

Date: February 2015

Abstract

The very high strength, enhanced ductility and long-term durability of ultra-high performance concrete (UHPC) makes it an ideal material to be used for building structures in the future. The non-heat treated UHPC requires less quality control than heat treated UHPC, which makes it more relevant to be applied in South Africa. This research focuses on developing non-heat treated UHPC with locally available materials, with the exception of short, straight, high strength steel fibre.

While UHPC mix design guidelines have been proposed, ingredient materials available locally, but which do not necessarily comply with recommended property ranges, may be compensated for by particular strategies. The local ingredient materials are compared based on their mineralogy, specific surface area, particle size and grading by researchers who successful developed non-heat treat UHPC. The majority of local materials were found not that ideal for UHPC. Under such circumstances, following the general UHPC mix design, it is difficult to reach the same designated strength as those achieved by the other researchers.

One of the problems for non-heat treated UHPC is its large shrinkage caused by very low water to cement ratio. A new mix design philosophy is developed for UHPC by making use of steel fibre to improve its compressive strength. Instead of avoiding the large shrinkage, this method uses shrinkage to improve the bond between steel fibre and matrix through the mechanism of shrinkage induced clamping pressure. Subsequently, the mechanism of bridging effect of steel fibre is used to confine shrinkage evolvement in UHPC. Through such a mix design philosophy, the steel fibres are pre-stressed inside UHPC so that it both improves the compressive strength and ductility. A UHPC strength of 168 MPa is achieve in this research.

After the UHPC has successfully been developed, factors that can affect UHPC strength are tested. It is found that the environmental temperature of UHPC, cement composition and

specimen cover during the moulded period significantly influence UHPC strength by approximately 24%. It is also found that after two days of de-moulding, the UHPC exposed to the air, achieved similar strength as that cured in water, which is helpful for future industrial application.

Keywords: UHPC, fibre reinforced, non-heat treated, local materials, shrinkage induced clamping pressure.

Acknowledgements

This research cannot be completed without the support of many individuals and organizations. I would like to first present my sincere gratitude to my study leader, Professor van Zijl, for his time, guidance, patience, support and encouragement. I also appreciate the support of the following people and organizations and sincerely thank them for their time, guidance, and their expertise.

- University of Stellenbosch Civil Engineering academic staff: Professor Jan Wium, Professor WP Boshoff, Prof JV Retief and Dr. JAvB Strasheim for their ideas and support.
- University of Stellenbosch Civil Engineering laboratory manager and working staff, for their support of laboratory work.
- University of Stellenbosch, for support and financial assistance.
- The companies: PPC, Chryso, Sika, Mapei, Bekaert, Hulse reinforcing for their support.
- Finally, all the others who helped me with my research.

Contents

List of Tables

List of Figures

List of Symbols

$A_{c,i}$ Section i area in compression zone;

$A_{t,i}$ Section i area in tension zone;

$d_{c,i}$ The distance from centroid of section i in compression zone to neutral axis;

d_f Equivalent diameter of the fibre;

$d_{t,i}$ The distance from centroid of section i in tension zone to neutral axis;

f_c First cracking strength from flexural test;

f_p Ultimate tensile strength from flexural test;

f_{ct} First crack tensile strength;

f_{pt} Peak tensile strength;

f_{cf} First crack flexural strength;

f_{pf} Peak flexural strength;

f_{cu} Compressive strength;

f_t Tensile strength;

$f_{t,i}$ Average tensile stress of section i in tension zone;

L_{em} The embedded length of the fibre;

n   Number of steel fibres in pull out cross-section;

M_t The total applied bending moment.

P_{max} Maximum pull out load;

PE_{total} Pull out energy until the fibre is completely pulled out;

S   Fibre spacing;

V_f Applied volume content of steel fibres in %;

ε_{cr} Crack strain;

ε_{ult} Ultimate strain;

$\delta_{c,i}$ Average compressive stress of section i in compression zone;

σ_{cr} Crack stress;

τ_{max} The average bond stress.

xvi

List of Abbreviations

AS   Autogeneous shrinkage;

AS'   Part of autogenous shrinkage;

B_{ft} Box girder top flange width;

B_{fb} Box girder bottom flange width;

B_w Bleeding water;

C   Cement;

COV   Coefficient of variation;

DS   Drying shrinkage;

h_{ft} Box girder top flange height;

h_{fb} Box girder bottom flange height;

FE   Finite element;

GP   Glass powder;

H   Hydration products;

H_{ave} Average box girder height;

P   Pore;

PS   Plastic shrinkage;

SF   Silica fume;

SP   Superplasticizer;

Std   Standard deviation;

t_{wl} Box girder left flange thickness;

t_{wr} Box girder right flange thickness;

UHPC   Ultra-high performance concrete;

UHPM   Ultra-high performance mortar;

UHPP   Ultra-high performance paste;

W   Water;

W/C   Water to cement ratio.

Chapter 1: Introduction

Ultra-high performance concrete (UHPC) is a relatively new material which was developed in France during the 1990s. UHPC is also known as ultra-high performance fibre reinforced concrete (UHPRFC) and was defined by the Association Française de Génie Civil (AFGC) as a material that has a compressive strength of over 150 MPa and which contains steel fibres (AFGC, 2002). Steel fibres in UHPC ensure the non-brittle behaviours of this type of material.

Even if heat curing of UHPC can enhance UHPC strength, it is not easy to be applied in the industry. Instead, non-heat cured UHPC has great potential to be used in the future, but limitations exist for the ingredient materials used in UHPC according to the experience of various researchers. This research will focus on developing UHPC under normal curing conditions and making use of local available materials.

1.1. RESEARCH MOTIVATION

The application of this material in the construction of bridges, such as UHPC I-girder bridge in the United States and pedestrian bridges shown in Figure 1-1, have exploited and demonstrated the high strength of this material.
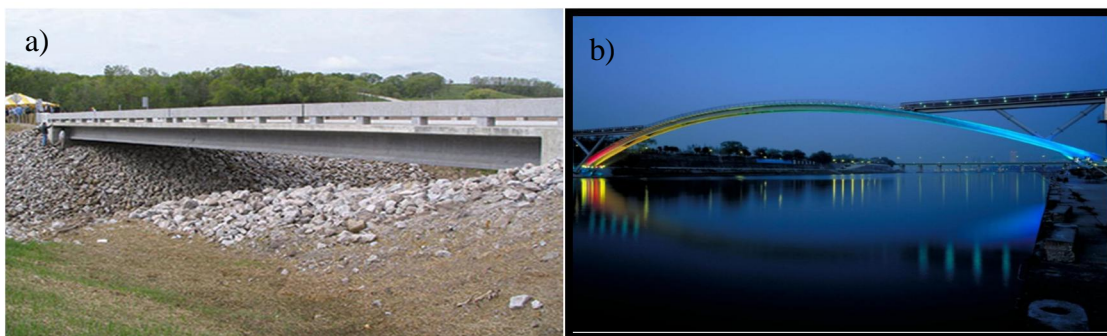
Figure 1-1: UHPC bridges: (a) The Mars Hill Bridge, located in Iowa's Wapello County (Graybeal, 2009); and (b) The Footbridge of Peace in Seoul (Brouwer, 2001).

1

The mix design of UHPC differs slightly in different countries according to their local materials. Various UHPC parameters have been systematically tested in many countries in order to provide useful data for future application. The high strength and enhanced ductility of UHPC enable it to minimize the section dimension of the building structures. In addition, the high tensile strength of UHPC enables bridge girders to be designed without shear reinforcement. Besides the strength and ductility, UHPC also exhibits high durability such as superior resistance to chloride ion penetration and freeze-thaw deterioration. In addition, the high fracture energy in UHPC makes such material ideal to be used in seismic resistance building structures. Based on the above mentioned superior properties of UHPC, much research has already been done despite the fact that it has only been developed over the last two decades. However, non-heat treated UHPC has not been implemented in South Africa yet and consequently there is a need for UHPC to be developed using local materials.

1.2. RESEARCH OBJECTIVES AND SIGNIFICANCE

The objective of this research is to develop non-heat cured UHPC with local available materials. Even if each material contributes to the strength of UHPC, the ultra-high strength paste (UHPP) is one of the key factors that involves chemical reaction to provide UHPC strength. The major objective of this research is then to develop a proper UHPP mix design for UHPC. The relatively non-ideal materials available locally for UHPC mix design make it impractical to simply adjust the UHPC mix design developed by other researchers, who have already done much research on which they built their reference UHPC mix. Instead, the UHPC has to be re-developed based on the local available materials. The effect of various mix design parameters on UHPC strength is gradually studied through the mix design and laboratory testing program here.

2

1.3. RESEARCH SCOPE

This research focuses on the development of UHPC, using the materials that are commonly used in South Africa. Besides high strength straight steel fibres that are imported, the locally available materials in the Western Cape are as follows:

- Cement: CEM I 42.5N and CEM I 52.5N;

- Silica fume: grey silica fume with specific surface area of 23 $\pm$ 3 m^2/g;

- Superplasticizer: Chryso 310, Mapei Dynamon SP1, Sika Viscocrete 10 and Sika Viscocrete 20HE;

- Natural sands: Philippi and Malmesbury sand;

- Coarse aggregate: 6.7 mm Greywacke stone;

Heat curing is not included, not even as a reference, due to lack of time, but primarily because of the prime objective of developing non-heat cured UHPC. The mix designs and test programs will only focus on the development of UHPC, either to verify the key findings from other researchers or to gradually improve the strength of locally developed UHPC.

Once UHPC has been developed with adequate compressive strength, the tensile behaviour is tested based on the available laboratory equipment that can provide fundamental structural design parameters. The shrinkage of UHPC is not tested in this research even though it is postulated to contribute to UHPC strength. However, UHPC shrinkage development reported in the literature by other researchers is used as reference.

1.4. STRUCTURE OF DISSERTATION

This dissertation comprises eight chapters as shown in Figure 1-2 which show the progress of this research. Chapter 1 provides an overview of this research. Chapter 2 introduces related experimental results and experience from researchers which help to guide the UHPC

development in this research. Chapter 3 compares the local available materials with the materials used by other researchers, so that the corresponding UHPC strength with local materials can be understood. Chapter 4 presents a UHPC mix design philosophy that can guide UHPC development. Chapter 5 elaborates on the phase mix design of UHPP, UHPM and UHPC based on the mix design philosophy in this research. Once the UHPC has been successfully developed in this research, the factors that can influence UHPC strength are studied and tested. Chapter 6 compares tensile and flexural behaviour and characterises the tensile strength of UHPC developed in this research. Chapter 7 presents the post tensioned box girder test and FE analysis on a structural level. The final chapter concludes the findings in this research and recommends items for future research.

```
┌─────────────────────────────┐
│         Chapter 1            │
│        Introduction          │
└─────────────────────────────┘
              │
┌─────────────────────────────┐
│         Chapter 2            │
│       Literature review      │
└─────────────────────────────┘
              │
┌─────────────────────────────────────────────────┐
│                  Chapter 3                        │
│ Comparing local materials with typical materials  │
│                used for UHPC                       │
└─────────────────────────────────────────────────┘
              │
┌─────────────────────────────┐
│         Chapter 4            │
│ The Philosophy in developing │
│            UHPC              │
└─────────────────────────────┘
              │
┌─────────────────────────────────────────────────┐
│                  Chapter 5                        │
│ UHPC development with local materials and factors │
│           that affect UHPC strength               │
└─────────────────────────────────────────────────┘
              │
┌─────────────────────────────┐
│         Chapter 6            │
│ Tensile and flexural         │
│   behaviour of UHPC          │
└─────────────────────────────┘
              │
┌─────────────────────────────┐
│         Chapter7             │
│ Post tensioned box girder    │
│      test and analysis       │
└─────────────────────────────┘
              │
┌─────────────────────────────┐
│         Chapter 8            │
│ Conclusions and future       │
│        research              │
└─────────────────────────────┘
```

Figure 1-2: Layout of Dissertation.

4

Chapter 2: Literature review

2.1. INTRODUCTION

This chapter introduces related literature that helps to develop UHPC in South Africa. The typical way to develop UHPC is first introduced. Then, types of shrinkage in UHPC are introduced. Subsequently, the concept of shrinkage-induced clamping pressure is introduced and the UHPC bond stress results are obtained from the literature.

2.2. UHPC DEVELOPMENT

In this sub-section, the general way on how to develop UHPC under normal curing conditions is introduced. The effect of curing regime, cement, sand, and silica fumes on UHPC is elaborated.

2.2.1. The effect of curing regime on the UHPC compressive strength

Even if UHPC has only been developed over approximately one decade, a substantial amount of research has already been done on UHPC. Because UHPC exhibits a relatively large shrinkage compared to normal strength concrete, heat curing treatment is normally applied to accelerate shrinkage caused by the hydration of cement at early age. According to Graybeal (2006), four types of curing regimes are commonly used, namely:

- Steam curing: Steam UHPC at 90 ℃, 95 percentage relative humidity (RH) for 48 hours after casting;

- Tempered steam curing: Steam UHPC at 60 ℃, 95 percentage RH for 48 hours after casting;

- Delayed steam curing: Steam UHPC at 90 ℃, 95 percentage RH for 48 hours starting

5

15 days after casting;

● Water curing: Cure UHPC in the water tank of 23 ± 2 ℃ after 48 hours of casting.

For the same mix design, the UHPC strength under different curing regimes is summarized in Table 2-1. It can be seen that the heat curing condition does help to increase the compressive strength significantly and the higher curing temperature leads to higher compressive strength.

Table 2-1: The 28 days UHPC strength under four curing regimes (Graybeal, 2006).

Curing regime	28 days strength (MPa)
Steam curing	181
Tempered steam curing	154
Delayed steam curing	173
Water curing	112

2.2.2. General method of developing UHPC

Even if heat cured UHPC has higher strength compared with water cured UHPC, it is not easy to apply heat curing treatment in the industry. This research is focused on the water cured UHPC because its application in industry is more flexible. However, more limitations on ingredient material usage are needed for water cured UHPC in order to achieve the designated strength of at least 150 MPa due to its relatively lower strength, compared with UHPC under heat cured conditions as shown in Table 2-1.

Even though UHPC has superior strength compared with the normal strength concrete, it still belongs to the concrete family and thus follows the general behaviour of concrete. The UHPC could generally be achieved through two ways: one way is to increase cement content by reducing the water to cement (W/C) ratio, while the other way is to improve the packing density of UHPC. It is common knowledge that reducing the W/C ratio can increase the paste strength, which contributes to increased UHPC strength. In addition, improving the aggregate

6

packing density can contribute to increased UHPC strength.

The essential ingredient materials for UHPC are cement, silica fume (SF), aggregate, superplasticizer (SP), steel fibre and water, as described below:

- Cement: Hydration of cement determines the concrete compressive strength (Yogendran *et al.* 1991:691).
- SF: The SF acts as reactive powder and has two functions in UHPC. From the physical point of view, SF can act as filler in UHPP that improves the paste packing density. From the chemical point of view, the pozzolanic reaction of SF can further increase UHPC strength (Yogendran *et al.* 1991:691).
- Aggregate: Either fine aggregate or coarse aggregate can be considered as inert filler. Fine aggregate, such as fine sand, is normally used for UHPC under water curing conditions. Coarse aggregate, such as small particle stone of 6 mm in diameter, is normally used for heat cured UHPC.
- SP: Helps to disperse solid particles of cement and SF under very low water content (Schroefl *et al.* 2008:383).

By combining all ingredients except the aggregate and steel fibre, the ultra-high performance paste (UHPP) is formed. UHPP provides the chemical reaction to increase UHPC strength. By adding fine aggregate, ultra-high performance mortar (UHPM) is formed, and once fibres are also included, UHPC is complete.

Besides the above mentioned, two ways of developing UHPC by most researchers are followed, which are the use of a low W/C ratio and ensuring a high packing density, the relatively higher shrinkage in water cured UHPC can cause quite substantial limitations for the materials to be used, especially cement type. Therefore, more understanding of each material and its role are needed to successfully develop water cured UHPC.

2.2.3. The packing density

2.2.3.1. Aggregate packing density

The aggregate is an essential constituent in concrete mix. The spatial dispersion of this non-reactive material affects the concrete strength. Therefore, some packing models have been developed by researchers to optimize their aggregates. Among these models, Larrard and Sedran (1994:997) developed the Solid Suspension Model (SSM) which was derived from Mooney's suspension viscosity model, and they successfully applied this model in the development of UHPC.

The parameters for those packing models can be used as an indication to better understand the concept of the packing of the aggregate. Mooney's model takes into consideration the following parameters: minimum and maximum grain size, specific packing density, loosening effect and wall effect (Mooney, 1951:162). The SSM model modifies Mooney's model through changing the reference specific packing density to make it more practical. It can be seen from the above models that the size and grading of sand are quite important for aggregate selection.

2.2.3.2. Paste packing density

The particle size of SF is generally between 10 times and 20 times smaller than that of cement. Therefore, some researchers used filler to fill in the gap between SF and cement to improve the packing of paste to further increase UHPC strength (Park *et al*. 2008, Wille *et al*. 2011).

Fillers with mean median grain size of 100 micron (μm) and 13 μm respectively were used to compare the effect of filler on UHPC compressive strength by Park *et al*. (2008:105-112). The grain size of 100 μm filler lies between cement and sand. The grain size of 13 μm filler lies between SF and cement. It was found that the 100 μm filler has limited effect on strength

8

increment while the 13 μm filler results in a 31% of increased compressive strength with the increment value of 55 MPa according to Park *et al*. (2008:105-112). However, the filler was normally used in UHPC under heat curing conditions in previous years. For the normal water cured UHPC, Wille *et al*. (2011:46) selected a filler with the median grain size of 1.7 μm and achieved paste strength of approximately 180 MPa.

2.2.3.3. Overview of packing density

Because the materials used for UHPC by researchers from various countries are not of the same origin and thus composition, there is not enough information to select the type of sand and filler that perfectly match their material when developing UHPC locally. Instead, a systematic trial approach is required.

2.2.4. The effect of sand on UHPC strength

Higher packing density of sand causes fewer voids between sand particles that require less paste volume to fill in these voids. Less paste volume can reduce the side effect of shrinkage, whereby this cause of compressive strength reduction may be reduced. However, higher performance concrete requires a higher cement content that leads to a higher paste volume, which requires enough thickness of paste around the aggregate to provide enough concrete strength (Kovler & Zhutovsky, 2006:827). Therefore, increasing UHPC strength cannot be achieved purely by improving the packing of the aggregate. The sand used for UHPC is normally very fine sand with minimal ratio between smallest and largest grain size to minimize the wall and loosening effect. It can be observed that researchers typically incorporate a sand to cement ratio of between 1.1 and 1.4 (Wille *et al*. 2012:309) to maintain a certain paste volume in UHPC. In addition, the fine sand can reduce the differential stress between paste around sand particles and sand.

As mentioned in Section 2.2.3.3, the role that sand effectively plays in UHPC differs between

researchers. Except the packing model, the improved bulk packing density is also used to increase the UHPC compressive strength and this reduces the cost. With optimised sand, Wille *et al*. (2011:46) achieved a compressive of 194 MPa for UHPC without steel fibres while the paste strength achieved approximately 180 MPa, leading to an increased strength of approximately 8%. A lack of enough literature makes it difficult to compare the contribution of sand on UHPC strength from other researchers.

2.2.5.   The effect of silica fume on concrete compressive strength

It is generally believed that pozzolanic reaction of SF can further increase the concrete compressive strength. Chatterji *et al*. (1982:781) argued that the increased concrete compressive strength was due to the filler effect of SF instead of the pozzolanic effect. However, when comparing the effects of carbon black and SF on concrete compressive strength, it is found that the pozzolanic reaction of SF is dominant in improving the concrete compressive strength (Detwiler & Mehta, 1989:609). The carbon black and SF have similar particle size characteristics and the only difference is that the carbon black does not participate in a pozzolanic reaction. Through replacement of 10% of cement by weight with carbon black and SF respectively, the effect of the SF on concrete compressive strength can be compared as shown in Table 2-2.

It can also be seen from Table 2-2 that the pozzolanic reaction has only a limited effect on concrete compressive strength on 7 days while the pozzolanic reaction is dominant in increasing concrete strength over 28 days. From the physical point of view, the filler effect of carbon black only results in a slight strength increment over 28 days while it leads to a reduction in compressive strength on 7 days.

Table 2-2: Concrete compressive strength contains silica fume and carbon black (Detwiler & Mehta, 1989:609).

Type of mix	Water to cement ratio	7 days compressive strength (MPa)	28 days compressive strength (MPa)
Plain cement		80.3	91.6
90% cement + 10% SF	0.25	80.3	108.9
90% cement + 10% Carbon black		74.8	93.3

The above analysis shows that the pozzolanic reaction of SF does help to increase concrete strength. The effect of SF content on UHPC strength was studied by Park *et al*. (2008:105-112) as shown in Figure 2-1. By changing the SF content while the content of the rest of the materials remains the same, the UHPC strength follows a parabolic curve as shown in Figure 2-1. The UHPC strength increases with increased SF content when SF/C is less than 0.25. Once the SF/C is larger than 0.25, the UHPC strength decreases with the increased SF content.
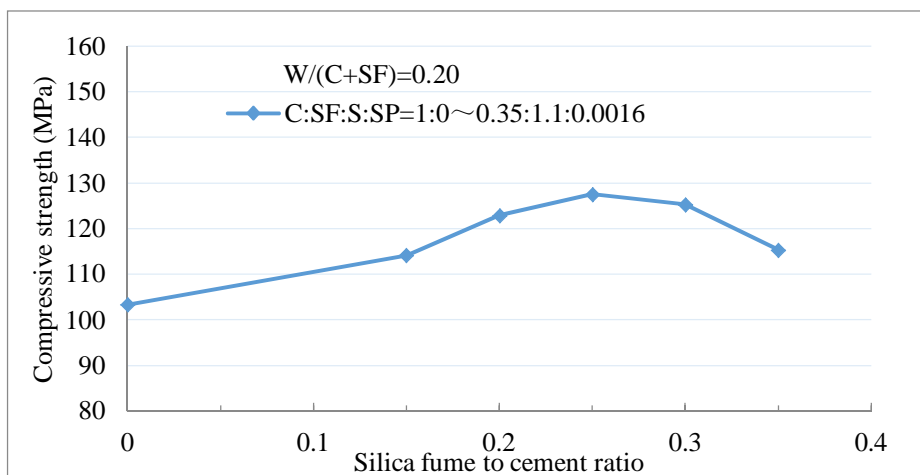
Figure 2-1: Effect of silica fume content on UHPC strength (Park *et al*. 2008:105-112).

2.3. EFFECT OF SHRINKAGE ON UHPC

Shrinkage is the natural phenomenon in concrete due to differences in humidity and pore sizes

and it is generally accompanied by internal differential stresses or even worse, micro cracks. The UHPC specimens under laboratory conditions are normally covered with a lid, plastic or wet burlap to prevent moisture loss which will reduce the plastic shrinkage for UHPC during the moulded period. Due to a very low water to cement (W/C) ratio, the increased cement content in concrete causes relatively larger shrinkage and the autogenous shrinkage is believed to be the most dominant shrinkage that affects the UHPC. The autogenous shrinkage will not be high if the W/C ratio is greater than 0.42. However, when the W/C is lower than 0.42, the autogenous shrinkage may be significant according to (Aitcin *et al*. 1997:35). In addition, the incorporation of more SF in UHPC will further increase the autogenous shrinkage. Therefore, with the decrease of W/C ratio and increase in SF content, the autogenous shrinkage in UHPC will be increased (Zhang *et al*. 2003:1687). The early age stress and/or crack are mainly caused by the combinations of thermal dilation, drying shrinkage, autogenous shrinkage and possibly plastic shrinkage.

2.3.1. Thermal dilation

Thermal dilation refers to a volume change in response to a change of temperature during the early and later ages of concrete. During the early ages, the cement hydration causes the temperature to rise which causes the expansion of concrete. Then, the concrete starts to cool down (after the heat of hydration) which results in the contraction of concrete. The thermal gradient can cause thermal strains and possible cracks during the early ages of concrete. Especially for any large project that requires massive amounts of concrete, the thermal strain will be caused by a differential in temperature between the interior of concrete and exterior surface caused by environmental changes.

2.3.2. Drying shrinkage and plastic shrinkage

Drying shrinkage refers to the concrete volume reduction due to the loss of moisture at constant temperature and relative humidity, which shows an important property of hardened

cement paste. The main mechanisms for drying shrinkage have been explained to be capillary tension, solid surface tension and loss of interlayer water (Bažant, 2001:27). Plastic shrinkage refers to the very first hours of volume change caused by the loss of water either by evaporation from the surface of concrete or by the absorption from aggregate when the concrete is still plastic.

Under laboratory conditions, researchers generally protect their freshly cast UHPC specimens with a plastic sheet or some other device to retain the moisture and to minimize plastic shrinkage. However, a condition of no top cover is more applicable to in situ construction. The current published research works lack corresponding information on how plastic shrinkage affects water cured UHPC, but the curing conditions during the moulded period do have a significant influence on the compressive strength of UHPC. Ambient conditions, such as temperature and relative humidity, affect UHPC early-age compressive strength, which result in an approximately 52% of the target compressive strength, especially in relatively cold temperature (Soliman, 2011).

For the drying shrinkage, mass change was studied under different exposure conditions and the results are shown in Figure 2-2 where the drying conditions were controlled with temperature: 20 ± 1 ℃, relative humidity: 40% and the submerged conditions refer to water controlled with temperature of 20 ± 2 ℃. It was found that a lower mass change of approximately 25% and 58% under the drying and submerged conditions when the W/C equals to 0.22 compared with that of 0.25 (Soliman, 2011). Gain and loss of water in concrete are associated with positive (swelling) and negative (shrinkage) volume changes respectively. According to Soliman (2011), the lower volume change for cement with lower W/C ratio is caused by: a) reduced porosity; and b) lower capillary suction of water and reduced diffusion coefficient.
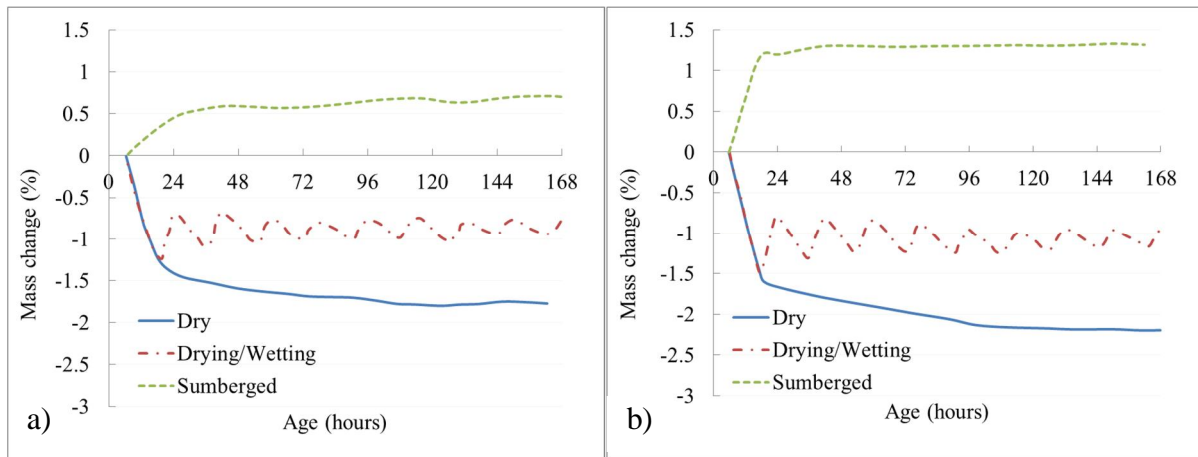
Figure 2-2: Mass change of controlled mixture (a) W/C=0.22 and (b) W/C =0.25 under different exposure conditions (Soliman, 2011).

2.3.3. Autogenous shrinkage and chemical shrinkage

The term autogenous shrinkage was defined to be a macroscopic reduction in volume without any moisture migration to or from the concrete and under a constant temperature (Tazawa *et al*. 1995:288). The chemical shrinkage however is the reduction in the volume of hydration products compared with un-hydrated constituent materials before hydration, which can be considered to be the main driving mechanism behind the autogenous shrinkage (Tazawa *et al*. 2000:21). The difference between autogenous shrinkage and chemical shrinkage is shown in Figure 2-3. The chemical shrinkage refers to absolute volume reduction (internal reduction), while autogenous shrinkage is regarded as apparent volume change (external volume change).
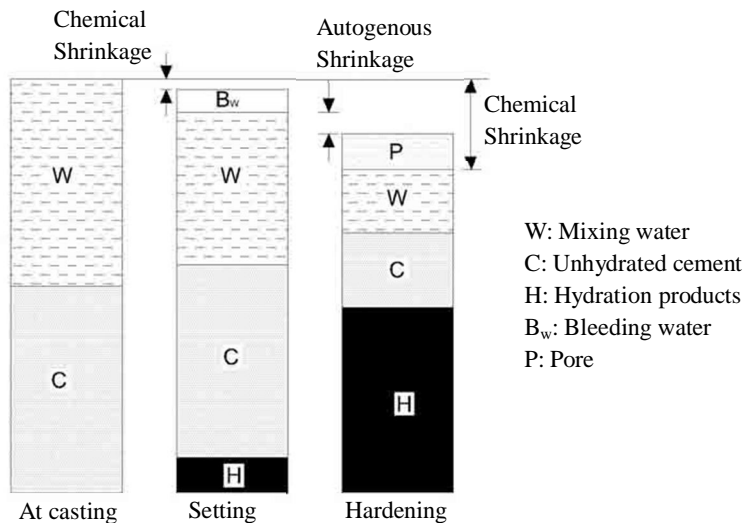
Figure 2-3: Concrete autogenous shrinkage and chemical shrinkage (Mihashi & Leite, 2004:141).

2.3.4. The formation of concrete

The concrete undergoes three phases after the mixing is finished, namely the liquid phase, skeleton formation phase and hardened phase as shown in Figure 2-4. For the first phase, the concrete is still in a liquid state and the autogenous shrinkage is equivalent to chemical shrinkage as indicated in Section AB in Figure 2-4. A few hours after casting, the stiffening of concrete paste starts to form a skeleton, which can resist some of the stresses caused by the chemical shrinkage. The setting of concrete will occur soon after the initial skeleton has formed as shown in Section BC in Figure 2-4. After point C, the skeleton is strong enough to resist stress caused by autogenous shrinkage and the concrete has attained the hardened phase.

15
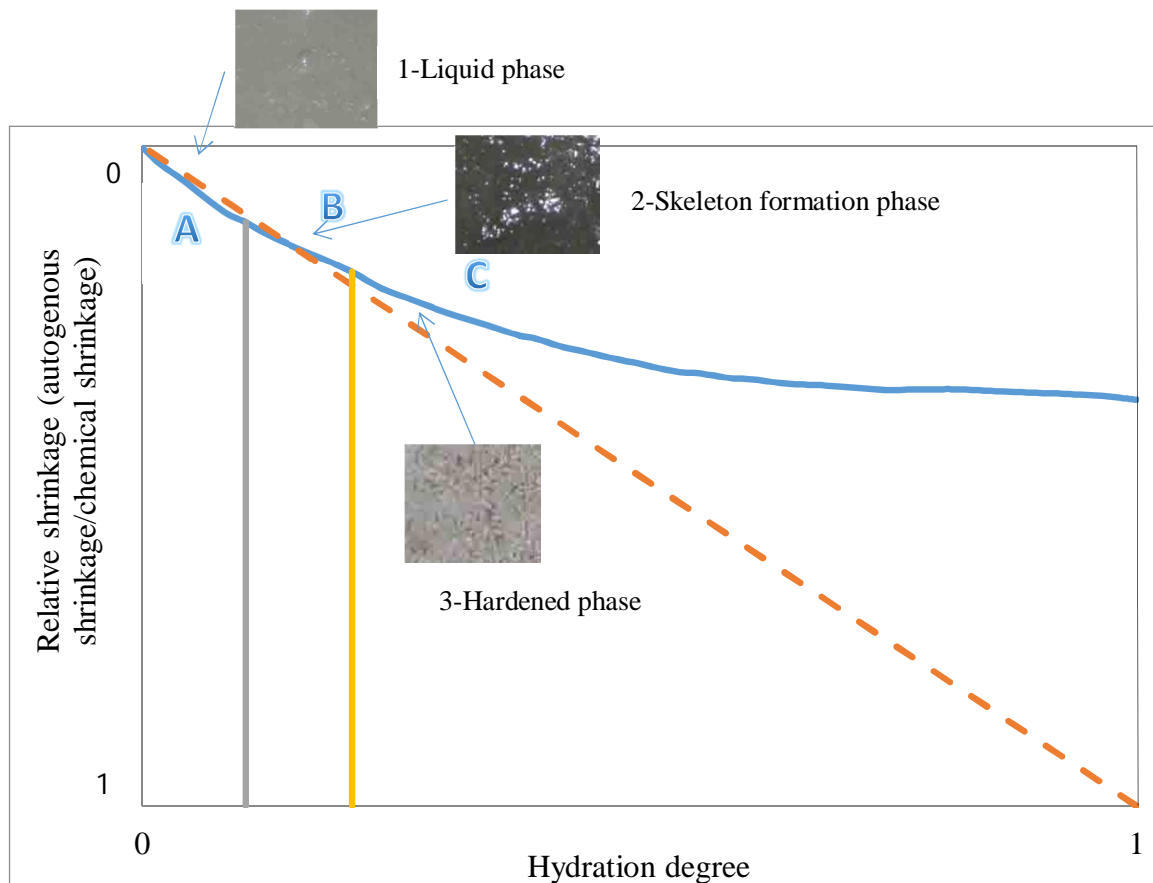
Figure 2-4: Autogenous shrinkage and chemical shrinkage during different phases, as a function of hydration degree (Esping, 2007, Holt, 2001, Soliman, 2011).

2.3.5. Factors that affect UHPC shrinkage

The main types of shrinkage discussed above are not independent, but are inter-related to each other. The shrinkage, especially early age shrinkage, affects the formation of the skeleton which determines the UHPC compressive strength for later ages. Soliman (2011) concluded that the main factors that affect shrinkage are: a) rate of hydration that is affected by the type and content of the cement and SF; b) the aggregate content that confines the paste to reduce shrinkage; c) the water content that affects the autogenous shrinkage; d) pozzolanic materials that affect autogenous shrinkage; and e) curing conditions. Even if the actual UHPC shrinkage will never be exactly the same between UHPCs with different materials and mix design, understanding the mechanisms of shrinkage helps to understand the UHPC performance either in compression or in tension. These mechanisms are especially helpful for decision

16

makings during the development of water cured UHPC in this research.

2.3.5.1. The temperature effect on autogenous strain

Once the materials for UHPC are determined, autogenous strain is mainly affected by the curing conditions. Figure 2-5 shows the autogenous strain for the controlled W/C of 0.25 under sealed conditions (Soliman & Nehdi, 2011:879). It can be seen from Figure 2-5 that a higher curing temperature leads to the acceleration of early-age autogenous strain for the first 24 hours, then the strain increment rates are similar under different curing temperatures. Such autogenous shrinkage increments indicate that relatively higher curing temperatures can help to release more shrinkage at early age which in turn may lead to a relatively lower long-term shrinkage.
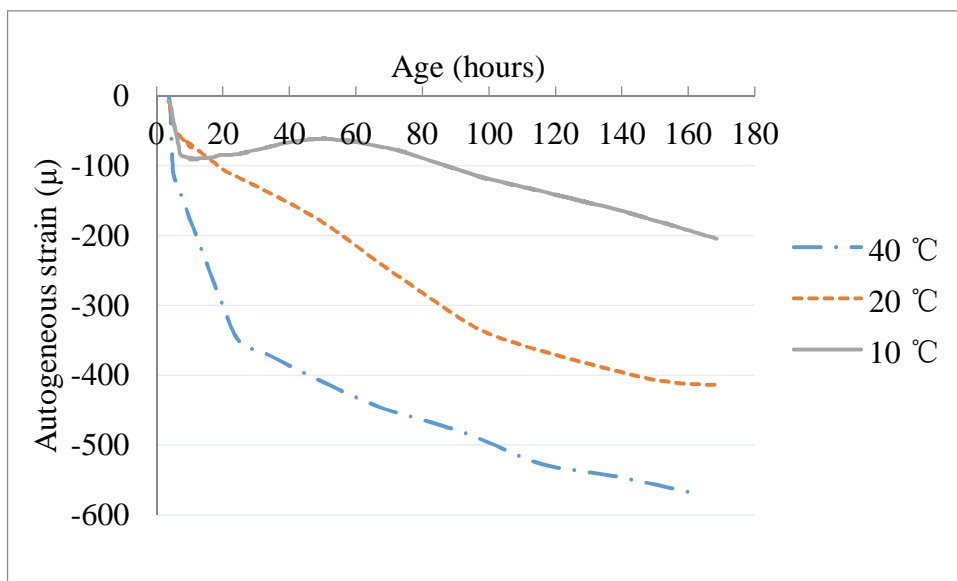
Figure 2-5: Autogenous strain for controlled mixture under 10, 20 and 40 ℃ (Soliman & Nehdi, 2011:879).

2.3.5.2. The curing condition influence on UHPC compressive strength

The different curing temperature during the moulded period was found to have a significant influence on 28 days UHPC strength as shown in Figure 2-6. The general trend is that a

higher curing temperature and a higher relative humidity results in a higher compressive strength. In addition, it is also common knowledge that the compressive strength increases with reduced W/C ratio.

However, for 7 days and 28 days strength, some results show that the reduced W/C ratio causes lower compressive strength under fixed temperature and relative humidity as shown in Figure 2-6, which is contradictory to the general trend. Such a phenomenon indicates the complexity of curing conditions on UHPC compressive strength. The combinations of reactions are inter-related with each other, either physically or chemically, and they determine the UHPC strength. Therefore, understanding the mechanisms can help researchers to further increase UHPC compressive strength.
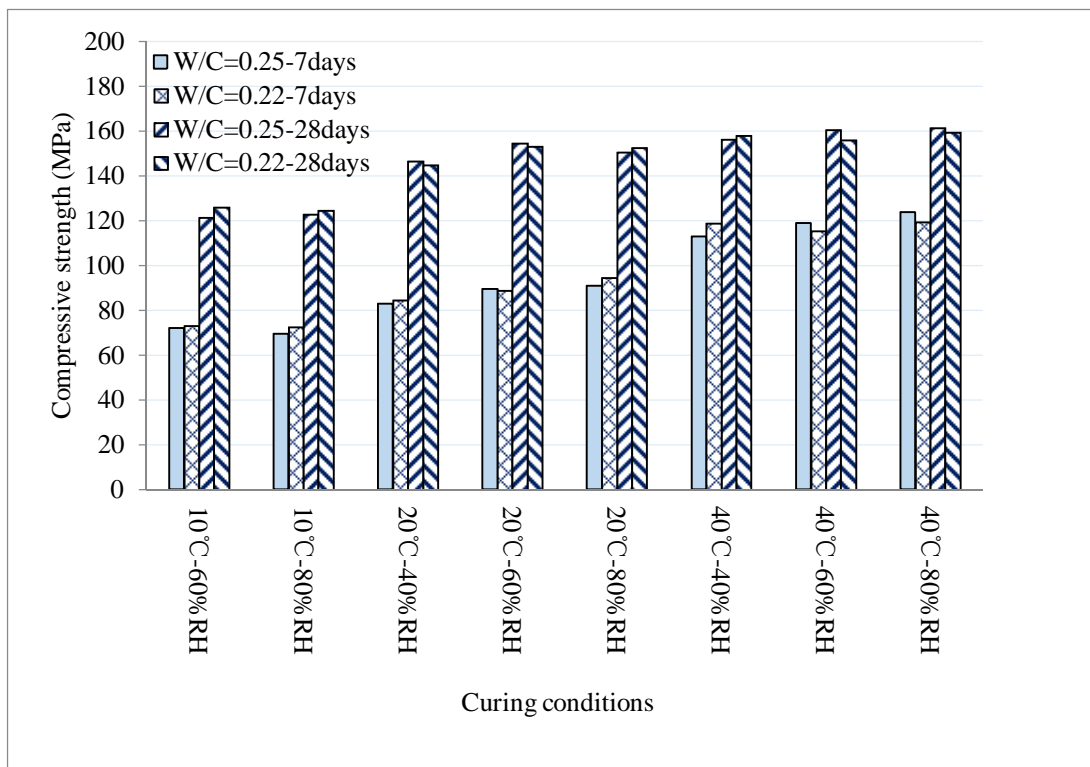
Figure 2-6: Effect of W/C on compressive strength under different curing conditions (Soliman, 2011).

2.4. EXPERIENCE OF UHPC SHRINKAGE FROM OTHER RESEARCHERS

Having found that the shrinkage can be affected by the content of materials in the UHPC mix and the curing conditions, the typical shrinkage results from researchers are introduced.

2.4.1. The influence of W/C ratio on UHPC early age volume change

Different water to cement ratio results in different apparent autogenous shrinkage for UHPC during early age. Under the sealed condition with the ambient temperature fixed at 20 ℃, the relative volumetric variation is shown in Figure 2-7, with the corresponding mix design listed in Table 2-3.

The main difference for the two mixes is the different W/C ratio. It can be seen from Figure 2-7 that lower W/C ratio leads to a relatively higher volume change during early age, which indicates a higher autogenous shrinkage. Such volume change is mainly caused by more cement content in the case of lower W/C ratio, which changes the hydration rate.

Table 2-3: The mix design for different water to cement ratio (Feylessoufi *et al.* 2001:1573, Morin *et al.* 2002:1907)

W/C ratio	SF/C ratio	Solid SP in percentage of cement weight	Sand to cement ratio
0.16	0.25	0.018	1.1
0.21	0.25	0.015	1.1

19
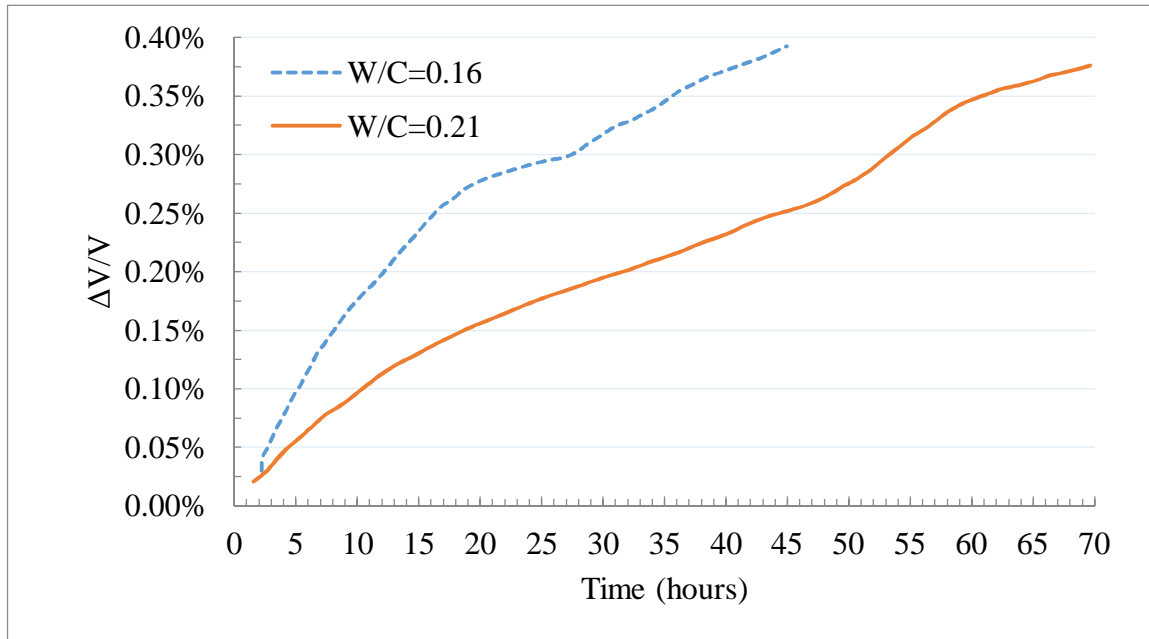
Figure 2-7: Relative volumetric variation for W/C of 0.16 and 0.21 respectively (Feylessoufi *et al*. 2001:1573, Morin *et al*. 2002:1907).

2.4.2. The effect of W/C ratio and superplasticizer dosage on drying shrinkage

The different W/C ratio and SP dosage will also influence the drying shrinkage. The effect of different W/C ratio and the SP dosage on ultra-high performance mortar (UHPM) drying shrinkage is shown in Figure 2-8. By changing the W/C ratio while fixing other materials in the mix design, the lower W/C ratio of UHPC results in a lower drying shrinkage (Tam *et al*. 2012:79). When only changing the SP dosage while fixing the W/C=0.26, the UHPM drying shrinkage reduced with lower SP dosage (Tam *et al*. 2012:79). Such a phenomenon also confirms the finding that a lower percentage of SP leads to a reduced shrinkage rate which can provide a higher strength (Morin *et al*. 2001:63).
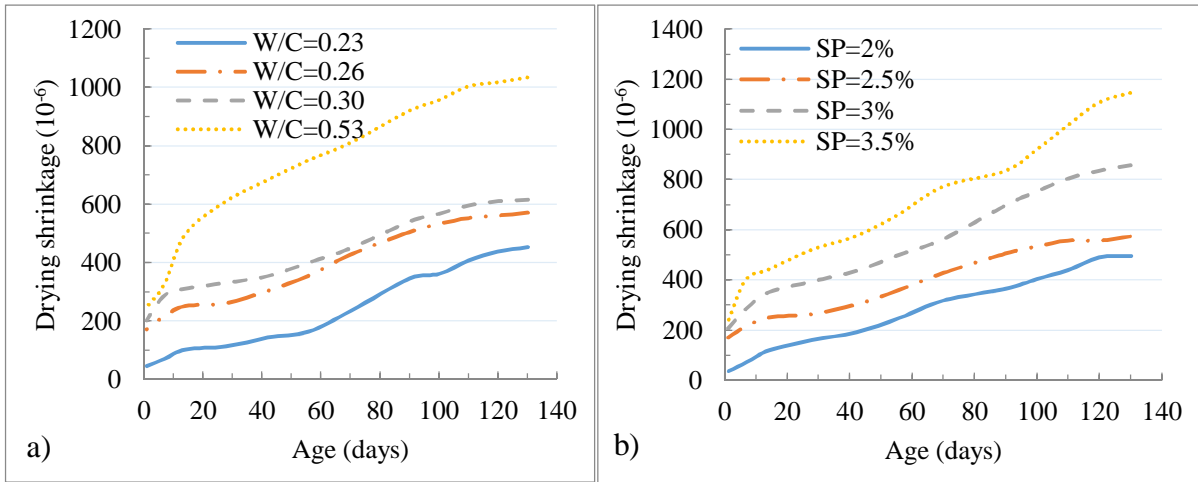
Figure 2-8: Drying shrinkage of UHPC with (a) different water to cement ratio and (b) with different superplasticizer dosage (W/C=0.26) under various ages (Tam et al. 2012:79).

2.4.3. The effect of silica fume content on UHPM autogenous shrinkage

The effect of SF on autogenous shrinkage is shown in Figure 2-9. It can be seen that more SF content leads to a higher autogenous shrinkage. In addition, the autogenous shrinkage increases quickly for the first 14 - 21 days and at a significantly lower rate after that. Ma *et al.* (2003:255) also indicate that the pozzolanic reaction of SF further increases the autogenous shrinkage for UHPC.
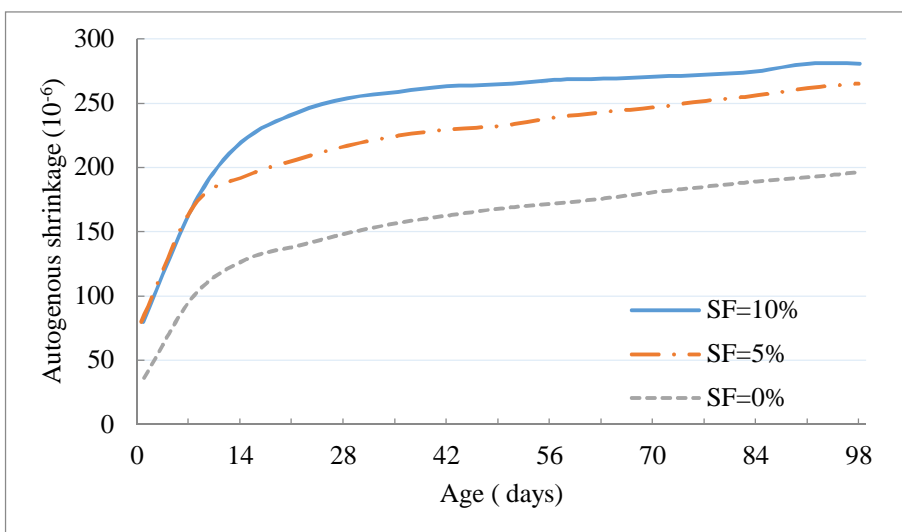
Figure 2-9: Effect of SF content on UHPM autogenous shrinkage (Zhang *et al.* 2003:1687).

21

2.4.4. The major shrinkage for UHPM: autogenous shrinkage compared with drying shrinkage

From the previous sub-sections, it can be seen that both autogenous shrinkage and drying shrinkage contribute to the total shrinkage of UHPC. Quite a few factors affect UHPC shrinkage which make it difficult to distinguish the exact shrinkage between different researchers because the materials used by researchers are different.

Shrinkage of UHPM was studied by measuring the total shrinkage and autogenous shrinkage by Zhang *et al*. (2003:1687). They cast prisms with the dimensions of 400×100×100 mm in steel moulds, covered them with plastic sheet and left them in the casting room at the temperature of 30 ℃ for 24 hours. The prisms were then de-moulded and cured in a moist-curing room with temperature of 30 ℃ and relatively humidity larger than 95%, until the day of testing.

The autogenous shrinkage (AS) was measured through a strain transducer and a thermocouple that was embedded horizontally in the centre of the prism right after casting of the prisms. The total shrinkage was measured by two pins at a distance of 200 mm glued to both sides of the side-casting prism surfaces 1.5 hours after drying. A Demec gauge was used to measure the distance every week so that the changing length can be compared with the initial length. The total shrinkage of prisms was monitored at 30 ℃ and relatively humidity of 65% after 7 days of moist curing. Therefore, the total shrinkage includes plastic shrinkage (PS), drying shrinkage (DS) and part of the AS (AS'), where AS' is developed in UHPM during 7 days of moist curing.

The total shrinkage and AS are shown in Figure 2-10. Based on the test setup of Zhang *et al*. (2003:1687), it is not possible to obtain DS by directly subtracting the AS from the total shrinkage. However, the difference can be compared according to Table 2-4. It can be seen from Table 2-4 that for lower W/C ratio, the AS is nearly the same as that of total shrinkage.

22

Zhang *et al.* (2003:1687) shows that the AS increased with the decreased W/C ratio. The W/C ratio for most UHPCs developed nowadays is lower than 0.22 which further reduces the DS and increases AS. Therefore, AS can be regarded as the major shrinkage for UHPC.
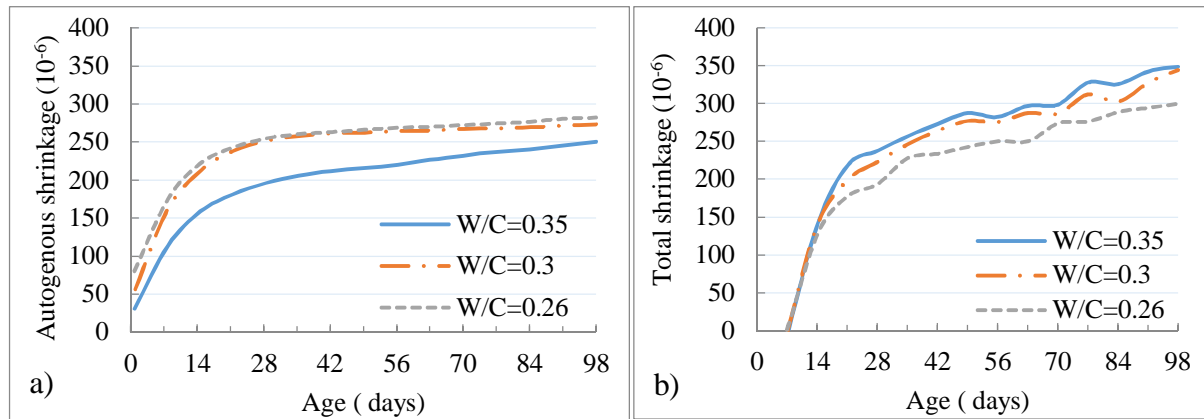
Figure 2-10: UHPM (CF/C=0.1) shrinkage: (a) The autogenous shrinkage and (b) The total shrinkage (Zhang *et al.* 2003:1687).

Table 2-4: The relationship between autogenous shrinkage and drying shrinkage at 98 days (Zhang *et al.* 2003:1687).

W/C	AS (10^{-6})	PS+DS+AS' (10^{-6})	AS/(PS+DS+AS') (%)
0.26	282	298	95
0.30	274	346	79
0.35	251	344	73

2.4.5. Autogenous shrinkage of UHPP

Having found that autogenous shrinkage is the main shrinkage for UHPC, the autogenous shrinkage for UHPP is quite important. However, there is not much research on UHPP itself available because most researchers have focused on the overall performance of UHPC. One research done by Schachinger *et al.* (2002:1341-1354) shows the autogenous shrinkage for UHPP under various W/C ratios and SF contents, which is quite valuable for this research. In order to better observe shrinkage evolving in early age, the first 7 days autogenous shrinkage is shown in Figure 2-11 (a) and the total tested autogenous shrinkage is shown in Figure 2-11

23

(b).

It can be seen from Figure 2-11 (a) that the majority of autogenous shrinkage developed within 24 hours. From Figure 2-11 (b), for SF/C=0.3, the shrinkage increasing rate between 1 day and 28 days is higher than that after 28 days. However, for W/C=0.27 and SF/C=0.18, there is a sudden jump of autogenous shrinkage at 14 days and the reason why the test stopped at 17 days for UHPP (W/C=0.27 and SF/C=0.18) shrinkage is unknown. But such a jump in autogenous shrinkage at 14 days may show the reason why the UHPP strength reduces after 14 days of casting found in this research, which will be elaborated in Chapter 5.
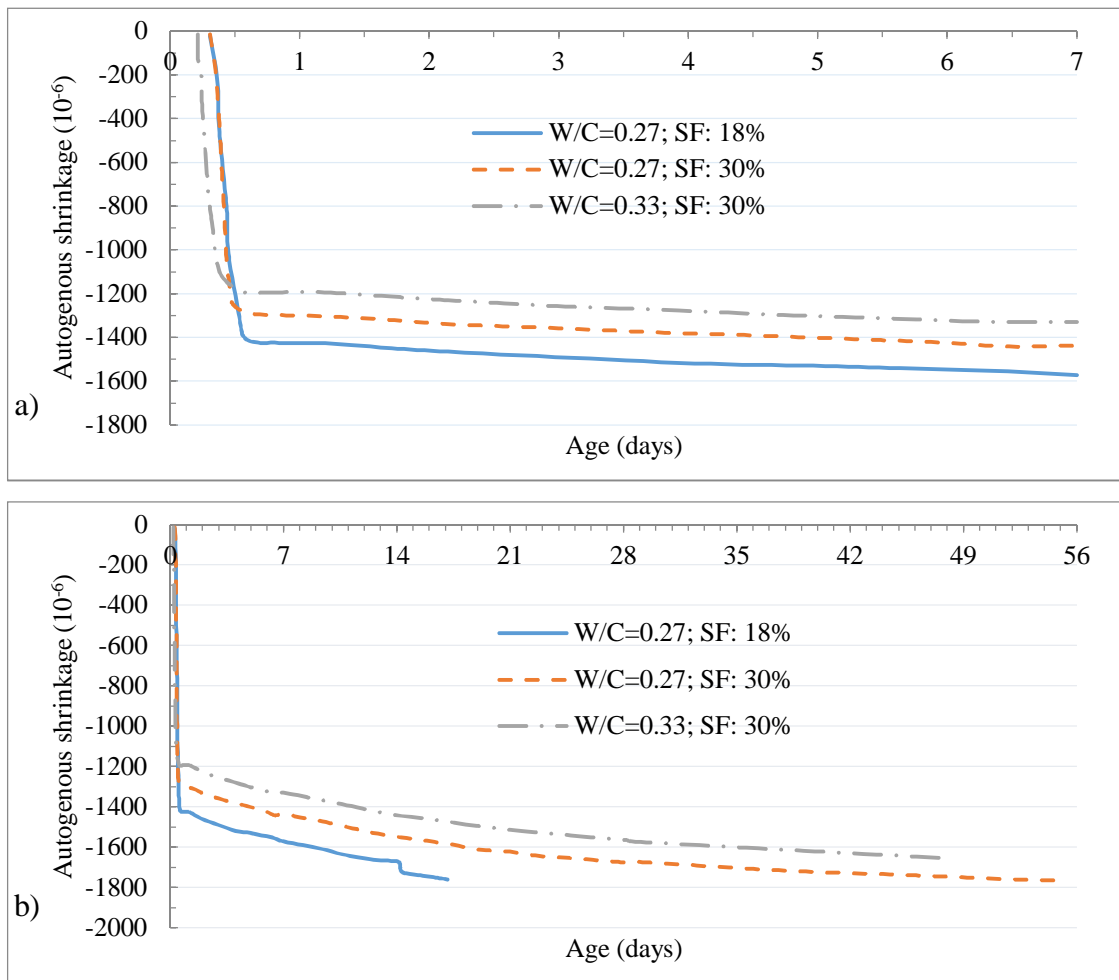
Figure 2-11: The UHPP autogenous shrinkage (a) up to 7 days and (b) up to 56 days.

By comparing autogenous shrinkage of UHPP (W/C=0.27, SF/C=0.18) with that of UHPM (W/C=0.26, SF/C=0.10, S/C=1.5) in Section 2.4.4, it can be seen with similar W/C content

and 8% difference of SF by cement weight, the UHPP autogenous shrinkage reaches as high as 1800 micro-strain while the UHPM autogenous shrinkage only reaches approximately 300 micro-strain. A significant reduction in autogenous shrinkage in UHPM reflects that higher sand content does help to reduce shrinkage.

2.5. BOND STRESS BETWEEN STEEL FIBRE AND UHPM

According to the report of ACI 544.1R-96, the steel fibres can not only restrain crack development, but can also help to resist material deterioration such as fatigue, impact, shrinkage and thermal loads. The clamping pressure caused by matrix shrinkage helps to increase fibre-matrix bond stress and might be an important mechanism for FRC (Stang, 1996:106). The relatively higher shrinkage in UHPC will further help to increase the clamping pressure around steel fibres. For smooth straight steel fibres, the pull out work under friction is approximately two to three orders of magnitude larger than that under de-bonding which indicates the importance of friction on fibre bond stress (Alwan *et al*. 1991:247). Wille & Naaman (2013:451) showed that the average fibre bond stress in UHPC of 8.9 MPa is approximately three times that of 3.2 MPa in high strength concrete (Naaman & Najm, 1991:135) through single fibre pull out tests. Understanding how to increase the bond stress will help to make better use of steel fibres in UHPC.

2.5.1. Clamping pressure caused by shrinkage

Stang (1996:106) used a laboratory mercury thermometer as a pressure sensor to measure the shrinkage induced clamp pressure on steel fibres. The clamping pressure and effective shrinkage for paste with W/C ratio of 0.3 and different SF to cement content was compared as shown in Figure 2-12. It can be seen that the paste with 10% SF by cement weight has three stages of shrinkage development. The first stage of effective shrinkage increment occurs until 50 hours after casting. The second stage of effective shrinkage increment occurs between 50 and 210 hours with a reduced gradient. For the third stage, the effective shrinkage continues

25

to increase with time until the test is stopped. The corresponding clamping pressure increased with effective shrinkage as well.

The effective shrinkage for paste without SF has similar early age effective shrinkage as that of paste with 10% SF for the first 50 hours. Without the contribution of SF, the shrinkage reduces between 50 and 210 hours. After that, the effective shrinkage slightly increases but the shrinkage increment rate is lower than the paste with SF. Since the clamping pressure is induced by the effective shrinkage, the corresponding clamping pressure also follows the trend of effective shrinkage in this case.
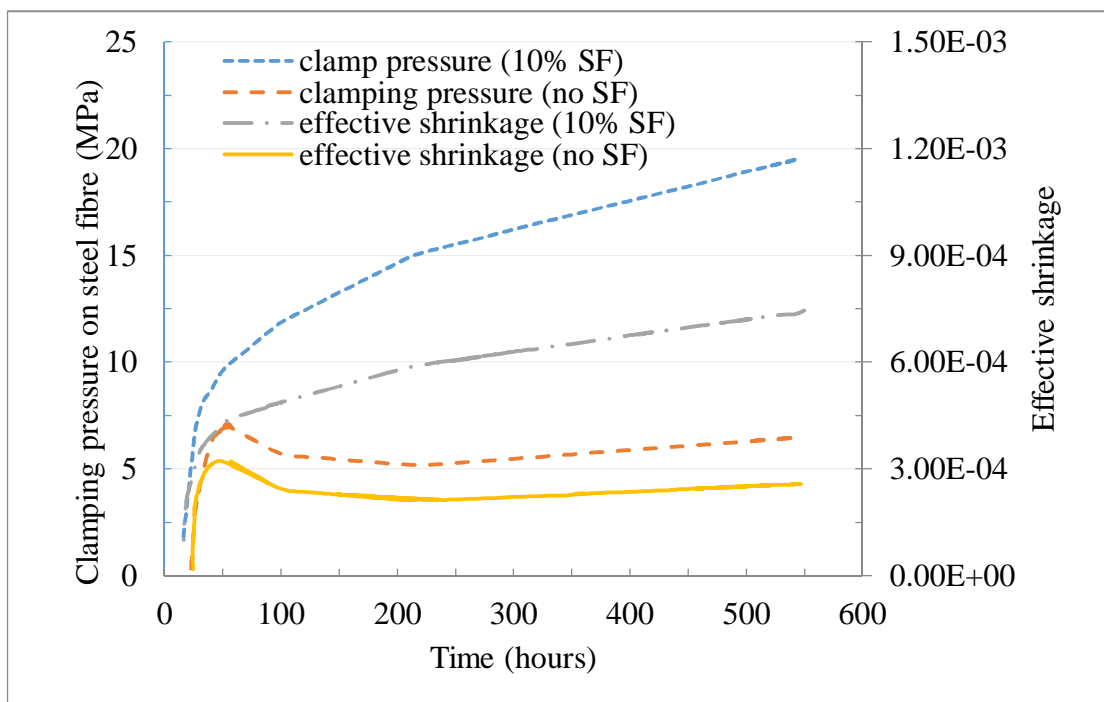
Figure 2-12: The effective shrinkage and corresponding clamping pressure on steel fibre for paste with and without SF (Stang, 1996:106).

Based on the test results from Stang (1996:106), the effect of SF on paste shrinkage can be observed. Even if SF in the paste increases its effective shrinkage, the clamping pressure is also increased correspondingly, which may be beneficial for steel fibre pull out resistance in UHPC.

26

2.5.2.   The effect of sand on steel fibre bond stress

The shrinkage of ultra-high performance paste (UHPP) is the driving mechanism of clamping pressure and thus increases the bond stress between steel fibre and UHPP. However, fine sand is also found to have a positive effect on the bond stress. Three types of fine sand of SS40, SS60 and SS80 were studied by Kang *et al*. (2013:1421). The particle diameter for SS40 ranges from 0.15 mm to 0.7 mm with the average particle size of 0.42 mm; the particle diameter for SS60 ranges from 0.1 mm to 0.3 mm with the average particle size of 0.22 mm and SS80 is the very fine micro silica with particle diameter less than 0.2 mm. The 0.3 mm in diameter and 30 mm in length smooth steel fibre was tested for concrete with W/C=0.35 and without SF. The equivalent bond stress calculated from Equation (2-1) is listed in Table 2-5.

$$\tau_{equ} = \frac{\mathbf{2}PE_{total}}{d_f L_{em}^2}$$
(2-1)

Where:

PE_{total}:   pull out energy until the fibre is completely pulled out;

d_f: equivalent diameter of the fibre;

L_{em}:   the embedded length of the fibre.

It can be seen from Table 2-5 that for the fixed sand to cement ratio, the equivalent bond stress increases when the sand particle size in mortar is finer. In addition, the increased sand content increases the pull out resistance of smooth steel fibre. Because the pull out mechanism governs the mechanical interaction between steel fibres and matrix, the sand particle size and content significantly affect the bond stress (Kang *et al*. 2013:1421).

Table 2-5: Equivalent bond stress for three type of sand under different S/C ratio (Kang *et al*. 2013:1421).

Sand to cement ratio	Sand type	Equivalent bond stress (MPa)
1	SS40	1.480
	SS60	2.441
	SS80	3.975
1.5	SS40	3.148
	SS60	3.696
	SS80	4.947

2.5.3. Effect of silica fume on bond stress

The incorporation of SF in concrete was found to increase the bond stress between matrix and steel fibres (Chan & Chu, 2004:1167, Stang, 1996:106, Wille & Naaman, 2013:451). The average bond stress is defined in Equation (2-2) and the corresponding bond stress is shown in Figure 2-13. It can be seen that the average bond stress continues to increase for contents from 0% to 30% of SF by cement weight and the bond stress increased approximately 14%. Further addition of SF above 30% will result in a reduction in bond stress. Also, the bond stress increasing rate is low when SF content is between 20% and 30%.

$$\tau_{max} = \frac{P_{max}}{n\pi d_f L_{Em}}$$
(2-2)

Where:

τ_{max}:   The average bond stress;

P_{max} :   Maximum pull out load;

n: Number of steel fibres in pull out cross-section;

28
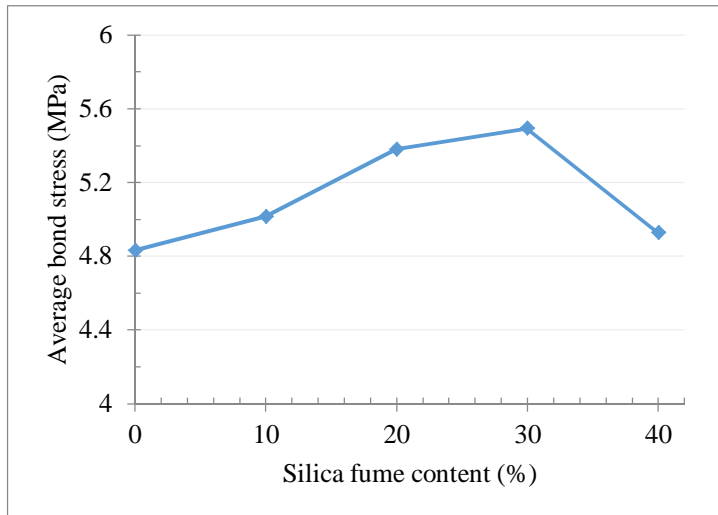
Figure 2-13: Effect of silica fume on bond stress for UHPC (Chan & Chu, 2004:1167).

2.5.4. Bond stress in UHPP, UHPM and UHPC

Knowing that UHPP can provide a high bond stress between steel fibre and matrix, the effect of sand and steel fibre on bond stress was studied through single fibre pull out tests by Wille and Naaman (2013). The bond stress of UHPP, UHPM and UHPC is compared with sand to cement ratio of 1.38 and 2.5% by volume of steel fibre under the same UHPP. It can be seen from Figure 2-14 that the pull out behaviour for UHPC and UHPM is similar and both of them have higher shear stress than that of UHPP. The increased bond stress further indicates that the sand does have a positive effect on bond stress.

The average bond stress based on Equation (2-2) for UHPP, UHPM (no steel fibre) and UHPC (contains steel fibre) result in the values of 5.5 MPa, 8.9 MPa and 8.5 MPa respectively. Only fine sand was used as aggregate in his mix. It does not seem that there is much difference in average bond stress between UHPM and UHPC. On the contrary, the average bond stress in UHPC is slightly lower than that of UHPM, which shows the 2.5% by volume of steel fibre in UHPC does not help to increase the bond stress. The higher bond stress was only achieved at a relatively larger slip as shown in Figure 2-14.

29
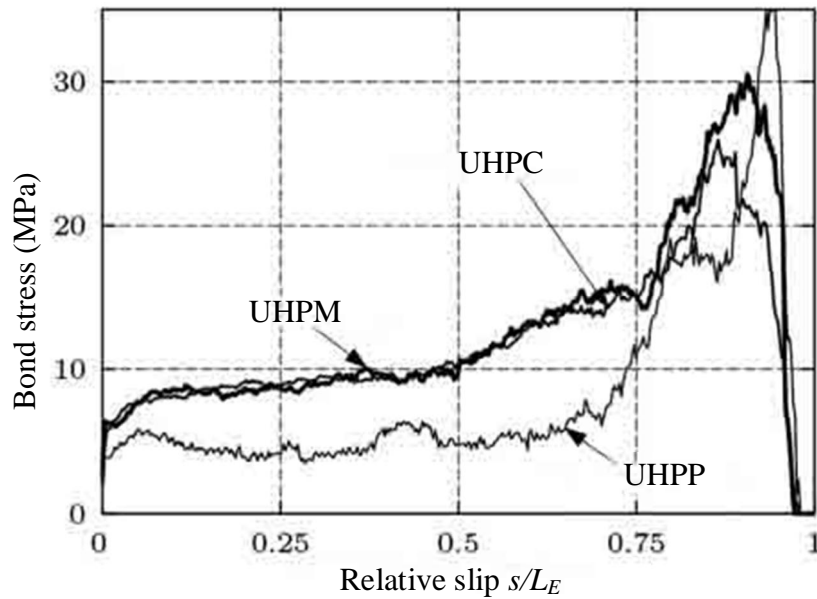
Figure 2-14: Influence of sand and fibre on pull out behaviour (Wille & Naaman, 2013:451).

2.6.   CONCLUDING REMARKS

This chapter shows that the general way for developing UHPC is through reduced W/C ratio and increased density of UHPC. The low W/C ratio and relatively high SF content cause high shrinkage, which may influence UHPC strength. By comparing various shrinkages, the autogenous shrinkage is found to be the major source of shrinkage for UHPC. High shrinkage can induce high clamping pressure to improve the bond stress between steel fibre and matrix and the bond stress of UHPP is much higher than that of high strength concrete. In addition, the sand and SF also help to further improve the bond stress between steel fibre and matrix. These mechanisms hold potential for an alternative philosophy in UHPC design, namely fibre pre-stressing by exploiting the high clamping pressure for fibre bridging of shrinkage-induced matrix cracking.

Chapter 3: Comparing local materials with typical materials used for UHPC

3.1. INTRODUCTION

Nowadays, most UHPC developers are choosing better constituent materials to achieve better UHPC performance. However, the local constituent materials are not that ideal as recommended by other researchers who successfully developed non-heat cured UHPC. This research focuses on the development of UHPC with utmost use of local available non-ideal materials and, therefore, a good understanding of the philosophy of developing UHPC is needed. This holds the potential that, if the UHPC could be developed under such conditions, significant improvement in its performance might be achieved with better materials in the future. In this section, the constituent materials used for this research are introduced and compared with other researchers who successfully developed UHPC under normal curing conditions. The essential constituents are cement, SF, SP, sand, 6.7 mm stone, steel fibre and water. Except for the steel fibre (which is imported), the other materials can be found in the local market.

3.2. CEMENT USED IN UHPC

Cement is the most important material in UHPC mix because the hydration of cement provides the fundamental way to achieve concrete strength. The strength and workability are two key parameters for cement used in UHPC. It is of common knowledge that a reduction in the W/C ratio can improve the concrete compressive strength. However, the reduction in W/C ratio under a certain value will reduce the paste workability, which potentially increases the porosity and thus lowers the concrete strength. Therefore, simply reducing W/C ratio under the critical value is one reason why the compressive strength cannot be further improved. UHPC requires a very low W/C ratio which confines the type of cement to be used. The Bogue result for cement was found to be one of the key parameters that affects the mix design of UHPC.

31

It is found that little C_3A content minimizes water demand (de Larrard, 1988) which in turn will affect the viscosity of the paste. In addition, the fitness also governs the viscosity of paste (Bonen & Sarkar, 1995). Sakai *et al.* (2008) state that the cement with less than 8 weight percentage of the C_3A content according to the Bogue analysis does not have a significant influence on the paste viscosity. As shown in Table 3-1, the cement used for this research is OPC in the form of CEM I 52.5N with 6.77% of C_3A content, which meets this requirement.

Besides the workability, the hydration of cement determines the paste strength. Therefore, researchers normally choose the cement with high C_3S and C_2S content. The typical C_3A, C_2S and C_3S in the content of cement used for UHPC by researchers, are compared and listed in Table 3-1.

It can be seen from Table 3-1 that the water cured UHPC which achieves a compressive strength over 150 MPa has a similar percentage of C_3A and C_3S in cement. The UHPC developed by Montreal has similar C_3S and C_2S content compared with the local CEM I 52.5N but contains much less C_3A content. The cement used in Toronto has similar C_3A and C_3S content with this research but contains less C_2S content. The UHPC in both Montreal and Toronto achieves the compressive strength of less than 130 MPa, i.e. significantly lower than that achieved by the same lead author Habel *et al.* (2008:217) of 168 MPa in an earlier work, which emphasizes the importance of cement in UHPC.

Habel *et al.* (2008) point out that most cements used in Europe contain approximately 4% of C_3A and 73% of C_3S which enable good workability and strength development. The worst workability was found for cement containing 7% of C_3A, which was discarded when UHPC was developed in Montreal. This finding differs from that of Sakai *et al.* (2008), who indicate that less than 8% of C_3A does not have significant influence on paste workability. The one local OPC used in this research, CEM I 52.5N, contains 6.77% of C_3A and was also found to cause a relatively low workability compared with the findings of Wille *et al.* (2011), which agrees with the finding by Habel *et al.* (2008). The detailed information will be provided in a

later chapter.

Table 3-1: Cement major chemical content and corresponding compressive strength for UHPC.

28 days Strength (MPa)	Cement weight % according to Bogue analysis			Reference
	C_3A	C_3S	C_2S	
164.9 (water curing)	4.11	67.23	14.50	France (de Larrard & Sedran, 1994:997)
168 (water curing)	4.00	73.40	10.00	(Habel *et al*. 2006:1362)
192 (without steel fibre) 201 (2.5% steel fibre)	5.00	74.30	14.10	U.S. (Wille, Naaman & Parra-Montesinos, 2011:46)
121 (water curing)	2.00	60.00	16.00	Montreal (Habel *et al*. 2008:217)
128 (water curing)	9.00	60.00	10.00	Toronto (Habel *et al*. 2008:217)
168 (water curing)	6.77	61.61	17.22	CEM I 52.5N in 2012; this research
136 (water curing)	6.70	59.20	19.00	CEM I 52.5N in 2013; this research
128.6 (without steel fibre)	7.26	59.00	19.00	CEM I 42.5N in 2011; this research

Two types of cements are used for this research which are CEM I 42.5N and CEM I 52.5N, while only the latter leads to sufficient compressive strength to be classified as UHPC. However, it was found that the CEMI 52.5N used in 2013 had a relatively lower C_3S content compared with the same type of cement used in 2012 according to the Bogue results as shown in Table 3-1. The relatively lower C_3S results in a reduction in UHPC strength of 136 MPa which will be elaborated on in Chapter 5 supported by laboratory test results that further indicate the importance of cement on UHPC strength as shown by other researchers.

The corresponding chemical composition and Bogue results of CEM I 42.5N and 52.5N in 2012 and 2013 are summarized in Appendix A which was provided by the local supplier. The CEM I 42.5N was used at the start of this research as the only OPC available locally, but CEM I 52.5N became available recently when the local supplier upgraded their products to include CEM I 52.5N.

3.3. SILICA FUME

SF normally has two functions in UHPC mix: one is its pozzolanic reaction, that further enhances the concrete strength, and the other is to act as a filler to fill the gap between cement particles.

From the chemical point of view, the chemical content of SF is of key importance. According to Park *et al*. (2008:105-112), 25% of SF by cement weight can improve UHPC strength by 23.5%. However, the UHPC strength appears to be insensitive to the type of SF (Habel *et al*. 2008:217, Wille *et al*. 2011:46).

From a physical point of view, the size of SF determines the grading, and thereby packing, of the paste. Wille *et al*. (2011) found that medium size of SF with specific surface area of 12.5 m^2/g has a better effect on the workability and compressive strength than the common SF with a specific surface area of 21.9 m^2/g. However, the UHPC developed by Wille *et al*. (2011) uses Glass Powder (GP) with particle size between that of cement and SF to improve the grading of the paste. The GP only acts as filler and does not involve any chemical reactions. Besides the quality of SF, the addition of GP further improves the grading and this may provide one reason why a higher spread value was achieved in their UHPP mix. For SF itself, Habel *et al*. (2008) showed that a relatively high specific surface area of SF of between 15-20 m^2/g which they used, caused a high water demand of UHPC and thus does not perform as good as the SF used in Europe with specific surface area of 12 m^2/g.

Based on the above analysis, it can be seen that the granular size of SF is the most important parameter for UHPC. The SF with specific surface area of approximately 12 m^2/g is the best option for the moment as discovered by those researchers who successfully developed UHPC. There is only one type of grey SF with a specific surface area of 23 ± 3 m^2/g and with a silica content of more than 92 percentage available in South Africa. In addition, the particle size of local SF is approximately 20 times finer than cement, whereas the granular size of SF used for

general UHPC is approximately one tenth of that of cement (Schrofl *et al*. 2012:1401). This is shown in a later section which explicates that the local SF has a significant influence on UHPC workability.

3.4. SUPERPLASTICIZER

Very low W/C ratio makes SP essential for UHPC to achieve the required good workability and spread. The SP used for UHPC is normally based on polycarboxylate ether containing different lengths of side chains (Schroefl *et al*. 2008:383).   The side chain density is the main mechanism of controlling the workability of the paste (Zingg *et al*. 2009:153). Due to the chemical reaction between SP and cement/SF, different types of SP are compatible with the corresponding cement and SF. The SP based on methacrylic acid ester polycarboxylate disperses cement better than SF, while the allylether based polycarboxylate disperses SF better than cement. Therefore, a blend of SPs that could both effectively disperse cement and SF is preferred in UHPC mix (Plank *et al*. 2009:5). In order to achieve a highly flowable paste, an effective dispersion of SF, and not cement, is necessary for SP (Plank *et al*. 2009:5).

The dosage of SP used for UHPC mix also contributes to the compressive strength. Different amounts of SP were compared and it was found that a lower percentage of SP leads to a reduced shrinkage rate which in turn may lead to a higher strength (Morin *et al*. 2001:63). Therefore, if the type of SP is not efficient enough to disperse cement and SF of paste, the addition of more SP might cause a higher shrinkage and result in a reduction in UHPC strength.

Although the theoretical role of the types of SPs matching the types of cement and SF were focused upon by researchers as discussed above, the side chain length and density are normally kept secret by chemical companies and no detailed information could be obtained in this research. For this reason, there are no simple chemical balance equations from which to derive the optimal dosage, but a systematic, empirical test program was followed to measure

spread values representing the workability of paste according to Artelt and Garcia (2008:633).

In this research, four types of SP were used, which are Chryso 310, Mapei Dynamon SP1, Sika Viscocrete 10 and Sika Viscocrete 20HE, all available in the local market. Based on the local cement and SF, Sika Visocrete 20HE exhibits the best performance in spread value results for the test mixes reported here.

3.5.   FINE AND COARSE AGGREGATE

3.5.1.   Aggregate particle size and shape

Better graded aggregates provide better packing density in concrete mix and reduce the cement content simultaneously. Such reduction in cement usage can make the concrete more economical and the inter-locking behaviour of aggregate may also improve the concrete performance. The compressive strength was found to decrease when the voids inside the matrix increase (de Larrard & Sedran, 1994:997) when the packing density of aggregate for UHPC was optimized. Therefore, besides the normal concrete, the packing density also influences performance of high strength concrete, which was proved by Aitcin and Neville (1993:21).

The paste for UHPC has stronger strength and larger shrinkage than those of normal concrete, and this leads to a change in mechanics during the failure of the concrete. Such effects influence the larger grain size aggregate in terms of compressive and tensile strength, due to stress concentrations caused by a relatively high shrinkage of paste, compared with normal strength concrete. In addition, when the inter-locking behaviour by aggregate cannot balance the bond between aggregate and paste, shear failures of aggregate tend to occur. Therefore, most researchers only choose fine sand as aggregate in UHPC under normal curing conditions. This is in agreement with de Larrard and Tondat (1993:505) who indicate that a small size aggregate leads to a higher strength in high strength concrete. The sands used by some

researchers, who successfully developed their UHPC under normal curing conditions, are listed in Table 3-2 below.

It can be seen from Table 3-2 that most of the researchers chose fine sand of grain size approximately between 0.2 and 0.8 mm. The sand from most researchers was supposed be obtained from their local suppliers but whether the sand is re-graded or not is not reported in their research. This research will only use the local available sand as aggregate instead of sieving and re-grading them.

Table 3-2: Types of sands used by some researchers for water cured UHPC.

Reference	Sands type and sizes
France (de Larrard & Sedran, 1994:997)	Three type of quartz sand S125, S250 and S400 are used. S125 range between 0.063 mm and 0.125 mm; S250 range between 0.1 mm and 0.25 mm; S400 range between 0.125 mm and 0.4 mm;
(Habel *et al*. 2006:1362)	Quartz sand with the maximum grain size of 0.5 mm.
U.S. (Wille *et al*. 2011:46)	Two types of fine silica sand with the maximum grain size of 0.2 mm and 0.8 mm respectively.
Montreal, (Habel *et al*. 2008:217)	Silica sand with the mean grain size of 0.25 mm.
Tonroto, (Habel *et al*. 2008:217)	Silica sand with the mean grain size of 0.2 mm.
U.S. (Graybeal, 2006)	Fine sand with grain size range between 0.15 mm and 0.6 mm.

Two types of natural sands, Philippi and Malmesbury that are commonly used in the Western Cape, South Africa, were chosen. The gradings of these sands are shown in Figure 3-1. Malmesbury sand is generally preferred for normal concrete due to its wider range in particle sizes. However, it contains particles larger than 2.4 mm while all Philippi sand particles pass through the 1.2 mm sieve.

In addition, Malmesbury #2 sand (arrived in July 2013) with the grain size much finer than that of Malmesbury #1 sand (arrived in March 2012) is also examined on UHPC strength even if the UHPC had already developed locally. Based on the local experience, the different

37

sand from different batches follows certain standards and it only slightly differs in its grading and particle size, which virtually has no effect on compressive strength of the normal concrete. But, the Malmesbury #2 sand is an exception. More percentage of fine particles can be found in Malmesbury #2 sand compared with that of Malmesbury #1 sand.

Besides the sand, the effect of small particle stone on UHPC was also observed by adding 6.7 mm Greywacke stone, the most commonly used aggregate from the local quarry in the Western Cape, with approximately 84% of them smaller than 6.7 mm.

Figure 3-1: The grading of three types of sands used in this research.

Besides the grading, the shape of the aggregate also contributes to the workability of concrete. For the similar grain sand, well-rounded smooth sands flow much better than the angular sand during the mixing procedure and lead to fewer voids in the UHPC performance. Therefore, well-rounded, smooth sand particles are better suited for UHPC. The overview of three types of sand is listed in Figure 3-2, with a clear view on the shape of sand at each grain size, with corresponding enlarged sand photos that were taken and listed in Table 3-3.

38
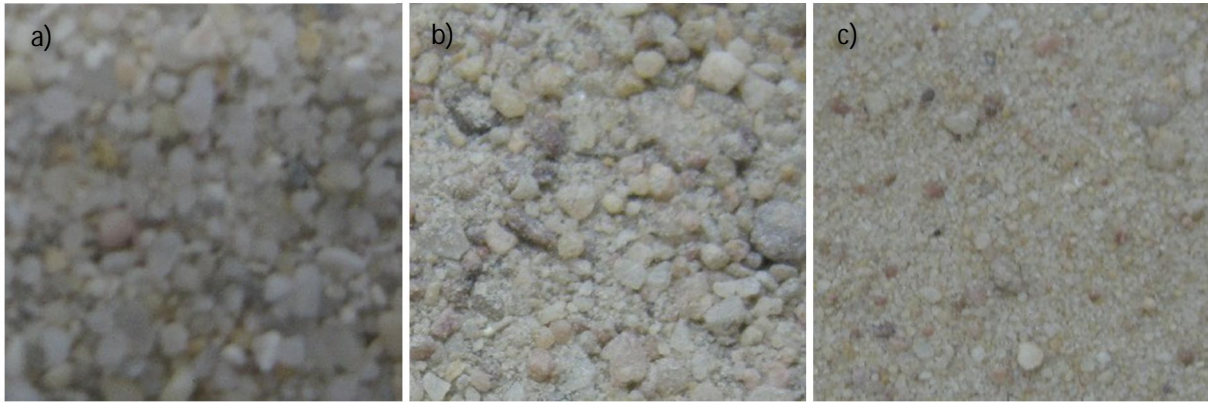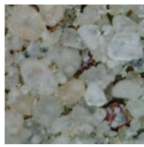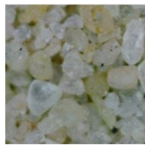
Figure 3-2: Photos of sands: (a) Phillipi; (b) Malmesbury #1; and (c) Malmesbury #2.

The shape for each size is shown in Table 3-3 with magnification up to a factor of about 200 for better observation. For the sand size smaller than 600 μm, the shape of Malmesbury #2 sand is similar to that of Phillipi sand and both of them have a better shape than that of Malmesbury #1 sand. Especially for very find sand with grain size smaller than 300 μm, Malmesbury #2 sand appears a more spherical shape than that of Phillipi sand and both of them appear to have a smoother surface than that of Malmesbury #1 sand. For the sand size larger than 600 μm, the shape of Malmesbury #2 sand is better than that of Malmesbury #1 sand, but worse than that of Phillipi sand.

For the sand content in UHPC, most researchers found that the optimized sand to cement ratio to be between 1.1 (Park *et al.* 2008:105-112) and 1.4 (Wille *et al.* 2012:309). The improved sand content can make UHPC more economical by making full use of the function of fine sand. When the local sand is applied, it was found that the increasing sand content causes a large reduction in workability and reduces the UHPC compressive strength. An optimized sand to cement ratio of 0.6 was found with local Malmesbury #1 which will be introduced in detail in Chapter 5.

Table 3-3: Particle shapes for three South African sand types.

Size (μm)		Phillipi		Malmesbury #1		Malmesbury #2	
Between		Photo	Magnitude	Photo	Magnitude	Photo	Magnitude
2360	4750				34		46
1180	2360				55		30
600	1180		35		42		35
300	600		173		176		138
150	300		181		184		168
75	150		195		195		197
<75			203		199		199

In addition, when Malmesbury #2 sand arrived, it was used in comparison with Malmesbury #1 because they are of the same regime sand but with different grain sizes and shapes. Under the fixed sand to cement ratio of 0.6 and the fixed other materials for UHPC, a significant improvement in UHPC compressive strength is obtained, indicating that a relatively easier way to improve UHPC strength is available through adjusting better quality sand.

3.5.2. The strength of aggregate

Besides the grading of the sand, the strength of the sand is also important. It can be noted from Table 3-2 that most of the researchers used strong silica sand or quartz sand as their aggregate. The aggregate is supposed to have a higher strength than the designated UHPC (de Larrard & Tondat, 1993:505). The shear failure of sand in UHPC can be observed with the tested specimen in this research as shown in Figure 3-3.

Clear images with a magnification of 30 were shown on the right side of Figure 3-3 to present a clear view of the compressive splitting/shear failure of sand in UHPC specimen. Through the compressive splitting/shear failure surface of UHPC specimen, the sand with different grain size is measured and marked on the right side of Figure 3-3.
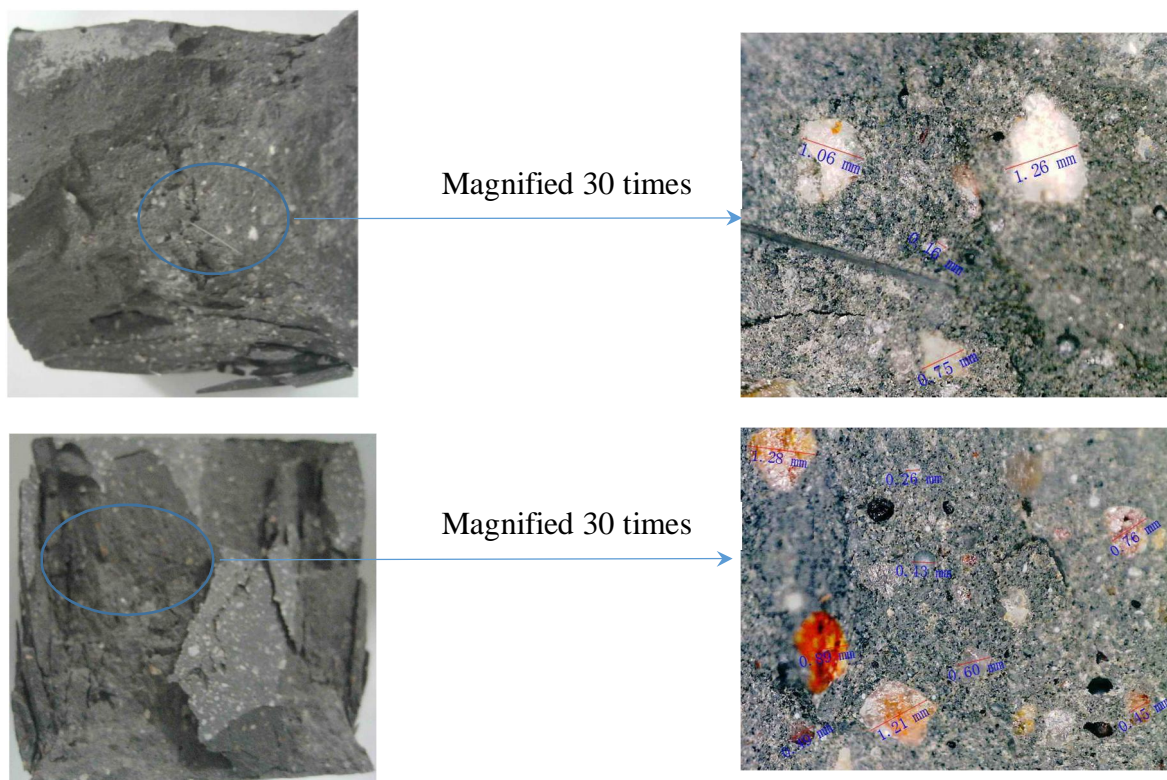
Figure 3-3: Shear failure of sand in UHPC specimens after compressive test.

The reason for compressive splitting/shear failure of sand can be attributed to the lack of strength of sand compared with that of paste according to Larrard and Tondat (1993:505).

41

Such a comment provides an indication why most researchers chose strong silica sand or quartz sand for UHPC. However, the compressive splitting/shear failure was also observed with the 6.7 mm Greywacke stone in this research. The strength of local 6.7 mm Greywacke stone can provide the strength of approximately 230 MPa which is much higher than the maximum UHPC strength achieved in this research of approximately 168 MPa. This is contradictory to the opinion of Larrard and Tondat (1993:505). Based on this phenomenon in this research, the opinion provided by Larrard and Tondat (1993:505) can only be partially true for the general UHPC with a relatively larger content of aggregate.

3.5.3. The effect of aggregate on shrinkage

Besides the above mentioned advantages, better graded aggregate enables larger sand content that lowers the paste content, which in turn reduces the overall shrinkage of UHPC. The aggregate has a positive confinement effect on the cement paste (de Larrard & Sedran, 1994:997) which indicates that the aggregates act as an internal restraint to reduce the shrinkage. Other researchers indicated that the better grading aggregate could reduce the volume of cement paste which could result in a lower chemical shrinkage (Esping, 2007, Holt, 2001). Such confinement of optimised aggregate provides a useful mechanism to reduce the overall shrinkage that helps to improve UHPC strength.

3.6. STEEL FIBRE

3.6.1. The property of steel fibre

Short high strength steel fibres are normally used in UHPC. Since no South African company manufactures high strength steel fibres yet, the steel fibres are imported. Bekaert straight steel fibre of 13 mm in length, 0.16 mm in diameter with a minimum tensile strength of 2600 MPa and brass coating is used in this research. Steel fibres used for UHPC by different researchers

are similar and are commonly used to improve the ductility of UHPC.

3.6.2. The effect of short straight steel fibres content on UHPC performance

Usually, steel fibres mainly improve concrete ductility. This is because only once the concrete cracks, the fibre is significantly stretched to develop resistance in bridging the crack. Therefore, the steel fibre has a limited effect on concrete crack strength, whether in (splitting) tension or compressive splitting.

The effects of steel fibre content on UHPC are different under various curing conditions. Park *et al*. (2008:105-112) found that a 2% volume of steel fibre results in a 13% improvement in compressive strength under heat curing conditions. For non-heat treated UHPC, an improved compressive strength of 6.7% is achieved with a 1.5% volume of steel fibres and an improved compressive strength of 9.8% is obtained with 2.5% steel fibres (Wille *et al*. 2012:309). It can be seen from work of other researchers that the effect of steel fibres on UHPC compressive strength is less significant under the normal curing conditions as that of the heat curing conditions. In addition, lower steel fibre content results in a lower improvement in compressive strength for UHPC.

3.6.3. The spacing and dispersion of steel fibres in UHPC

The dispersion and spacing of steel fibres will affect the tensile strength, especially the concrete post crack strength. In addition, the uniform distribution of steel fibre is quite important for UHPC to maintain a homogenous property. Furthermore, the spacing of the steel fibre also influences the tensile strength. A relatively higher volume of steel fibres that can be dispersed well in concrete will result in a closer spacing that leads to a higher first crack load of the matrix because the fibres reduce the matrix stress intensity factor (Edward & Nawy, 2008).

The effects of fibre dimension and content on fibre spacing were studied by several researchers, who also proposed formulae for fibre spacing. Among those formulae, the typical expression for continuous fibre is shown in Equation (3-1) (Romualdi & Mandel, 1964:657); the expression that considers the length of steel fibres is shown in Equation (3-2) (Mindess & Young, 1981) and the spacing for random oriented steel fibres in Equation (3-3) (McKee, 1969). Equation (3-3) was also accepted in European standard EN 14487-1 as a requirement for minimum dosage of steel fibres used in fibre reinforced concrete (FRC) to ensure minimum overlap between fibres.

Despite the fact that the fibre spacing expressions were originally used to evaluate the tensile behaviour of FRC, they might also be used as an indication to choose the maximum aggregate size (Markovic, 2006). However, the actual dispersion of fibres is more complicated and it is unlikely that fibres arrange in a complete regular grid as assumed by the formulae. The factors that affect fibre dispersion include: the confinement of formwork, fibre size and content, aggregate size, matrix viscosity, vibration, etc. Researchers are developing models that could better simulate the fibre dispersion but there are still substantial limitations. However, it is useful to consider theoretical steel fibre dispersion in the mix design.

$$S = 13.8d\sqrt{\frac{1}{V_f}}$$
(3-1)

$$S = 13.8d\,\frac{\sqrt{l_f}}{V_f}$$
(3-2)

$$S = \sqrt[3]{\frac{\pi d^2 l_f}{4V_f}}$$
(3-3)

Where:

S: Fibre spacing;

d: Fibre diameter;

V_f: Applied volume content of steel fibres in %;

44

Figure 3-4 shows the relationship between the volume percentage of steel fibres and fibre spacing as obtained from the above three expressions. The maximum aggregate size that better fits between steel fibres differs significantly when the steel fibres content is low and such variation narrows when the steel fibre content is high.

It can also be seen from Figure 3-4 that for Equation (3-3), the fibre spacing does not change that much with different percentage of steel fibres since the main focus for this expression is to guarantee enough overlap of steel fibres. The fibre spacing for Equation (3-2) becomes more constant after 3% of steel fibres, while for Equation (3-1), the fibre spacing reduces with the increased volume percentage of steel fibres and has a high decreasing rate when the steel fibre content is less than 3%.
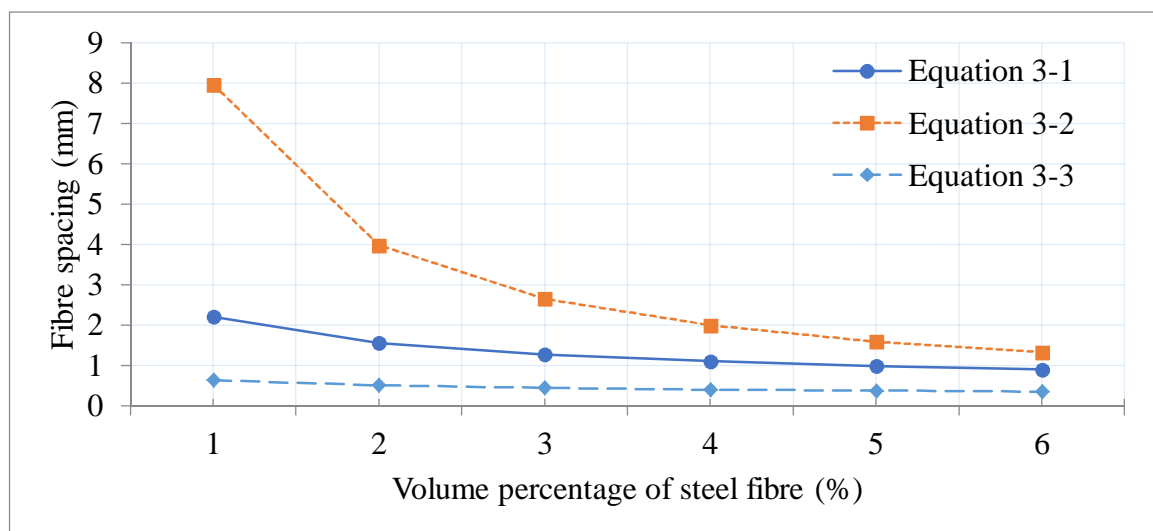
Figure 3-4: Fibre spacing corresponding to volume percentage of steel fibre.

In order to provide a good dispersion of steel fibres, the fibre length should be typically 2 to 4 times that of the maximum aggregate size (Grünewald, 2004). For Malmesbury sand, approximately 98% of the particles are smaller than 2.36 mm according to the sieve test as shown in Figure 3-1, which complies with the above fibre length requirement. In addition, based on Equation (3-2), a 1.5% volume of steel fibre corresponds to approximately 2 mm of maximum sand particle size. Besides the relationship between fibre spacing and maximum aggregate size, the fibre spacing should be lower than 0.45 l_f for a minimum overlap

45

according to EN 14487-1 and Equation (3-3). With 1.5% of steel fibres, the fibre spacing is approximately 0.56 mm as shown in Figure 3-4, which is smaller than 0.45 l_f (= 5.85 mm) and meets the requirement. When considering the 6.7 mm aggregate, the fibre length of 13 mm is approximately 2 times that of the stone size that meets the suggestion from Grünewald (2004). In addition, according to Equation (3-1), 1.5% of steel fibres volume corresponds to a fibre spacing of approximately 7 mm that meets the requirement of 6.7 mm Greywacke stone.

Beside the above considerations, the steel fibres are the most expensive constituent in UHPC mix and the tensile capacity of practical structural element can be enhanced through adding more reinforcements/pre-stressing tendons from the structural point of view. Mindess *et al.* (2002) also indicated that fibre reinforcement is generally not a substitute for conventional steel reinforcement. Therefore, the more economical and practical way of structural application of UHPC is to use minimum required steel fibre and incorporate this with reinforcements/pre-stressing tendons to obtain the maximum structural integrity.

Based on the above analysis, a 1.5 volume percentage of steel fibre was chosen in this research. In this way, a uniform dispersion of steel fibre is expected. By balancing the particle size and fibre spacing, this research aims to exploit good fibre packing as part of a tight skeleton, whereby paste shrinkage-induced anchorage may lead to significant fibre-enhanced compressive strength.

3.6.4.   The real steel fibre dispersion in UHPC

As can be seen in Figure 3-5 (a), the actual dispersion of steel fibres in fine aggregate FRC with 1.5 volume percentage of steel fibres in 150 mm cube specimens may be non-uniform, and thus not ideal as in the above mentioned equations. The settling of steel fibres is caused by the combined effects of steel fibre gravity, viscosity and vibration time (Głodkowska & Kobaka, 2013:645).

46

The phenomenon of steel fibre settlement was also observed with longer vibration times in this research. Figure 3-5 (b) shows the steel fibre dispersion in a 40 mm thick dumbbell shaped specimen with the vibration time of one minute, while Figure 3-5 (c) shows a 16 mm thick dumbbell shaped specimen with the vibration time of two minutes. It can be seen from Figure 3-5 (c) that with longer vibration time, the steel fibre settlement tends to occur. Moderate vibration may prevent steel fibre settlement as shown in Figure 3-5 (b), which indicates good dispersion of steel fibres in this research under such considerations.

Besides the fibre dispersion, voids in UHPC can be eliminated with longer vibration time. This can also be observed when comparing Figure 3-5 (b) and (c). The location of voids close to the top surface of the specimen in Figure 3-5 (c) indicates that longer vibration time does help to reduce the voids. Settlement of steel fibre should, however, be avoided in structural application.
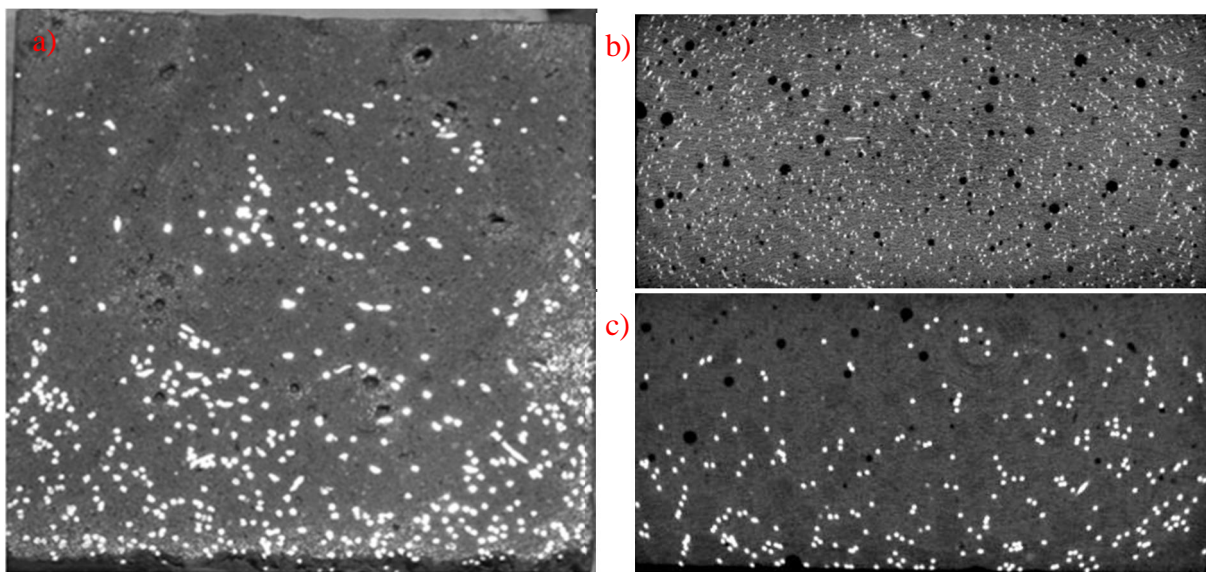
Figure 3-5: Steel fibre dispersion in (a) Fine aggregate concrete (Głodkowska & Kobaka, 2013:645); (b) 40 mm thick dumbbell shaped specimen with moderate vibration (this research); (c) 16 mm thick dumbbell shaped specimen with excessive vibration (this research).

3.7. SUMMARY OF THE MATERIAL USED IN THIS RESEARCH

It was described that non-ideal constituents for UHPC are available locally in South Africa

compared with what is available. Only steel fibres that are not locally available are imported. The quality of aggregate is comparatively easy to be improved. One merely needs more investment in the selection and careful grading to produce better aggregate. However, the chemical and mineral composition of cement is not that easy to be changed according to PPC, the local cement supplier. In addition, the SF with high specific ratio is not ideal to be used in UHPC due to the large surface area, or relatively fine particle size. All of these will bring a challenge to developing UHPC in South Africa. This demands clear understanding of the underlying principles, to successfully develop UHPC despite non-ideal ingredients.

Chapter 4: The Philosophy in developing UHPC

4.1. INTRODUCTION

In this Chapter, the philosophy for UHPC development with local materials is introduced. Even if all the materials could contribute to the ultimate UHPC strength, the ultra-high performance paste (UHPP) strength is the fundamental parameter to provide UHPC strength because the chemical reaction of UHPP is the main reason to obtain UHPC strength. This chapter will introduce the step development of UHPP, UHPM and UHPC development with local materials.

4.2. SPECIMEN PREPARATION AND TESTING

Due to the non-heat treated UHPC that is developed in this research, the specimens are prepared according to following procedure. When mixing of the UHPC is completed, the fresh UHPC is cast into the moulds and vibrated for one minute. The specimens are then covered with a plastic sheet and stored in the laboratory at room temperature for 48 hours, expect for one batch which was stored for 24 hours for comparison purpose as listed in Table 5-5. The specimens are then de-moulded and stored in a water tank with the temperature controlled to $23 \pm 2 \ ℃$ until the day of testing. On the day of compressive test, the specimens are taken out of the water tank for measurement 15 minutes before the test starts. The specimens are then tested in the Contest compressive materials testing machine in a surface dry state.

4.3. UHPC DEVELOPMENT PHILOSOPHY

The design philosophy in this research is based on the experience from other researchers and the analysis from local test results. Traditionally, concrete parameters such as creep and

shrinkage are only tested after a certain type of concrete has been developed and it is not realistic to measure such parameters beforehand. For UHPC, the shrinkage can only be measured after a reference UHPC mix design has been developed. The side effect of shrinkage plays an important role in UHPP strength, where the experience from other researchers provides key importance in UHPC development with local materials.

4.3.1. UHPP development

Followed by the mix design methods, an empirical UHPP approach was used. The first step was to reduce W/C ratio to improve the UHPP strength. However, it was found that further reduction of the W/C ratio could cause increased voids in UHPP and thus reduce UHPP strength (de Larrard & Sedran, 1994:997). Therefore, besides reducing the W/C ratio, the UHPP packing density should also be optimized. The UHPP slump flow is an efficient way to optimise the paste packing density and a value of 300 mm was recommended by Wille *et al*. (2011:46). The tests T8 and T9 as shown in Phase 1b of Table 5-1 shows the above mentioned mechanisms that, when the W/C is reduced from 0.22 to 0.2, the 28d UHPP strength reduces as well as the UHPP slump flow reduces from 320 mm to 290 mm. It is postulated that the low slump flow in T9 makes it difficult to get all the entrapped air out of the mixture, thus resulting in an increased porosity and a decreased UHPP strength in T9.

Even if the requirement of reduced W/C ratio and the maintenance of the slump flow of over 300 mm is satisfied at the same time, the local UHPP experienced strength reduction at the age of two weeks, which is not mentioned by other researchers. As elaborated in Section 3.2 and Section 3.3, the cement and SF are not as ideal as those that researchers selected, which lack sufficient UHPP strength increment. Followed by the general UHPC development theory and general concrete development knowledge, the reduction of UHPP strength after two weeks is generally regarded as poor mix design. Simply reducing W/C ratio can results in increased UHPP strength with time, but the 28 days UHPP strength is far from the designated strength. Therefore, unless a new mix design methods is developed, following the traditional

UHPC development methods is unlikely to achieve the designated UHPC strength with local materials. However, even if the UHPP strength reduction occurs after two weeks, the first two week UHPP strength increment rate is quite high as elaborated in Chapter 5, which is helpful for skeleton formation during the early age. The reason why UHPP strength reduction occurred with local materials needs to be understood before further adjustment in UHPC mix design can be made.

It can be postulated that the reduction in UHPP strength after two weeks is caused by a relatively high autogenous shrinkage for the following reasons. The autogenous shrinkage can be regarded as the major shrinkage for UHPC as elaborated in Section 2.4.4. According to Schachinger *et al*. (2002:1341-1354) and shown in Figure 2-11, there is a sudden drop of shrinkage on 14 days, which may lead to the strength reduction in UHPP afterwards. Especially the optimised UHPP with the W/C of 0.2 will result in a relatively larger autogenous shrinkage because it is much lower than that of 0.27 that Schachinger *et al*. (2002:1341-1354) tested. Because the UHPP met the requirement of slump flow larger than 300 mm, the reduction of UHPP strength cannot be the reason of improved voids in UHPP according to Larrard and Sedran (1994:997). It is of common knowledge that the UHPP strength continues to increase with hydration and pozzolanic reaction continues for water cured specimens. The reduction in UHPP strength can be caused by chemical reactions, but the appearance effect is crack formation due to internal strain gradients and exceedance of tensile strength. The following two cases can be postulated to explain such phenomenon:

● Case one: The improved shrinkage increment rate.

When considering UHPP to be homogeneous from macroscopic point of view, the sudden drop in autogenous shrinkage in 14 days will not be caused by differential stress inside UHPP. Instead, the improved shrinkage increment rate will cause stress concentration inside UHPP due to its sudden volume change. The autogenous shrinkage is caused by the hydration of cement and pozzolanic reaction of SF and the UHPP strength increases

51

with the increment of shrinkage. When the increased strength of UHPP cannot balance the stress caused by the autogenous shrinkage, such as a sudden drop of autogenous shrinkage in 14 days, internal differential stress or micro-cracks will occur, which leads to reduced UHPP strength.

- Case two: The differential stress in UHPP.

From the microscopic point of view, the UHPP includes cement and SF with different particle sizes. The hydration and pozzolanic reaction is heterogeneous along UHPP which will cause differential stress that causes weak spots or even micro-cracks when such differential stress is larger than the tensile resistance of UHPP that leads to a sudden drop in autogenous shrinkage in 14 days.

Each of the above two postulated cases or a combination of the two cases may explain the autogenous shrinkage jump in 14 days found by Schachinger *et al.* (2002:1341-1354), which can be regarded as the main reason for reduction in UHPP strength after two weeks in this research.

4.3.2. UHPM development

Even if Larrard and Sedran (1994:997) developed the Solid Suspension Model (SSM) and applied it for UHPC as elaborated in Section 2.2.3, it is generally applied to heat cured UHPC where the majority of shrinkage occurs before the moulded period. Wille *et al.* (2011:46), who developed the highest non-heat cured UHPM strength of 192 MPa for the moment, did not apply any packing model, but chose types of sand through empirical methods.

It is already recognized that optimised sand size and content do help to confine the UHPP shrinkage (de Larrard & Sedran, 1994:997). By increasing the sand packing density, the sand content in UHPM will increase; however, simply adding more sand content is not an efficient

way to reduce autogenous shrinkage for modern concrete such as high performance concrete (HPC) or self-compacting concrete (SCC), which have the characteristics of UHPC. For HPC, a high cement content and, therefore, high paste volume are needed to obtain HPC strength according to Kovler and Zhutovsky (2006:827). For SCC, a higher aggregate content leads to reduced paste content and the aggregate friction will block the paste flow and thus reduce the workability, especially for concrete with low W/C ratio (Soliman, 2011). Therefore, the sand and paste content need to be balanced for UHPM to provide enough workability and UHPM strength. Based on the UHPM strength and slump flow as elaborated in Chapter 5, the Malmesbury #1 sand to cement ratio of 0.6 is optimised for UHPM.

4.3.3. UHPC development

With the introduction of the shrinkage induced clamping pressure concept, as elaborated in Section 2.5.1, the optimised UHPP reduction in its strength after 14 days can be used for UHPC development based on the following two conditions: (a) The reduction of UHPP strength is postulated to be the high autogenous shrinkage in UHPP as elaborated in Section 4.2.1; and (b) Such optimised UHPP provide higher early age UHPP strength up to 14 days. The bond stress between steel fibre and UHPM improves gradually with the skeleton formation of UHPC as shown in Figure 4-1.

By following the iteration process in Figure 4-1, the skeleton starts to form based on two conditions. One condition is that when the bond strength is larger than the shrinkage of the matrix, the clamp enables the resistance between the interface of steel fibre and matrix from slipping. From this stage on, a contraction force is already applied to the steel fibre and will continue to increase its magnitude due to the increased shrinkage and clamping pressure in the matrix. The other condition is that when the hardened UHPP is strong enough to resist UHPP shrinkage, the hardened UHPP can form a skeleton to prevent UHPP from further shrinkage. When both conditions are met, the UHPC skeleton formed by sand, hardened UHPP and steel fibre is strong enough to resist further UHPC shrinkage through this strong skeleton. The start

53

of skeleton formation may only happen a few days after casting and the skeleton grows stronger with time.

```
┌─────────────────────────────────────────────────────────────────┐
│ The chemical reaction: cement hydration and/or silica fume pozzolanic reaction │
└─────────────────────────────────────────────────────────────────┘

┌──────────────────────────┐          ┌──────────────────────────┐
│ Increased UHPP strength   │          │ Increased UHPP shrinkage  │
└──────────────────────────┘          └──────────────────────────┘

┌──────────────┐ ┌──────────────────┐  ┌──────────────────────────┐
│ Hardened UHPP │ │ Sand and steel fibre │  │ Increased Clamping pressure │
└──────────────┘ └──────────────────┘  └──────────────────────────┘

        ┌──────────────────────────┐    ┌──────────────────────────┐
        │ Skeleton formed by Hardened │    │ Improved bond stress between │
        │ UHPP, Sand and steel fibre  │    │ steel fibre and matrix       │
        └──────────────────────────┘    └──────────────────────────┘
```
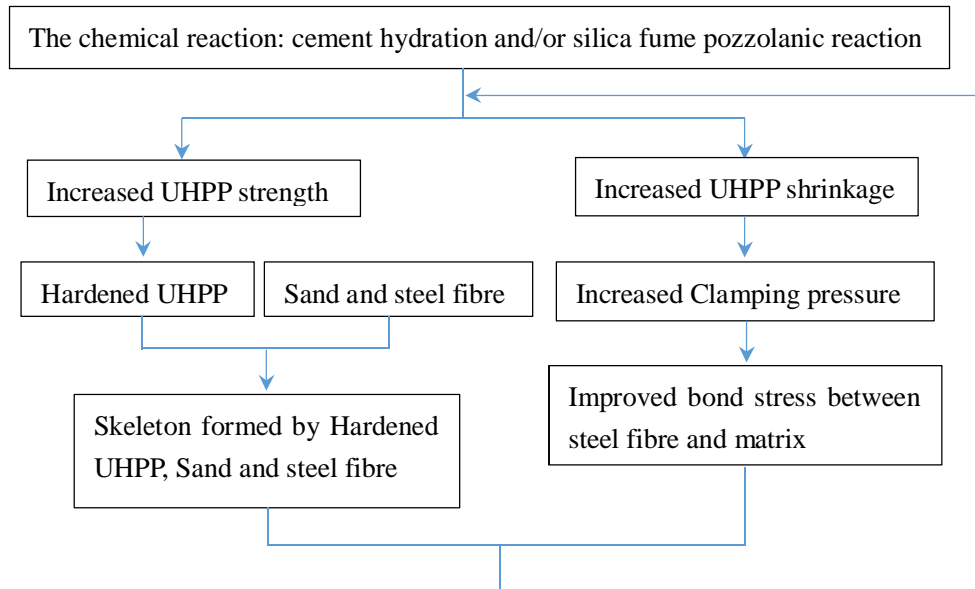
Figure 4-1: Skeleton formation procedure.

With a quick UHPP strength development up to 14 days, as was found in optimised UHPP as elaborated in Chapter 5, the skeleton becomes stronger and the pre-stressing force in steel fibre becomes larger. As mentioned in Section 3.6.3, the continuity of pre-stressing force in steel fibres is provided by enough overlap length which is easy to be met because most UHPCs incorporate approximately 2% of steel fibre. In addition, a uniform dispersion is required to provide a homogeneous UHPC property.

After 14 days, the UHPC strength can still increase even if the UHPP strength starts to decrease as found in this research. The reduction in UHPP strength after 14 days can be prevented by the combination of strong skeleton that formed up to 14 days, enough bond stress between steel fibres and matrix, adequate steel fibre lap length, and the bridging effect of steel fibres that are uniformly dispersed inside UHPC. As the hydration and pozzolanic reactions continue with time, the skeleton grows stronger and the steel fibres are able to effectively bridge micro-cracks that may develop in later days.

4.3.4. The comparison of volume change between UHPP, UHPM and UHPC

As elaborated in Section 2.4.5, a significant reduction in autogenous shrinkage in UHPM is obtained with higher sand content compared with that of UHPP. The low volume of steel fibre will not contribute to the autogenous shrinkage as shown in Figure 2-14, the similar bond stress between UHPM and UHPC according to Wille and Naaman (2013:451). The relationship of shrinkage between UHPP, UHPM and UHPC is depicted in Figure 4-2.

Based on the above mentioned mechanisms, a new strategy of UHPC mix design is developed. With the help of steel fibre, the quick development of UHPP strength in early days is of key importance to form a strong skeleton that can confine relatively large shrinkage in later days. Through following such mix design strategy, the optimised UHPP followed the spirit of such mix design method and a continuous development of strength UHPC is achieved with the help of steel fibres. Under the local non-ideal constituent materials, a UHPC compressive strength of 168 MPa is achieved on 28 days. Based on the local available sand, the optimised sand to cement ratio is only equal to 0.6, which is much lower than other researchers' findings. For higher sand content, such mix design strategy can theoretically be applied, but more limitations in sand property, such as shape and grading, may be required, which is ideal for future research.
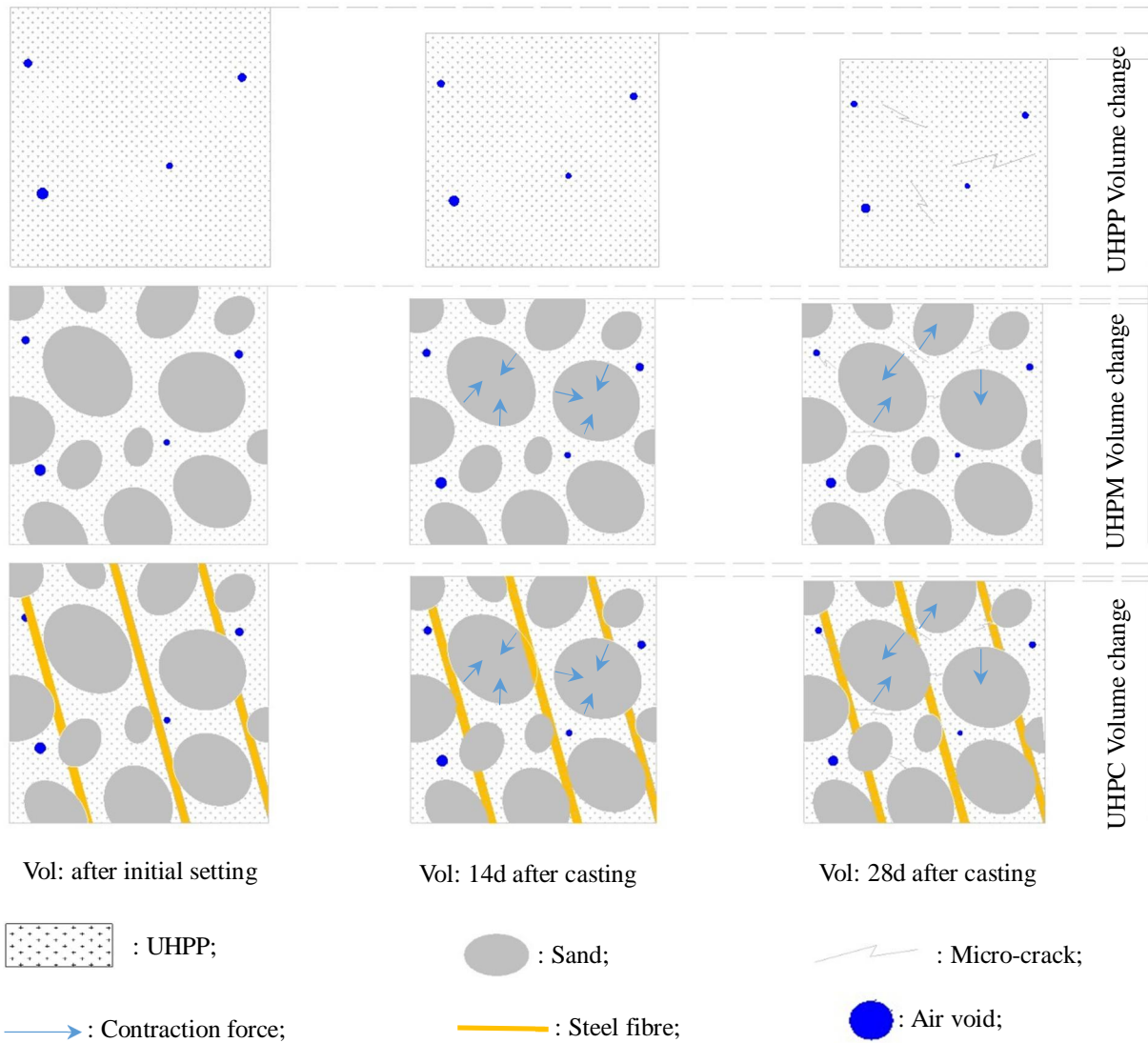
Figure 4-2: Skeleton development between UHPP, UHPM and UHPC

4.4. SUMMARY OF UHPC MIX DESIGN PHILOSOPHY IN THIS RESEARCH

This chapter introduces the main mechanisms that help to build the new mix design strategy in this research. Through the introduction of shrinkage induced clamping pressure, the steel fibre can bridge UHPM with adequate bond stress and lap length. With the increased UHPP shrinkage, the skeleton formed by sand, hardened UHPP and steel fibre grow stronger. The combination of this bridging effect and strong skeleton makes further reduction of W/C ratio in UHPP available where the relatively large shrinkage in later days can be balanced. In this way, the potential of steel fibre is used to further improve UHPC strength. In addition, one

56

advantage of such a mix design strategy is that the UHPC shrinkage in later days can be balanced by steel fibre and no special treatment to reduce shrinkage is needed, such as the addition of superabsorbent polymer (SAP) (Dudziak & Mechtcherine, 2008:425), or a shrinkage reducing admixture (SRA) (Soliman & Nehdi, 2014:81).

Chapter 5: UHPC development with local materials and factors that affect UHPC strength

5.1.   INTRODUCTION

When developing a new material locally, the option exists to import key ingredient materials. Alternatively, industrial processes during which ingredient materials are prepared, for instance sand and its grading, pozzolanic materials and their screening and grading, and even cement itself, must be changed. Both options may hold considerable cost implications, and could have been avoided, apart from using short high strength steel fibres. Fortunately in South Africa, where this UHPC material is developed through this project, cement that complies with European standards is used. However, differences in key ingredient materials such as condensed SF and sand, are of significance, and proved particularly challenging in developing UHPC locally. Even if local cement follows the European standards, the Bogue analysis shows that the local cement is less efficient for UHPC compared with the cement used by other researchers who have successfully developed UHPC.

The CEM I 42.5N was used at the start of this research as the only OPC available locally in the Western Cape Province (CEM I 52.5N was available elsewhere in South Africa, but it was decided not to make use of those), but CEM I 52.5N became available locally in 2012 when the local supplier upgraded their product. Through following the mix design philosophy, the test programs followed a UHPP, UHPM and UHPC design process and an iterative process could be acquired.

5.2.   MIXING AND TESTING EQUIPMENT AND PROCEDURES

Compressive strength of UHPC is generally regarded as the major characteristic of UHPC, while the tests for this stage are mainly focused on the compressive test. In addition, the slump flow was evaluated because slump flow is an efficient way to optimise the paste

packing density (Wille *et al*. 2011:46).

5.2.1. The mixing procedure

The mixing procedure for this research is similar to the other researchers but all the dry materials were mixed together. Unlike the mix procedure in U.S. (Wille *et al*. 2011:46) where the SF is mixed with sand first, then cement is added (and possibly GP afterwards), there is no difference in the property of local materials whether the dry materials are mixed together or if they are mixed separately. The mixing procedure is as follows:

Step 1: Mix the dry materials together at a low speed for approximately 5 minutes;

Step 2: Add water uniformly to the mixed dry materials;

Step 3: Add the SP and then mix at low speed for 1 minute, then mix at high speed for approximately 4 minutes, after which the mix starts to become liquid;

Step 4: Mix for another 5 minutes to achieve better dispersion and to make the mix more flowable;

Step 5: Add steel fibres slowly to avoid cluster of steel fibres;

Step 6: Mix for another 1 or 2 minutes to ensure the uniform dispersion of steel fibres;

Step 7: When the mixing is over, vibrate fresh UHPC with moulds for approximately 1 minute to accelerate some of the air bubbles out, directly after casting.

The addition of SP will affect the slump flow of UHPP. The step addition of SP as elaborated in Section 5.3.2.2 generally results in a higher slump flow than that of direct addition. In order to maintain consistency, most of the mix followed the direct addition of SP in this research. An exception was made in one batch of the test where the slump flow was difficult to obtain, which will be pointed out in the following sub-sections.

As introduced in Section 4.2, the specimens are covered with plastic sheet and stored in the laboratory at room temperature for 48 hours. The specimens were then de-moulded and stored

in a water tank with the temperature of 23 ± 2 ℃ until the day of testing. Only one batch that is listed in Table 5-5 was de-moulded 24 hours after casting for comparison purposes.

5.2.2. Type of mixer used for this research

Three types of mixer were used in this research, namely a three speed Hobart 10 L bowl mixer, 50 L pan mixer with and without a lid. The majority of tests were executed using the 10 L mixer. The characteristic of each mixer for UHPC can be summarized as follows:

●   Three speed 10 L bowl mixer

The advantage of this mixer is that it has three speeds. The lower speed can mix the dry constituents so that no materials, especially light powders, will fly out during this stage. The higher speed can provide enough mixing energy after the water and SP had been added.

The capacity of the 10 L bowl mixer is a problem, as only approximately 3 L of UHPC could be produced at one time. This is because the dry materials fill two thirds of the mixer before the mix starts. After the water, SP and steel fibre are added, the volume of mixed fresh UHPC only fills approximately one sixth of the mixer.

●   The 50 L pan mixer with lid

This mixer was used for a larger batch of UHPC mix for four point flexural test beam specimen preparation. The lid is supposed to maintain the dry material from flying out during the dry mix. However, the lid was not sealed properly and a small portion of the dry materials leaked out during the first 5 minutes of dry mix.

- The 50 L pan mixer without lid

Unlike some other researchers (Wille *et al*. 2011:46), the normal pan mixer cannot be used for UHPC because it only has one mixing speed which is too high to mix the dry constituents. Under such speed, the blade could flush out quite a substantial amount of dry materials during the dry mixing when this research started. Therefore, the 50 L pan mixer was only used for box beam casting because the pan is moveable. In this case, the dry materials were all mixed with the 10 L mixer, sealed into plastic bags and stored in steel bins to avoid any moisture absorption. The mixing procedure could be started from step 2 onwards and no problems were experienced.

5.2.3. The measuring methods and testing equipment

- The moulds for compressive test

This research started with 100 mm cubic moulds for the first batch of the test only. Then the 50 mm cubic moulds were used for the rest of the mixes as indicated by the other researchers. The 50 mm cubic moulds have two advantages. Firstly, enough specimens could be cast from the 3 L batch mixed in the 10 L mixer. The other is that, in a case where the UHPC strength achieved a higher value as that of Wille *et al*. (2011:46) of more than 200 MPa, the Contest machine of 2000 kN capacity could still be used.

- Compressive test machine and the corresponding loading rate

A contest compressive materials testing machine with the capacity of 2000 kN was used to test the compressive strength. The loading rate for the UHPP was chosen according to ASTM C109 where the recommended loading rate is between 54 kN/min and 108 kN/min. The average value of 81 kN/min was chosen in this research to keep a semi-static test environment. The same loading rate is selected for UHPM and UHPC

61

during developing UHPC.

- Slump flow test equipment and test methods

The equipment used to measure the spread value of UHPP is a cone according to ASTM C230/C230M without compacting. The equipment for UHPM is the flow table according to ASTM C1437.

The measurement of UHPP is different from that of UHPM. As for the UHPP, the cone was located on a flat steel plate and filled with fresh UHPP. The top surface of the cone was levelled after filling the UHPP and no leakage was allowed between the cone and the plate. Upon removing the cone, the UHPP flowed under gravity. Measurement of the flow diameter was taken after 1 minute. In order to minimize the error, four measurements were taken. The UHPM flow test followed ASTM C1437 procedures for layered filling of the cone and tamping, levelling the upper surface, removing the cone, dropping the table 25 times within 15 seconds and subsequently measuring the spread value.

- Measuring the materials during UHPP mix

Unlike cement and SF, when water and SP are added into the 10 L mixer, it is easy to add a few more drops because the liquid attached to the surface of the plastic column makes it hard to control, especially for SP which is more sticky and the overall volume is much less than that of water. The 7.5 kg scale with the precision of 0.1 gram was used and great care was taken for each mix to ensure more precise control.

5.2.4. The UHPC mix design

The typical mix design in this research is listed in Appendix B. By fixing the cement content, the rest of the ingredient materials are adjusted step by step and elaborated in the following

sub-sections.

5.3. UHPC DEVELOPMENT WITH CEM I 42.5N

5.3.1. Introduction

The design method entails three phases, namely:

Phase 1: Design of high strength, yet sufficiently flowable UHPP;

Phase 2: Addition of fine aggregate in order to form sufficiently strong, flowable UHPM;

Phase 3: Addition of suitable fibre and fibre volume to complement the skeleton in UHPC.

This is not included in Section 5.3, but will follow in Section 5.4.

An iterative process may be required. This may be to redefine the flowability and/or strength threshold for the preliminary optimised UHPP composition if incompatibility between the paste and fine aggregate leads to UHPM of insufficient flowability or compressive strength.

In addition to compressive strength, the slump flow of UHPP was evaluated with a recommended threshold value of 300 mm (Wille *et al*. 2011:46). The new set of tests was designed based on the previous test results either to improve UHPP strength or to verify the findings from other researcher. Through varying paste ingredients of cement (C), SF (SF) and SP dosage for optimised strength, the optimised UHPP was gradually built up. Subsequently the effect of sand (S) and fine particle aggregate (Agg) on UHPP was examined.

The Chryso 310 SP and CEM I 42.5N cement was used as the only type for this stage. The phases of design, together with detailed mix proportions, spread, average compressive strength (f_{cu}) and standard deviation (Std) results, are summarized in Table 5-1. The detailed information is listed in Table C1 in Appendix C. In the following sections, the steps towards deriving an UHPC mix using local materials but no heat curing are elaborated.

Table 5-1: UHPC phased design, showing Phase I-UHPP, Phase II-UHPM.

Step	Batch No.	SF/C	W/C	S/C ratio		6.7 mm Agg	SP		Slump flow (mm)	CEM I 42.5N			
				P	M #1		%	% s		Age	f_{cu} (MPa)	No.	Std (MPa)
1a.	T1	0.18	0.30				2.8	0.8	342	28	109.2	3	5.2
	T2	0.18	0.28				2.8	0.8	327	28	112.6	3	5.8
	T3	0.18	0.26				2.8	0.8	321	28	125.2	4	4.4
	T4	0.18	0.28				2.4	0.7	312	28	113.1	4	7.7
	T5	0.25	0.27				2.8	0.8	229	28	124.1	4	4.7
	T6	0.2	0.30				2.8	0.8	326	28	111.1	4	6.1
1b	T7	0.18	0.24				3.3	1.0	307	14	138.6	4	6.9
										28	107.5	4	8.5
	T8	0.18	0.22				5.5	1.7	320	14	143.93	4	2.4
										28	131.59	4	3.4
	T9	0.18	0.2				5.4	1.6	290	14	148.41	4	5.9
										28	130.6	4	6.7
2a	23	0.18	0.22	0.8			6.8	2.0	215				
				1			6.8	2.0	189				
				1.2			6.8	2.0	152				
	24	0.18	0.22	0.6	0.2		6.8	2.0	214				
				0.75	0.25		6.8	2.0	185				
				0.9	0.3		6.8	2.0	158				
	25	0.18	0.22	0.2	0.6		6.8	2.0	227				
				0.25	0.75		6.8	2.0	209				
				0.3	0.9		6.8	2.0	185				
	26	0.18	0.22		0.8		6.8	2.0	235				
					1		6.8	2.0	220				
					1.2		6.8	2.0	198				
2b	T10	0.18	0.22		0.8		6.8	2.0	225	28	119.5	3	3.5
	T11	0.18	0.22		1.2		6.8	2.0	190	28	117.2	3	2.2
	T12	0.18	0.22	0.2	0.6		6.8	2.0	228	28	116.1	3	9.2
	T13	0.18	0.22	0.8			6.8	2.0	216	28	119.4	3	2.6
2c	T14	0.18	0.22				6.0	1.8	253	28	65.3	2	0.4
	T15	0.18	0.22		0.6		6.0	1.8	212	28	76.1	3	11.5
	T16	0.18	0.22		0.4		6.0	1.8	239	28	85.2	3	6.5
	T17	0.18	0.22		0.2		6.0	1.8	252	28	98.9	3	5.1
2d	T18	0.18	0.22		0.6		6.0	1.8	273	28	128.6	2	5.9
	T19	0.18	0.22		0.6	12	6.0	1.8		28	118.9	3	4.2
	T20	0.18	0.22		0.6	4	6.0	1.8		28	115.4	3	4.9
	T21	0.18	0.22		0.6	20.8	6.0	1.8		28	112.0	3	12.6

5.3.2. Phase 1 – Optimization of the UHPP

Since the UHPP provides the chemical reaction that governs the compressive strength of

UHPC, the mix design starts with the UHPP mix design, based on the established design guidelines of ingredient materials with desired physical and chemical characteristics and proportions elaborated in previous chapters.

5.3.2.1. Phase 1a: Role of W/C ratio and SF/C dosage

This is the only batch that used 100 mm cubic specimens. It was recommended that the optimised dry content for SP between 0.5% and 0.9% of cement by weight and the spread value between 300 mm and 350 mm would give the best results (Wille *et al*. 2011:46). In addition, the recommended SF content is between 25% and 30% of cement by weight. Therefore, the majority mixes of this batch had a slump flow of more than 300 mm. When SF content is selected to be 25% of cement by weight, a significant drop in slum flow can be observed in T5.

The role of W/C and SF/C on UHPP compressive strength is shown in Figure 5-1. The following characteristics can be observed with the changing in paste ingredient:

- The W/C ratio: T1, T2 and T3

  When the W/C ratio is reduced, the compressive strength increases. Through a comparison of three tests, T3 presents a continuous development of strength with time. This indicates that the improved UHPP strength is larger than the side effect of shrinkage and causes a continuous improvement in strength when W/C ratio is reduced from 0.30 to 0.26. Therefore, through increased cement content in UHPP by further reducing W/C ratio, the strength could be improved. Following this trend, further reduction of the W/C ratio in UHPP would lead to a high strength.

- SF/C content: T1 and T6

When the SF content was increased, the compressive strength increased. This supported the finding from other researchers that the UHPP strength improves with more SF content (Detwiler & Mehta, 1989:609).

- SP dosage: T2 and T4

The slump flow for both T2 and T4 was larger than the threshold of 300 mm and less SP dosage lead to a slightly higher compressive strength in 28 days. However, the compressive strength in 21 days is much higher for higher dosage of SP with higher slump flow.

Two mechanisms contributed to the strength development in T2 and T4. One is that the higher SP dosage caused a higher slump flow which indicates a higher packing density of UHPP, resulting in a higher strength. The other is that higher SP dosage caused a higher shrinkage that reduced the UHPP strength (Morin *et al.* 2001:63). The test results represented a combination of these two mechanisms and indicated that a high shrinkage occurred between 21 days and 28 days in T2.

- Higher SF/C content and lower W/C: T5 and T6

Compared with T6, T5 with higher SF content and lower W/C ratio lead to a significant reduction in slump flow with the same SP dosage. However, the strength development in T5 obtained a continuous strength increase up to 28 days while T6 experienced a slight strength reduction between 21 days and 28 days. This indicates that slump flow is only an indication for UHPP packing density, which represents the UHPP strength, but not necessarily determines UHPP strength. The combination of increased strength due to chemical reaction, and reduced strength due to shrinkage, together with the UHPP

66

packing will determine the real UHPP strength.

Among this batch of tests, the highest UHPP strength was found in T3 and T5 as shown in Figure 5-1. Based on the analysis above, two ways may further improve UHPP strength.

- Way One: Further reduction of W/C ratio

Further increase of cement content in UHPP is an efficient way to improve strength. The slump flow of T3 achieved a value of 321 mm which is much larger than the threshold value of 300 mm that makes further reduction in W/C ratio a possibility. However, further improved cement content will cause higher shrinkage which may cause strength reduction in later days.

- Way Two: Increase SF content

According to Park *et al.* (2008:105-112) as shown in Figure 2-1, for SF/C ratios less than 0.25, the UHPC strength increases with the increased SF content. Therefore, increasing the SF content within the above limited range would further improve UHPP strength, which is mainly caused by the pozzolanic reaction of SF according to Detwiler and Mehta (1989:609) as introduced in Section 2.2.5. Compared with T3, T5 has a higher W/C ratio but still presents higher strength evolvement in UHPP in this batch of tests, which further shows the effect of SF content on UHPC strength mentioned by Park *et al.* (2008:105-112). But the poor slump flow caused by the increased SF content makes it difficult to further adjust the mix design in this respect.
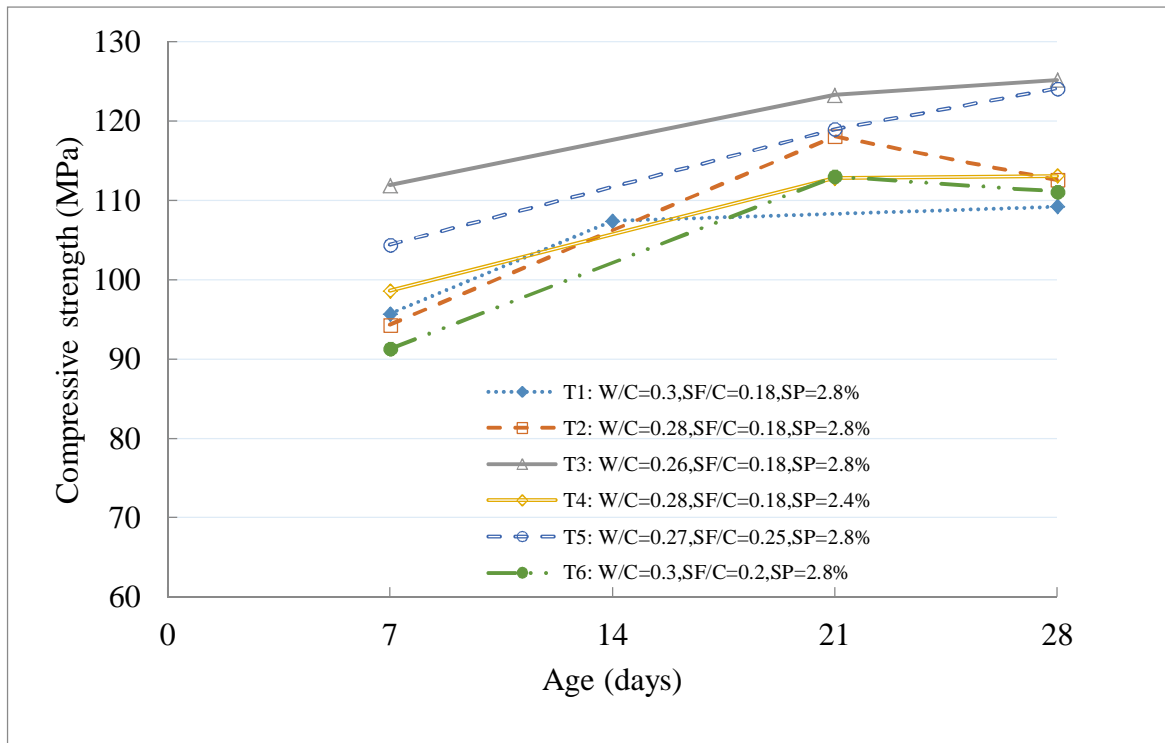
Figure 5-1: The compressive strength from T1 to T6 until 28 days.

Decisions should be made regarding which way to follow. It can be seen that the highest 28 days strength of 125.2 MPa (in T3) is far from the designated strength. In addition, the effect of sand on compressive strength still needed to be determined and whether the local sand could improve UHPM strength was unknown because it is not as ideal as the other researchers. On the other hand, the cement content in UHPP in T3 (W/C=0.26) is lower than those researchers (W/C=0.2) who successfully developed non-heat treated UHPC. The cement they used could provide much higher strength than local cement because of their higher C_3S and C_2S content. Therefore, the higher W/C ratio in T3 was unlikely to achieve the designated UHPM strength even if the same quality sands as other researchers were used. Further optimisation was required through increased cement content in UHPP by reducing W/C ratio.

Besides the above analysis and decision making, it was evident that the UHPP strength development with time could better represent UHPP property and the mechanisms in UHPP. The conventional way of only testing 28 days strength resulted in a lack of enough data to obtain the mechanisms, especially because there was no reference data available locally. Therefore, the following tests would track the strength on 7, 14, 21 and 28 days to obtain a

clear strength development in UHPP, UHPM and UHPC. Except for the 100 mm cubic specimens which were used for this batch, the rest of the tests only used 50 mm cubic specimens.

5.3.2.2. Phase 1b: Role of further reduction of W/C ratio on UHPP strength

Further reduction of the W/C ratio requires more SP dosage to disperse dry materials. However, different way of adding SP would cause the changing in UHPP slump flow. Step addition of SP, i.e. applying for instance half dosage at a time with continued mixing of several minutes in-between, can improve the slump flow compared with direct addition of SP (Tue *et al*. 2008:93). Such phenomenon was experienced in this set of tests, i.e. for T8, a much lower slump flow of 209.5 mm was achieved by direct addition method, while finally achieving a slump flow of 290 mm through step addition of SP. Step addition was used only in this batch from T7 to T9 to achieve a higher slump flow as shown in Table 5-1.

Further reduction in the W/C ratio of 0.18 was examined in one trial mix. Even with the step addition of SP, the slump flow only reached approximately 270 mm and could not be improved any further, indicating that further reduction of W/C ratio is not realistic under current conditions.

The role of W/C on UHPP compressive strength is shown in Figure 5-2. It can be seen that further reduction of W/C ratio will further improve the UHPP strength, which follows the indication from Phase 1a. The characteristics of this batch are as follows:

● Overall strength development: T7, T8 and T9

Further increased cement content in UHPP by reduction of W/C ratio resulted in a significant UHPP strength improvement between 7 and 14 days, but a large reduction in UHPP strength was found on 21 and 28 days. No literature could be found to explain the

69

reason for such reduction in UHPP strength. The most probable reason is due to a higher shrinkage in the later days because the strength increases by hydration over a period of time. The shrinkage was not measured in this research although it is normally measured after UHPC has developed, instead of during the developing stage. According to Schachinger *et al.* (2002:1341-1354) as shown in Figure 2-11 (b), there is a jump in shrinkage for UHPP on 14 days which may contribute to the reduction in strength of UHPP after 14 days.

The large shrinkage is mainly caused by a) increased cement content, and b) the higher SP dosage. After that, slight improvement in strength was found in T8 and T9 while T7 shows a slight reduction in its strength on 28 days. The point is that the UHPP strength reduction in later days is found in this batch, which differs from the traditional UHPP development without any strength reduction.

- The effect of slump flow on UHPP strength: T8 and T9

The strength development in T8 and T9 is similar, indicating further reduction of W/C from 0.22 to 0.2 does not have a significant improvement in UHPP strength. In addition, a slightly higher 28 days strength is achieved with W/C=0.22 in T8. With similar SP dosage, the slump flow in T9 of 290 mm indicates a lower UHPP packing density compared with 320 mm in T8. This phenomenon indicates that a lower packing density may increase the porosity in UHPP and lead to a reduction in strength even if with reduced W/C ratio (de Larrard, Sedran 1994).

- The threshold of slump flow: T7 and T8

When comparing the strength development between T7 and T8, it can be seen that a reduction in the W/C ratio from 0.24 to 0.22 while the slump flow of over 300 mm remains unchanged, results in a large improvement in UHPP strength. A further reduction

of W/C that leads to a slump flow of less than 300 mm did not improve UHPP strength. This phenomenon supports the postulation of Wille *et al.* (2011:46) that a slump flow of 300 mm can be regarded as a threshold to indicate a reasonable packing density of UHPP.
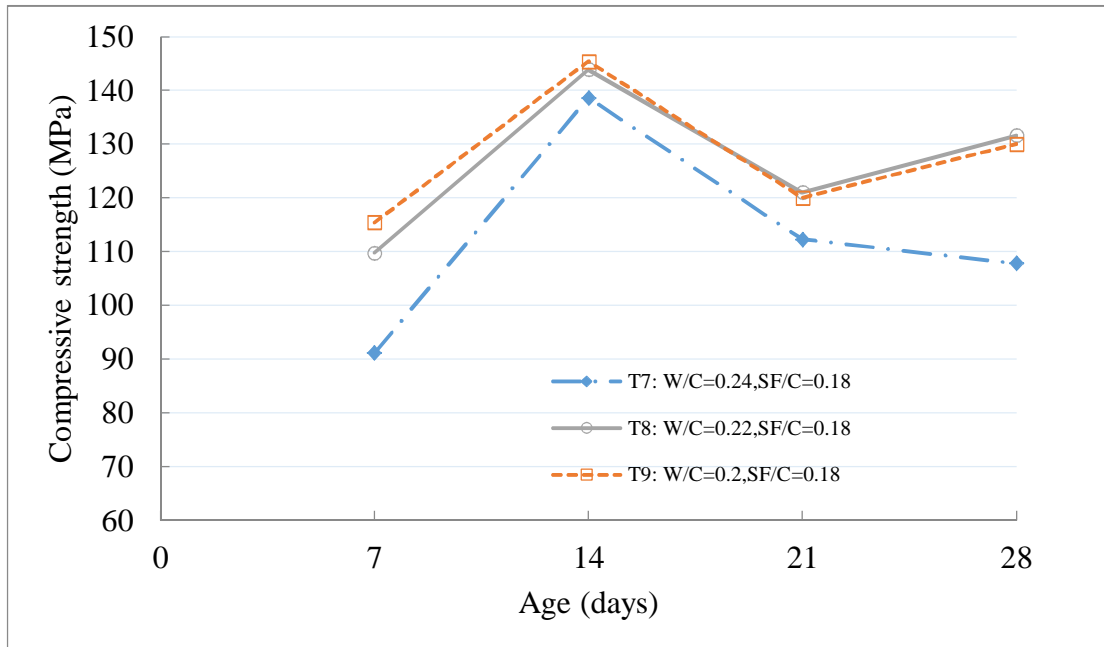
Figure 5-2: The compressive strength from T7 to T9 until 28 days.

Up to this stage, further improvement of UHPP strength based on the local materials is impossible. The Phase 1b already used step addition of SP to ensure higher slump flow with limited SP content, leading to a relatively lower shrinkage in later days, but still a big drop in UHPP strength was found between 14 and 21 days. Even if the strength fluctuated with time, the 28 days strength of 131.6 MPa (in T8) was still higher than that of 125.2 MPa (in T3) with continuous strength development – see Table 5-1. The addition of aggregate has a confining effect on UHPP and may lead to an increased UHPM strength. The best UHPP performance in test T8 is regarded as a reference UHPP up to this stage and used to further examine the effect of aggregate on UHPM strength.

5.3.3.   Phase 2 – Optimization of the UHPM

Once the UHPP was optimised, two types of local natural sand, Phillipi sand and

Malmesbury #1 sand, was used to optimise UHPM with the property introduced in Chapter 3. To limit the number of tests, slump flow is only considered in a first step, followed by a limited number of compression strength tests in a next step.

5.3.3.1. Phase 2a: Comparison of the two types of sands and their combinations on slump flow

For the fixed UHPP, the effect of sand on slump flow was measured through replacing Phillipi sand with Malmesbury #1 sand under various ratios and is shown in Figure 5-3. Two characteristics can be observed from this batch. One is the slump flow increases with the reduced S/C ratio, indicating the larger sand content causes more aggregate friction that blocks the paste flow and thus reduces the workability (Soliman, 2011). The other is that a slightly higher slump flow can be obtained through replacing more Phillipi sand with Malmesbury #1 sand under the same S/C ratio. Compared with Phillipi sand, Malmesbury #1 sand causes a slightly higher UHPM slump flow because it contains a wider range in particle sizes even if the particles are coarser and the shape is relatively angular.
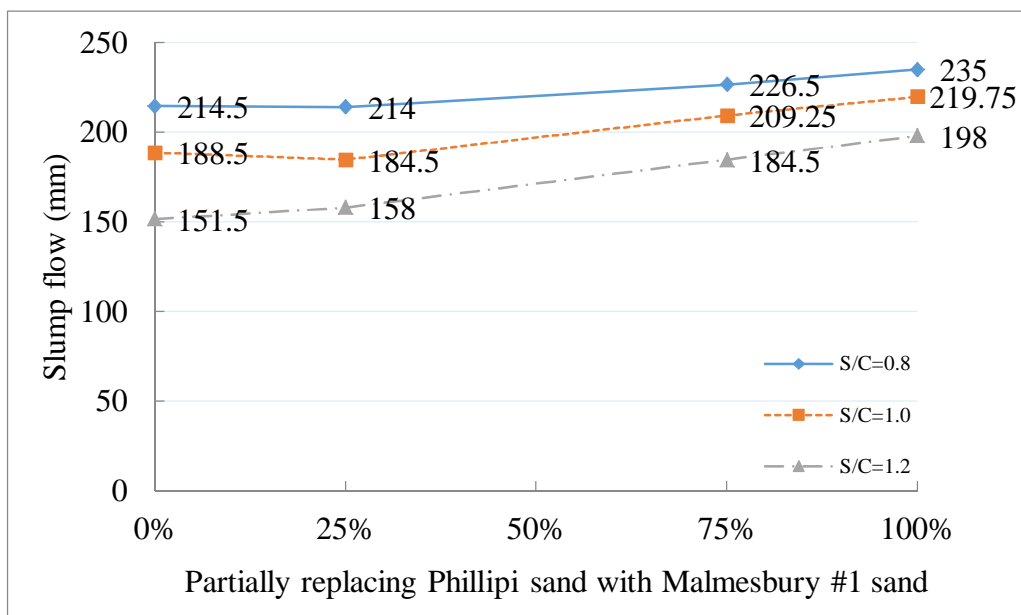
Figure 5-3: Influence of amount of Phillipi sand and Malmesbury #1 sand on slump flow.

However, the UHPM slump flow did not increase with the combination of two sands, indicating the combination of sand will not provide higher sand packing than Malmesbury #1 sand itself. This confirms that there is not much that can be done purely based on the local natural sands as the other researcher did, unless sieving and re-grading them, which may lead to ongoing research. Because S/C=0.8 gives the highest slump flow in this batch, three tests were chosen for UHPM with 0%, 75% and 100% of Phillipi sand replaced by Malmesbury #1 sand, so that the contribution of two local sand as well as sand combination on UHPM strength could be compared. Another test chose S/C=1.2 for UHPM with Malmesbury #1 sand to compare whether the higher amount of sand could improve UHPM strength. Therefore, four typical tests were chosen as shown in Table 5-1, Phase 2b for the next step.

5.3.3.2. Phase 2b: Effect of sand combination on UHPM strength

The strength for the selected four tests for Phase 2b is shown in Figure 5-4 with corresponding data in Table 5-1. The influence of sand combination and sand content on UHPM strength is compared. For the higher sand content of S/C=1.2, a significant reduction in slump flow as well as the strength can be found. As for S/C =0.8, the UHPM strength development is similar and the highest 28 days strength achieved in T10 of 119.5 MPa (Malmesbury #1 sand), with a slight reduction of 119.4 MPa in T13 (Phillipi sand).

There is a slight benefit that could be seen in Figure 5-4 when using the finer Phillipi sand rather than Malmesbury #1 sand because the 21 days UHPM strength with Phillipi sand is higher, which may be exploited in UHPC once the steel fibre is added to prevent later strength reduction as described in Chapter 4. Because further improvement in sand quality is recommended according to phase 2a, the Malmesbury #1 sand was chosen in this research for further tests based on two reasons: a) a higher slump flow, and b) a slightly higher 28 days UHPM strength because 28 days UHPM strength is generally regarded as standard strength.
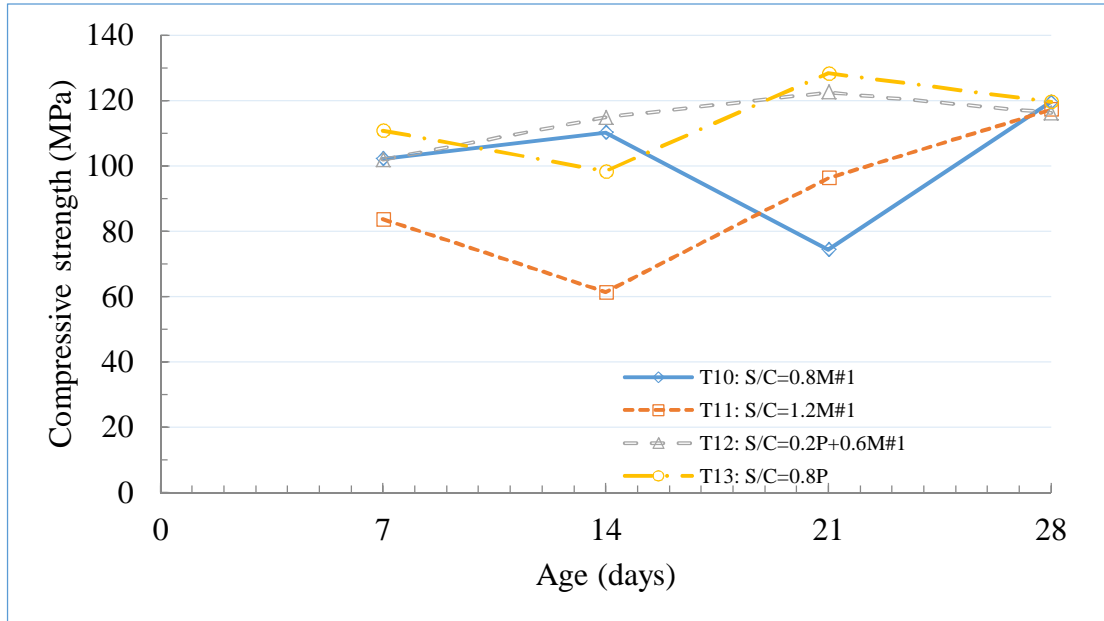
Figure 5-4: Influence of sand on UHPM strength: T10 to T13.

5.3.3.3. Phase 2c: Effect of sand combination on UHPM strength

There is nearly no improvement in UHPM strength with the incorporation of sand from Phase 2b. Further reduction of the S/C content will be examined in this batch. In addition, the UHPP strength is tested through the direct addition of SP.

The slump flow as well as the compressive strength of Phase 2c is listed in Table 5-1 and the strength development is shown in Figure 5-5. The erratic development of strength is mainly caused by: a) the lack of UHPP strength, poor dispersion of sand due to its smaller content; b) high dosage of SP caused higher shrinkage. Under the same UHPP mix, the slump flow of 252 mm (in T14), which is much lower than that of 290 mm (in T8), further indicates the direct addition as opposed to step-wise addition of SP leads to much less workability, which in-turn results in a lower strength.

74
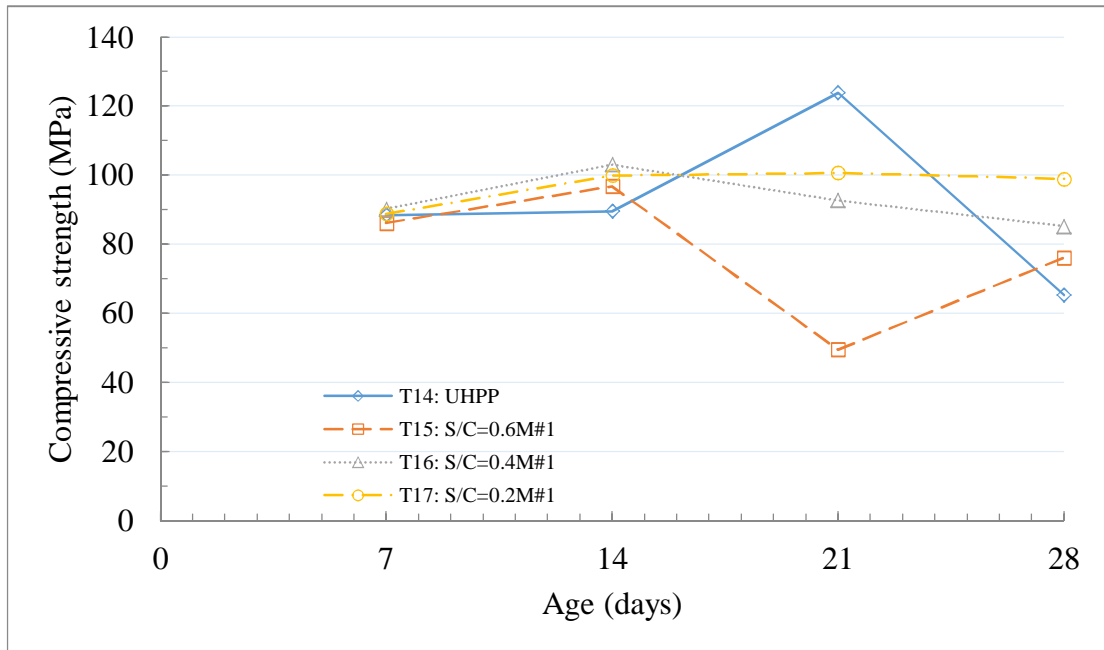
Figure 5-5: Effect of Malmesbury #1 sand on UHPM strength: T14 to T17.

5.3.3.4. Phase 2d: Effect of 6.7 mm aggregate on UHPM strength

Various volumes of 6.7 mm Greywacke stone is examined as listed in Table 5-1 and the strength development is shown in Figure 5-6. It can be seen from Table 5-1 that a reduction in SP/C by weight from 6.8% to 6% in UHPP, a higher slump flow of 273 mm (in T18) is achieved compared with that of 252 mm (in T14), which indicates that the slump flow cannot simply be improved by adding more dosage SP by the direct addition method. The strength development in T18 is much higher due to its higher slump flow and relatively lower SP dosage which both reflect a higher packing and reduced shrinkage of the matrix.

It can be seen from Figure 5-6 that the UHPM incorporating aggregate, results in a large strength reduction, which indicates why the aggregate is generally not recommended for UHPC mix under non-heat curing conditions. For the aggregate content, 12% by volume aggregate provides a higher 28 days strength than the other two. Therefore, through balancing the higher shrinkage and inter-locking behaviour of 6.7 mm aggregate, a 12% by volume aggregate leads to a relatively higher strength although still lower than that of UHPM (which only used sand as aggregate).

75
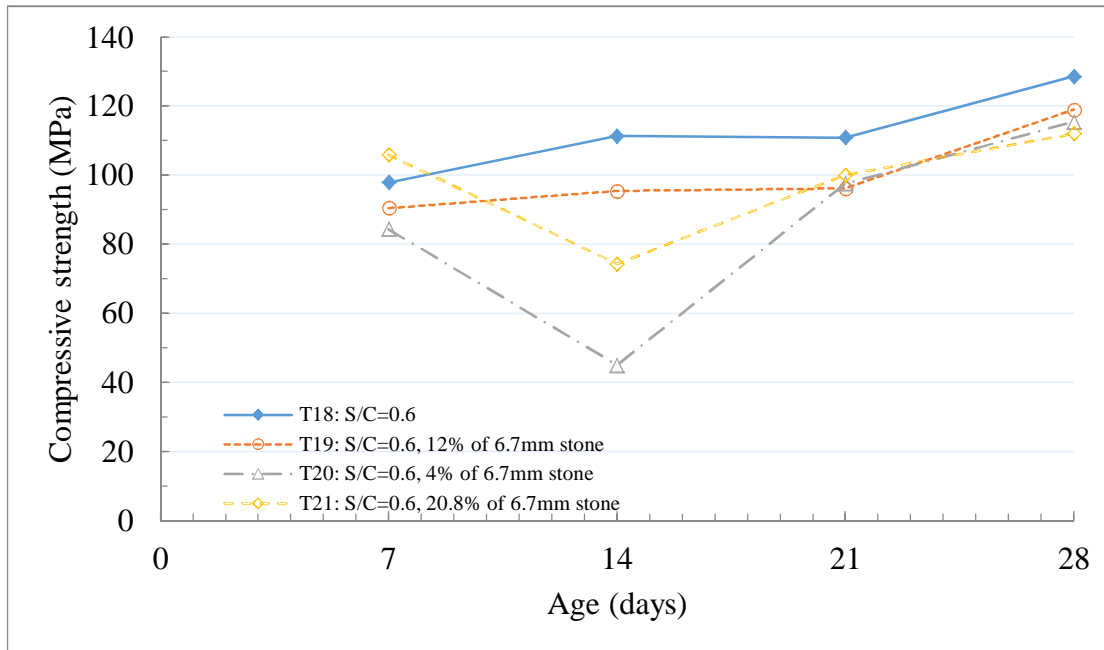
Figure 5-6: Effect of 6.7 mm aggregate on UHPM strength: T18 to T21.

5.3.4.   Conclusive remarks for mixing with CEM I 42.5N

Following the mix design procedure, the UHPP and UHPM is optimised using CEM I 42.5N cement and Chryso 310 SP. A lack of strength was found with UHPP and UHPM which indicates that stronger UHPP is required. However, the general UHPP and UHPM trends are obtained through the above phases.

For UHPP, it can be observed form Phase1a that either a reduction in W/C ratio or increased SF content can improve UHPP strength. However, the SF has a large influence on UHPP slump flow which in-turn affects the packing and, therefore, the UHPP strength. Further reduction in the W/C ratio in Phase 1b shows the threshold slump flow of 300 mm makes further reduction in W/C unable to increase UHPP strength. The W/C=0.22 is found to both satisfy higher UHPP strength and can provide slump flow of 320 mm. However, a significant reduction of UHPP strength is observed between 14 and 21 days which makes it impractical from a conventional way of thinking. In addition, step addition of SP in Phase 1b is used to further improve the slump flow, which turns out a higher UHPP strength than that of direct addition of SP. Except in Phase 1b, this research will stick to direct addition of SP for the

76

purpose of research and easy application in the industry. Step addition could possibly be used in future research to further optimise SP dosage to achieve a high spread value with less SP dosage.

For UHPM, the sand only shows limited confinement on UHPP based on Phase 2 tests. The best UHPM results with S/C=0.6 achieves 128.6 MPa (in T18) but still lower than UHPP strength of 131.6 MPa (in T8) – see Table 5-1. The 6.7 mm aggregate will not increase UHPM (with only sand as aggregate) strength and is thus not recommended, but better performance of aggregate was found to be 12% by UHPP volume through limited tests.

In order to improve the UHPM strength, it is more practical to introduce new quality sands, which can be used on its own, or mixed with the local available sands, e.g. the combination of sand will lead to a higher slump flow and strength as some researchers proved. The other way is through sieving and re-grading of the local available sands to further improve UHPM strength. Either way can lead to an economical way to improve UHPM strength, but it will not change UHPP property itself. The optimization of sand leaves room for further improvement in UHPC strength for future research. On the other hand, relative non-ideal sand in this research can better reflect the effect of steel fibres on UHPC strength by following the mix design philosophy in this research.

Following the mix design strategy, the incorporation of steel fibre may lead to an improved UHPC strength, and the reduction in strength at higher ages (beyond 14 days) found in Phase 1 could also be prevented. Before incorporating the steel fibre, the local cement company PPC upgraded their cement to CEM I 52.5N through using a commercial chemical additive strength enhancer, while using the similar clinker in their cement, to improve concrete strength. In addition, three other SPs are introduced from the local market, which may help to improve the UHPP slump flow. The next phase will optimise UHPP through comparing the new cement and SPs. Then, the iterative process will be followed again according to the mix design strategy to develop UHPC.

5.4. UHPC DEVELOPMENT WITH CEM I 52.5N

5.4.1. Introduction

The design method entails three phases, namely:

Phase 1: Design of high strength, yet sufficiently flowable UHPP;

Phase 2: Addition of fine aggregate in order to form sufficiently strong, flowable UHPM;

Phase 3: Addition of suitable fibre and fibre volume to complement the skeleton in UHPC.

In this stage, CEM I 52.5N will be used. In addition, three other types of SPs that are recommended from a local chemical company are introduced, which are: Mapei Dynamon SP1, Sika Viscocrete 10 and Sika Viscocrete 20HE.

By following the mix design strategy and the experience gained from UHPM development with CEM I 42.5N in Section 5.3, the phases of design, together with detailed mix proportions, slump flow and compressive strength results are summarized in Table 5-2. The detailed information is listed Table C2 in Appendix C

Table 5-2: UHPC phased design, showing Phase I-UHPP, Phase II-UHPM, Phase III-UHPC

Step	Batch No.	SF/C	W/C	S/C	6.7 mm Agg (vol %)	Steel fibre (vol %)	SP %	SP % s	SP Type	Slump flow (mm)	Age	f_cu (MPa)	No.	Std (MPa)
1a. SP type for UHPP slump flow (CEM I 42.5N)	S1	0.18	0.22				3.2	1.0	Mapei SP1	279				
	S2	0.18	0.22				5.5	1.7	Mapei SP1	259				
	S3	0.18	0.20				5.5	1.7	Mapei SP1	213				
	S4	0.18	0.22				3.4	1.0	Sika 10HE	315				
	S5	0.18	0.22				5.5	1.7	Sika 10HE	321				
	S6	0.18	0.22				3.2	1.2	Sika 20HE	347				
	S7	0.18	0.22				5.5	2.0	Sika 20HE	332				
	20	0.18	0.22				3.4	1.0	Chryso 310	276				
	22	0.18	0.22				5.5	1.7	Chryso 310	260				
1b. SF/C (CEM I 52.5N)	S10	0.18	0.22				3.2	1.2	Sika 20HE	346				
	S11	0.2	0.22				3.2	1.2	Sika 20HE	338				
	S12	0.16	0.22				3.2	1.2	Sika 20HE	363				
	S13	0.18	0.20				3.2	1.2	Sika 20HE	309				
	S14	0.16	0.20				3.2	1.2	Sika 20HE	329				
1c. SP dosage (CEM I 52.5N)	S15	0.16	0.20				4.0	1.5	Sika 20HE	323				
	S16	0.16	0.20				2.4	0.9	Sika 20HE	327				
	S17	0.16	0.20				1.6	0.6	Sika 20HE	279				
	S18	0.16	0.20				2.8	1.0	Sika 20HE	337				
	S19	0.16	0.20				3.6	1.3	Sika 20HE	330				
2. UHPP and UHPM (CEM I 52.5N)	T(20 HE)1	0.16	0.20				2.8	1.0	Sika 20HE	336	14	152.8	1	
											28	108.0	3	4.2
	T(20 HE)2	0.16	0.20	0.6			2.8	1.0	Sika 20HE	294	28	141.3	3	6.2
	T(20 HE)3	0.16	0.20	1.0			2.8	1.0	Sika 20HE	247	28	135.3	3	4.7
	T(20 HE)4	0.16	0.20	1.4			2.8	1.0	Sika 20HE	203	28	99.3	3	6.5
	T(SP 1)1	0.16	0.20				2.8	0.9	Mapei SP1	267	28	133.5	3	3.1
	T(SP 1)2	0.16	0.20	1.0			2.8	0.9	Mapei SP1	164	28	100.4	3	4.2
	T(20 HE)5	0.16	0.20	0.6	12		2.8	1.0	Sika 20HE		28	89.8	3	4
3. UHPC	T(20 HE)6	0.16	0.20	0.6		1.5	2.8	1.0	Sika 20HE		28	168.7	3	3.5
	T(20 HE)7	0.16	0.20	0.6	12	1.5	2.8	1.0	Sika 20HE		28	161.2	3	1.5

5.4.2. Phase 1 – Optimization of the UHPP

Following the experience from previous tests with CEM I 42.5N, it is learnt that slump flow of 300 mm can be regarded as a reference value that indicates the ability to pack UHPP densely. In addition, following the mix design strategy, further increase in cement content in UHPP by reducing W/C ratio can lead to a higher strength improvement in early days. Even if the strength reduction is experienced in later days due to larger shrinkage, it can be partially balanced by the incorporation of steel fibres. The purpose of following tests aims to optimise UHPP by satisfying the above mentioned two key parameters. The phase design in this batch starts with the examination of the efficiency of SPs and it starts with CEM I 42.5N in order to compare the test results with previous ones.

5.4.2.1. Phase 1a: Role of SPs and SP dosage on UHPP (CEM I 42.5N)

By checking the optimised UHPP from previous tests (with W/C=0.22, SF/C=0.18), the slump flow of 276 mm (in S20 from Table 5-2) is achieved with 5.5% SP by cement weight, which is similar to that of 273 mm (in T18 from Table 5-1) with 6% SP by cement weight.

The results are shown in Figure 5-7, where it is apparent that Sika 20HE achieves the highest slump flow for this particular base mix. This SP is selected for further mix optimization in subsequent steps. Cross checks with other SP types are performed from time to time to confirm that Sika HE20 is the most suitable for the UHPC developed here – see Table 5-2 for Phase 1a results.
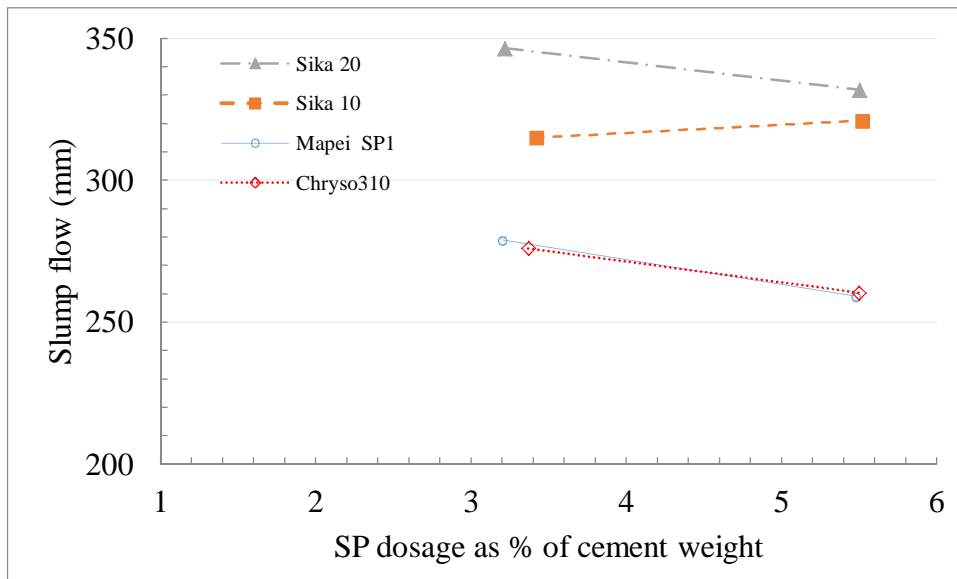
Figure 5-7: Effect of SPs and SP dosage on UHPP slump flow.

5.4.2.2. Phase 1b: Role SF/C and W/C on UHPP slump flow (CEM I 52.5N)

After comparing the efficiency of SPs on UHPP strength, CEM I 52.5N is used from this step on. It can be seen from Figure 5-8 that for the fixed W/C ratio and SP dosage, UHPP slump flow reduces with the increased SF content, which further indicates that a relatively high specific surface of SF causes a high water demand of UHPC (Habel *et al*. 2008:217).

In addition, some agglomerate could be observed in S11, and to a lesser degree in S10 and S13 with the higher dosages of SF – see Table 5-2. This causes heterogeneity of the mix and may form a weak spot in the UHPC. Therefore, the SF content is determined to be 16% of cement by weight based on the local conditions.
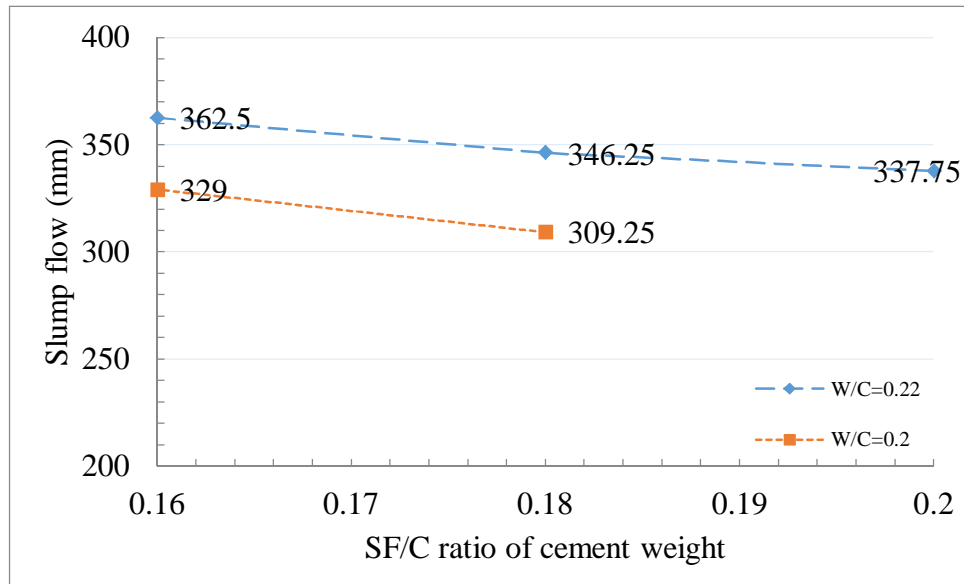
Figure 5-8: Influence of SF content and W/C ratio on UHPP slump flow.

5.4.2.3. Phase 1c: Optimise SP dosage to achieve a higher slump flow (CEM I 52.5N)

As mentioned before, higher slump flow reflects a high UHPP strength, while a lower SP dosage will cause reduced shrinkage to improve UHPP strength. The real balance is difficult to be achieved because the changing in each material property will change the entire result. However, the highest slump flow can be found with relatively lower SP dosage because it was found that additional SP dosage resulted in a reduced slump flow in previous tests by using the direct addition method.

Once the W/C ratio and SF/C content is determined from Phase 1a and Phase 1b, the optimised SP dosage on UHPP slump flow is tested. Because the effect of the SP dosage on the slump flow should follow a parabolic curve, limited tests provide the optimised SP dosage as shown in Figure 5-9. The best slump flow of 336.5 mm is achieved with the SP dosage of approximately 2.8% by cement weight.
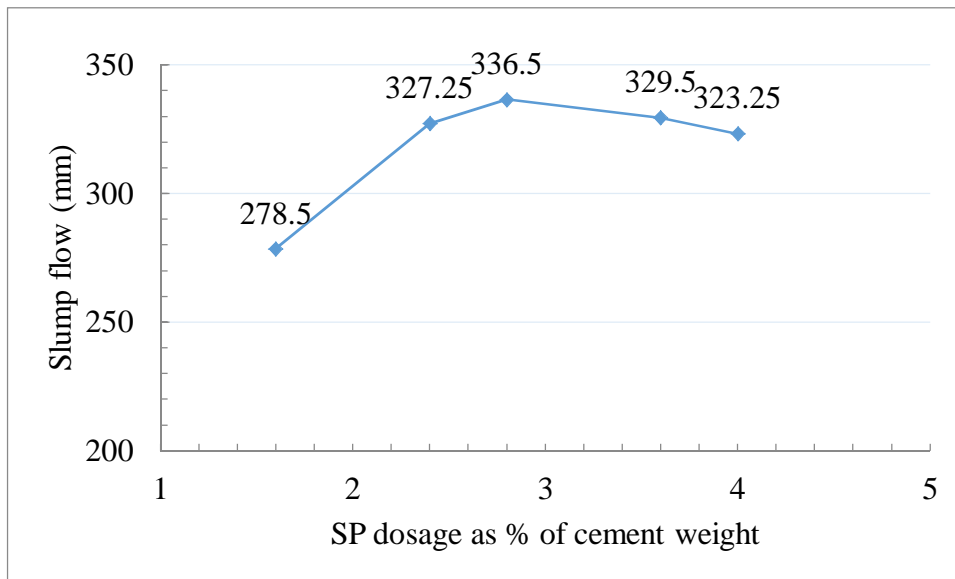
Figure 5-9: Effect of Sika 20HE SP dosage on UHPP slump flow.

5.4.3.   Phase 2: Effect of sand on UHPM strength (CEM I 52.5N)

Once the mix design for UHPP has been optimised, the effect of sand on UHPM strength is tested. Sika 20HE is used throughout, but some tests with Mapei SP1 are included. Even if Mapei SP1 leads to a relatively low slump flow, it contains the air reducing agent that can reduce the air bubbles during the mixing period, which in turn may improve the UHPP strength.

Clearly the maximum amount of sand will be beneficial from a cost point of view. For this reason three contents were tested, ranging from a relatively low value of S/C = 0.6, through to a typical value of S/C = 1 to a high value of S/C = 1.4 – see Table 5-2. The same trend was found as reflected in Figure 5-10 (a) that the UHPM slump flow decreases with the increased sand content. The relatively lower slump flow will reduce the UHPM workability, which may result in a lower UHPM packing and strength. The spread value of UHPM with S/C = 1.4 developed by Wille *et al*. (2012:309) is approximately 300 mm, stressing the importance of optimized fine aggregate and UHPP to achieve this.

The compressive strength results are shown in Table 5-2, and graphically depicted in

83

Figure 5-10 (b). The following characteristics can be seen.

● Effect of SP on UHPP strength: T(20HE)1 and T(SP1)1.

It can be seen from Figure 5-10 (b) that UHPP using Mapei SP leads to an increased UHPP strength until 28 days, which is the first-time it occurs in this research under the condition of UHPP slump flow smaller than 300 mm. Compared with UHPP using Sika 20HE SP, even if a much higher 28 days UHPP strength is achieved by T(SP1)1, it still appears a relatively lower strength development. This further indicates that a higher slump flow reflects a higher UHPP strength development rate in early days, which helps to form the strong skeleton. Nevertheless, the introduction of an air reducing agent may help to further improve UHPP strength that leaves room for UHPP strength improvement in the future.

● Effect of sand content on UHPM strength.

For Sika 20HE as SP, it is apparent from the graph that sand content S/C = 0.6 leads to a slight reduction of UHPM strength from 144 MPa (in 21 days) to 142 MPa (in 28 days), which shows certain confinement of sand on UHPP. Beyond this sand content, its inclusion in UHPM leads to erratic strength development, possibly also due to poor dispersion of relatively larger sand particles and sensitivity to test cube geometrical imperfection.

For Mapei SP1 as SP, the sand content S/C=1.0 and this leads to a big drop in UHPM strength, even if the UHPP strength does not experience any drawback. This further shows the fact that the local sand is not ideal and the inter-locking behavior of sand cannot balance the high differential stresses or micro-cracks due to a relatively higher shrinkage.

Based on the above analysis, the strength as well as the slump flow indicates that S/C=0.6 provide the best UHPM performance under the current local conditions and Sika 20HE provides better UHPM performance.
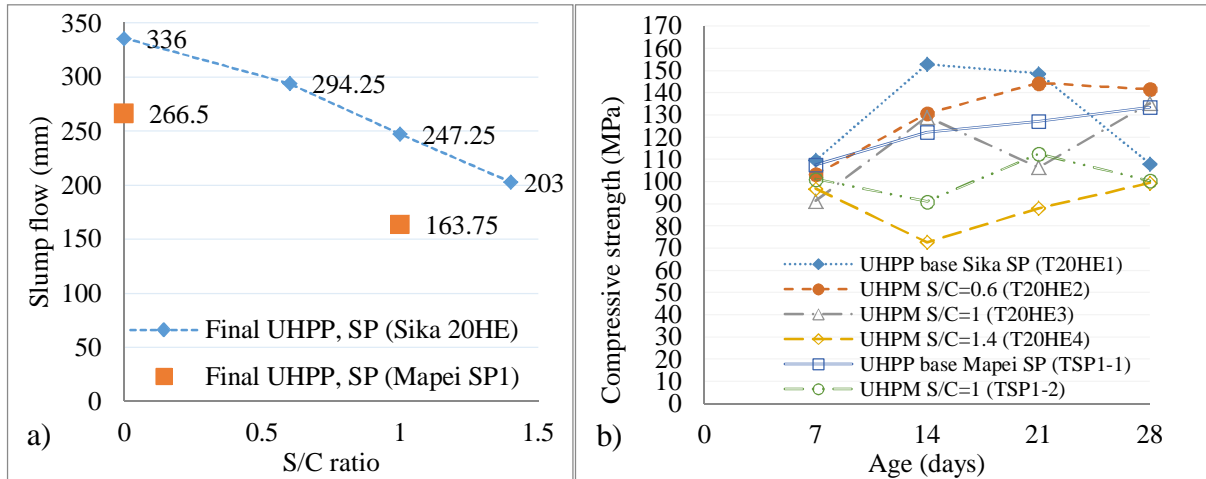
Figure 5-10: UHPM (a) slump flow; and (b) compressive strength development.

5.4.4. Phase 3: UHPC (CEM I 52.5N)

In the final stage, short steel fibres at 1.5% by total volume are added to the optimised UHPM. The resulting compressive strength development up to 28 days is shown in Figure 5-11 (a). For comparison, the strength development of the finally optimised UHPP and UHPM are shown in the figure as well. The steadily increasing strength development in time is evidence of a sound skeleton and bridging of micro-cracks induced by shrinkage of the UHPP. An ultimate strength of 168.7 MPa is achieved at the age of 28 days, succeeding in developing UHPC without heat curing.

Figure 5-11 (b) shows the results when, in addition to fine aggregate (Malmesbury #1 sand at S/C = 0.6), 12% by volume of small particle stone (6.7 mm) is added to both the UHPM and UHPC. Clearly, the UHPM strength development is erratic, but that of the UHPC demonstrates that the shortcomings are overcome once the 1.5% steel fibres are added. An ultimate strength of 161 MPa is achieved in this case. This successful achievement of UHPC

may be ascribed to the optimised UHPP. Also, the large aggregate particle size of 6.7 mm approaches the requirement that the fibre length is at least 2 to 4 times the aggregate particle size.
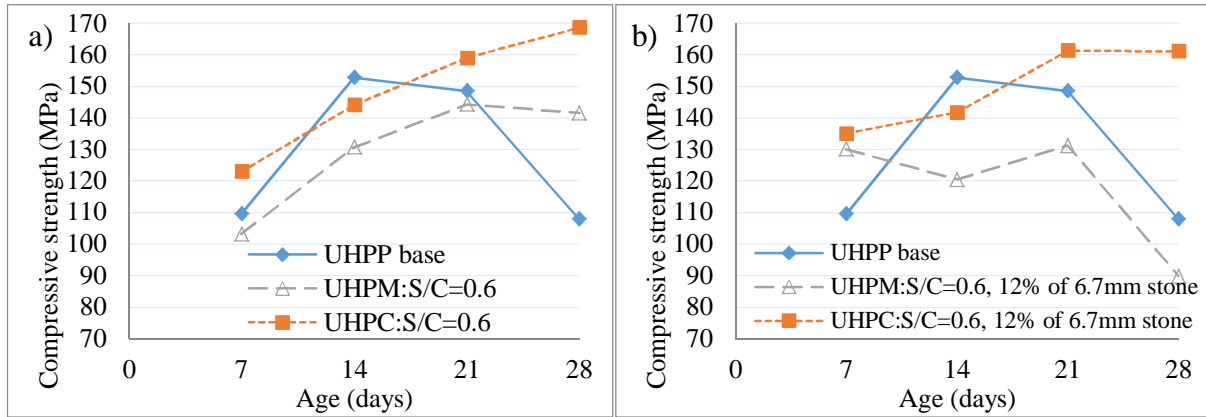
Figure 5-11: Compressive strength development of UHPC: (a) Phase 3 – UHPC, only fine aggregate; and (b) Phase 3 – UHPC, fine & coarse aggregate.

The final strength of UHPC is 19% higher than the UHPM strength, by the addition of only 1.5% by volume of short steel fibre. This is a significantly higher increase than reported by Wille *et al.* (2012:309, 2011:46) of 4.7% improvement with 2.5% steel fibres (2011), of 6.7% increase achieved with 1.5% steel fibres (2012) and 9.8% with 2.5% steel fibres (2012), which indicates the effective use of steel fibres in this research.

5.4.5. Concluding remarks for mix with CEM I 52.5

Following the mix design procedure, the phase designs are optimised through UHPP, UHPM and finally UHPC with upgraded CEM I 52.5N. Through better use of steel fibres, the UHPC with a compressive strength of 168 MPa is finally developed with local non-ideal materials. This indicates the successful application of the new mix design strategy by better use of the steel fibres with its development of strength as elaborated in Chapter 4.

Experience from UHPM development with CEM I 42.5N provides valuable references for the

phase design using CEM I 52.5N. The slump flow of over 300 mm is found to be one of the most important parameters for UHPP strength. Though SF content, W/C ratio and SP content also contribute to UHPP slump flow and affect UHPP strength, the maintenance of a proper slump flow is a much higher priority.

Further reduction of the W/C ratio, while retaining proper UHPP slump flow, provides an efficient way to improve UHPC strength, even if the UHPP strength reduction in later days is evident, as found in this research. Local sand is found to only provide limited confinement on UHPP and the optimised S/C ratio was limited to 0.6, which is too low compared with other researchers.

5.5. FACTORS THAT CAN AFFECT UHPC STRENGTH

Once the UHPC has successfully developed, factors that may affect UHPC strength were tested. Large UHPC post-tensioned box girders were cast and tested for structural verification and validation purposes as elaborated in Chapter 7, but a significantly lower cube compressive strength was found compared with the 168 MPa reported in Section 5.4.4. Therefore, the factors that can affect UHPC strength need to be addressed. These factors, which include cement type, setting and curing conditions, will be elaborated in this sub-section.

5.5.1. The effect of ambient temperature on UHPC strength

As introduced in Section 2.2.1, the ambient temperature will significantly affect UHPC strength. In addition, a slight change in room temperature of approximate 20 ℃ will also affect UHPC strength as introduced in Section 2.3.5.2. The laboratory temperature was also found to influence UHPC strength in this research. The trial mixes for post-tension box girder (T(20HE) TR), post-tension box girder (Box girder) together with some tests, are listed in Table 5-3. All these mixes used the same materials and the same mix design, but under

different ambient and curing conditions. The moulded period refers to specimens after casting and before de-moulding, while the curing period refers to specimens after de-moulding.

The specimens, cured at the ordinary (non-climate controlled) materials lab, experienced temperature changes during the moulded period, which are representative for the practical application. The specimens which cured at the PPC lab experienced a constant temperature of approximately 21 ℃ during the moulded period. Even if the UHPC strength under laboratory condition is difficult to compare due to the changing of the environmental temperature, it can still be seen that a relatively higher temperature causes a relatively higher UHPC strength with the ambient temperature of approximately 20 ℃ as shown in Table 5-3. When comparing T(20HE)TS3 and T(20HE)TR, it can be seen that an increase of 15 ℃ in ambient temperature results in a significant improvement in UHPC strength of approximately 20%. Such phenomenon follows the general trend of UHPC strength that higher ambient temperature cause higher UHPC strength (Soliman, 2011). Because a slight changing in ambient temperature can only cause a slight difference in UHPC strength, the significant reduction in UHPC strength between T(20HE)TR and post tensioned box girder is mainly caused by a specimen without a top cover during the setting period when the effect of curing conditions were ignored, namely the effect of either water or moisture on UHPC strength.

Table 5-3: Effect of ambient temperature on UHPC strength.

Batch No.	Ambient condition	Curing conditions	Specimen preparation	Temperature record during the day (℃)				Compressive strength (MPa)			
				08h00	11h00	14h00	17h00	Age	f_{cu} (MPa)	No.	Std. (MPa)
T(20HE)TR	Lab/2 days	Water	Plastic cover	25	33	33	30	28	163.4	6	2
Box girder	Lab/2 days	Moisture	No top cover	19	27	31	30	28	124.3	6	3.4
T(20HE)TS1	Lab/2 days	Water	Plastic cover	11	14	17	15	28	133.8	6	6.5
T(20HE)TS3	Lab/2 days	Water	Plastic cover	9	15	19	16	28	136.2	6	3.9
T(20HE)TS5	PPC lab/ 2 days	Water	Plastic cover	21	21	21	21	28	139.1	3	2.7

5.5.2. The effect of cement chemical composition on UHPC strength

The cement chemical composition, especially the C_3S content according to Bogue analysis, plays an important role in determining UHPC strength as introduced in Section 3.2. The cement used in T (20HE)6 has a relatively higher C_3S content than the cement used in T(20HE) TS3 as shown in Table 3-1. According to Table 5-4, for the same mix design, cement with higher C_3S content causes an approximately 24% improvement in UHPC strength under similar laboratory ambient temperature. The previous sub-section shows a slight change in laboratory temperature of approximately 2 ℃ can only cause a slight difference in UHPC strength. Therefore, the only reason left for such significant difference in UHPC strength is the chemical content in cement, especially the C_3S content that affects UHPC strength.

Table 5-4: Effect of cement on UHPC strength.

Batch No.	Ambient condition	Curing conditions	Specimen preparation	Temperature record during the day (℃)				Compressive strength (MPa)			
				08h00	11h00	14h00	17h00	Age	f_{cu} (MPa)	No.	Std. (MPa)
T(20HE) TS3	Lab/2 days	Water	Plastic cover	9	15	19	16	28	136.2	6	3.9
T (20HE)6	Lab/2 days	Water	Plastic cover	11	17	21	18	28	168.7	3	3.5

5.5.3. The effect of ambient and curing conditions on UHPC strength

In order to compare the effect of ambient and curing conditions on UHPC strength, the specimens, which are using the same mixing materials and under the same mix design, were cured in the PPC laboratory with a constant ambient temperature of approximately 21 ℃. For the moulded period of two days (i.e. specimens kept in the moulds for two days before de-moulding), the curing conditions have a slight effect on UHPC strength for specimens subsequently either cured in the water tank or exposed to the air as shown in set T(20HE) TS5 in Table 5-5. For the moulded period of one day as shown in set T(20HE) TS4, the water cured UHPC is approximately 6% stronger than that exposed to the air. It can be postulated

89

that the skeleton is not strong enough for moulded period of one day where the UHPC specimen is still affected by the environmental moisture. All the previous specimens were de-moulded after a period of two days, in which case the UHPC strength is less affected by curing conditions.

Table 5-5: Effect of ambient and curing condition on UHPC strength.

Batch No.	Sand	Specimen cover	Ambient condition	curing condition	Compressive strength				Density (kg/m³)
					Age	f_{cu} (MPa)	No.	Std (MPa)	
T(20HE) TS3	M#1	Plastic	PPC lab/2days	Water	28	136.2	6	3.9	2384
T(20HE) TS4	M#1	Plastic	PPC lab/1day	Air	28	134.4	3	1.3	2440.7
				Water	28	142.9	3	5.9	2440.9
T(20HE) TS5	M#1	Plastic	PPC lab/2days	Air	28	136.7	3	1.1	2433
				Water	28	139.1	3	2.7	2466

5.5.4. The effect of sand on UHPC strength

Compared with Malmesbury #1 sand (M#1), the new arrival Malmesbury #2 sand (M#2) has more fine particles and spherical shape, which was elaborated in Section 3.5.1. By simply replacing the same amount of M#1 with M#2 while the other mixing materials and curing conditions remain the same, the 28 days UHPC strength improve approximately 8%, which leave future opportunity to increase UHPC strength. In addition, the 56 days UHPC strength continues to increase, which shows that the steel fibre can effectively confine relatively larger shrinkage in later stage. This phenomenon further reflects the mix design philosophy for this research that no special treatment is needed such as SAP or SRA as elaborated in Section 4.3.

Table 5-6: Effect of sand on UHPC strength.

Batch No.	Sand	Specimen cover	Ambient condition	curing condition	Compressive strength				Density (kg/m³)
					Age	f_{cu} (MPa)	No.	Std (MPa)	
T(20HE) TS3	M#1	Plastic	PPC lab/2days	Water	28	136.2	6	3.9	2384
T(20HE) TS6	M#2	Plastic	PPC lab/2days	Water	28	147.6	6	5	2436
T(20HE) TS7	M#2	Plastic	PPC lab/2days	Water	56	156.5	6	2	2442

5.6. CONCLUSIONS

In this chapter, the practical application of mix design strategy was tested and elaborated through three phase designs: UHPP, UHPM and UHPC with local materials, without heat treatment. Based on the local non-ideal materials as compared in Chapter 3, the optimisation of UHPP and UHPM were unable to achieve the same paste and mortar strength as that of Wille *et al*. (2011:46) and the cement had to shift from CEM I 42.5N to CEM I 52.5N to achieve a relatively higher strength. The effect of each material on UHPC was studied through a series of tests under each phase. By following the mix design strategy that elaborated in Chapter 4, the UHPC was finally developed with the help of 1.5% steel fibres by UHPM volume of and achieved a compressive strength of 168 MPa. The UHPC strength was 19% higher than that of UHPM, indicating the successful application of mix design strategy and further shows the steel fibre did help to improve the UHPC compressive strength with proper mix design.

Once the UHPC had been successfully developed with the local materials, some factors were found to affect UHPC strength. Among these factors, cement composition, the ambient temperature and specimen preparation, whether specimens are sealed or not, significantly affect UHPC strength. Beside the above mentioned three key factors, the moulded period also influences UHPC strength, where the 48 hours of moulded period made UHPC specimens less affected by the curing conditions.

Chapter 6: Tensile and flexural behaviour of UHPC

6.1.   INTRODUCTION

The tensile behaviour of UHPC also provides a key parameter for structural analysis besides UHPC compressive strength. The tensile strength is generally obtained through direct tensile test (DTT) with great care. Besides the DTT, flexural test is also used by some researchers because of its standardized test setup. This chapter will introduce the DTT and flexural test for UHPC which were developed in this research.

6.2.   THE TENSILE STRENGTH RESULTS FROM THE DIRECT TENSILE TEST.

Careful direct tensile tests are performed to obtain the tensile response of UHPC in this research. The tensile behaviour of UHPC in this research was obtained through 40 mm thick notched dumbbell shaped specimens; however, 16 mm thick un-notched dumbbell shaped specimens were also tested to add information on size effect, which will be elaborated on in the following sub-section.

6.2.1.   Direct tensile test setup

Two hydraulic clamps that were fixed to the Zwick Materials testing machine (MTM) were used for the DTT as shown in Figure 6-1. The centre-line of the two clamps was aligned vertically. The hydraulic jack for each clamp extrudes out from both sides to clamp the specimen in position. The final setup of the specimen is shown in the right side of Figure 6-1 with the extensometer clamped to the specimen centre-line to measure the displacement. The specimen was carefully located in the hydraulic clamps to avoid misalignment by aligning the centre-line of the specimen to the centre-line of each hydraulic jack.

Pneumatic grips were used in the Zwick MTM. Each grip has two moving faces, controlled

92

pneumatically. This was selected instead of one-sided movable face only in order to assist the aligned grips to induce uniformly distributed tensile stress in the dumbbell shape specimens.

Figure 6-1: Direct tensile test setup.

6.2.2. Specimen dimensions

Two different sized dumbbell shaped moulds were used in this research. The first one is the 40 mm thick dumbbell shaped mould and the second one is the 16 mm thick dumbbell shaped mould as shown in Figure 6-2. The notations of dumbbell shaped specimen are shown in Figure 6-2 (c) with the width, depth and gauge length marked with w, d and l_g respectively. The corresponding dimensions are listed in Table 6-1.

Table 6-1: The dimensions for two types of dumbbell shape specimen.

	Width 'w' (mm)	Depth 'd' (mm)	Gauge length 'l_g' (mm)
40 mm thick dumbbell shape mould	80	40	108
16 mm thick dumbbell shape mould	30	16	80
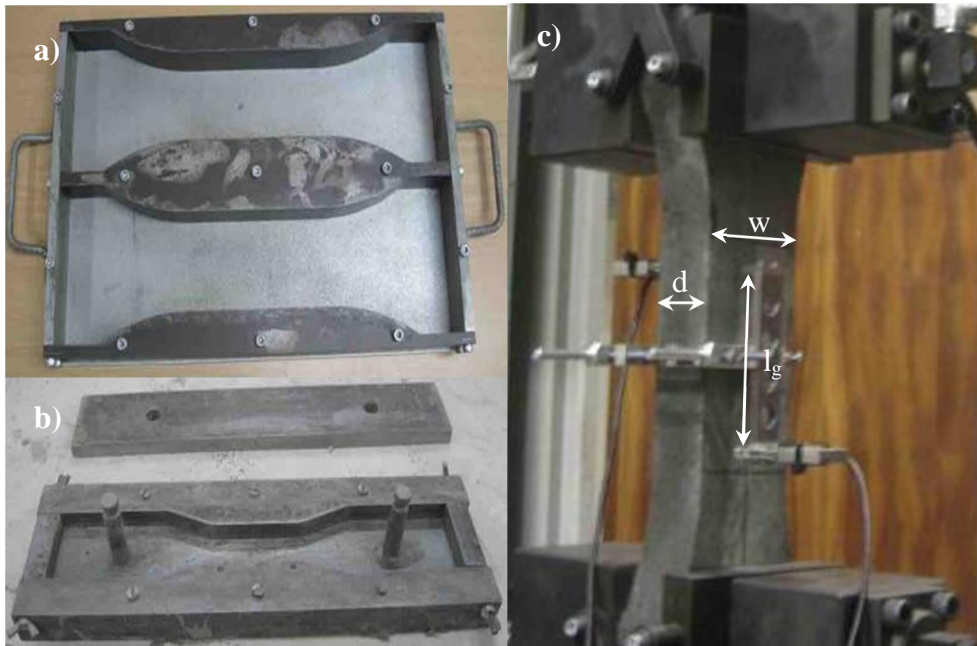
Figure 6-2: Dumbbell shaped specimen moulds, (a) 40 mm thick dumbbell shaped mould; (b) 16 mm thick dumbbell shaped mould; and (c) Dumbbell shaped specimen notation.

A complete calibration of size effect by extensive testing with both 40 mm and 16 mm specimens was not performed, due to unavailability of the large moulds. Such tests are recommended for future work.

6.2.3. Loading rate for DTT

Similar to the compressive test, the loading rate may also have an effect on the DTT results. Kim *et al*. (2009:399) compared four loading rates in DTT on high strength concrete and found that the strain rate of 0.006/min provides a pseudo static loading while the strain rate of 6/min provides a dynamic loading test environment. The loading rates of DTT chosen by researchers for the UHPC are listed in Table 6-2. In order to simulate a quasi-static test environment, the lowest strain rate of 0.001/min was chosen for UHPC in this research.

94

Table 6-2: The loading rate for direct tensile test of UHPC from researchers.

No.	Type of dumbbell shape specimen	Loading rate (mm/min)	Strain rate (/min)	Reference
1	Un-notched	0.1524	0.0015	(Graybeal & Baby, 2013:177)
2	Un-notched	0.4	0.0023	(Park *et al.* 2012:172)
3	Un-notched	0.4	0.0032	(Hassan *et al.* 2012:874)
4	Notched	0.2	0.001	(Kang & Kim, 2011:1001)
5	Notched 10 8mm	0.105	0.001	This research t=40 mm
6	Un-notched 80 mm	0.8	0.001	This research t=16 mm

6.2.4. Direct tensile test with 40 mm thick notched dumbbell shaped specimen

6.2.4.1. Introduction

The dumbbell shaped specimen is used to obtained tensile behaviour of UHPC. The 40 mm thick dumbbell specimen experienced first crack occurrence outside the middle section where the extensometer measures. Therefore, the conventional way of localizing the crack opening by applying the notch on the specimen, is used.

6.2.4.2. Specimen preparation

The casting of 40 mm thick dumbbell shaped specimen did not follow middle casting or layer casting methods so that the same casting method as the post tensioned box girder could be maintained, which will be elaborated on in the following chapter. The fresh UHPC could flow by itself due to its high workability and the surface of UHPC could be levelled automatically, especially after 1 minute of vibration. A 10 mm deep notch on each side and at the middle of the 40 mm thick dumbbell specimen was applied to localize crack opening location.

The notch was cut using a cutting machine resulting in a tolerance of less than 0.5 mm in depth. In order to attain more accurate dimensions, two measurements were taken on each face with a calliper with the resolution of 0.1 mm.

6.2.4.3. DTT results from 40 mm thick notched dumbbell shaped specimen

A total of 4 from 6 prepared specimens were successfully tested with cracks occurring in the gauge area; the test results are listed in Table 6-3 and the corresponding stress strain curve shown in Figure 6-4.

The notched dumbbell shaped specimens achieved an average first crack tensile strength of 5.29 MPa and peak tensile strength of 8.56 MPa. The relatively low standard deviation of 0.175 MPa for first crack strength reflects the high accuracy of DTT results. The grinding of the top and bottom surface together with the notch removed from the surface UHPC, where the UHPC strength can be affected by the environmental curing conditions, are taken out. However, the peak tensile strength appears to display a relatively large variation.

Table 6-3: Data from direct tensile test with 40 mm thick dumbbell shape specimen.

Specimen No.	Cracking		Maximum		E modulus (GPa)
	Stress (MPa)	Strain	Stress (MPa)	Strain	
#3	5.13	0.00012	9.06	0.0016	34.17
#4	5.20	0.00014	8.43	0.0014	33.99
#5	5.53	0.00013	8.95	0.0030	35.60
#6	5.30	0.00013	7.81	0.0024	34.23
Mean	5.29	0.00013	8.56	0.0021	34.50
Std.	0.175	0.000007	0.571	0.00073	0.742

6.2.4.4. Tensile stress-strain response of UHPC

A typical UHPC uniaxial tensile behaviour follows four phases as explained in Figure 6-3 by Graybeal and Baby (2013:177), which are: I) the elastic phase, where stress and strain evolve linearly before the first crack occurs; II) the multiple cracking phase, where the resistance taken by steel fibre reinforcement is larger than UHPM cracking strength; III) the crack straining phase, where crack opening increases but the steel fibres are still under partially de-bonding stage; and IV) the localization stage, where an individual crack opens while the rest of the cracks can remain in Phase III and the steel fibres that link this individual crack are

under fully de-bonding stage and slowly slide out.
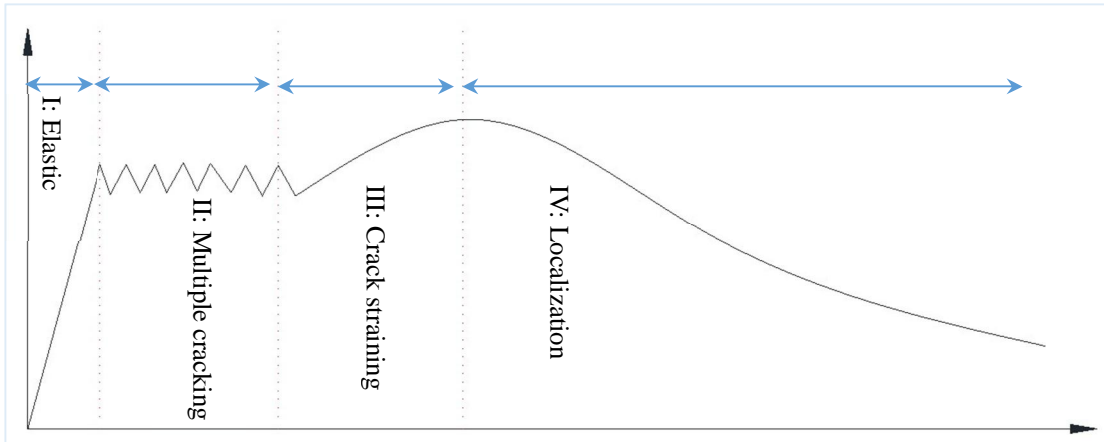
Figure 6-3: Idealize uniaxial tensile behaviour of UHPC (Graybeal & Baby, 2013:177).

It can be seen from Figure 6-4 (a) that the overall tensile behaviour of four specimens also follows the four phases as mentioned above. The tensile behaviour of four specimens in Phase I and Phase IV are similar. But it can be seen from Figure 6-4 (c), that there is slight difference between specimens in Phase II and Phase III. In order to see the fibre orientation, a 3D CT scanning of specimen 3 is shown in Figure 6-5.
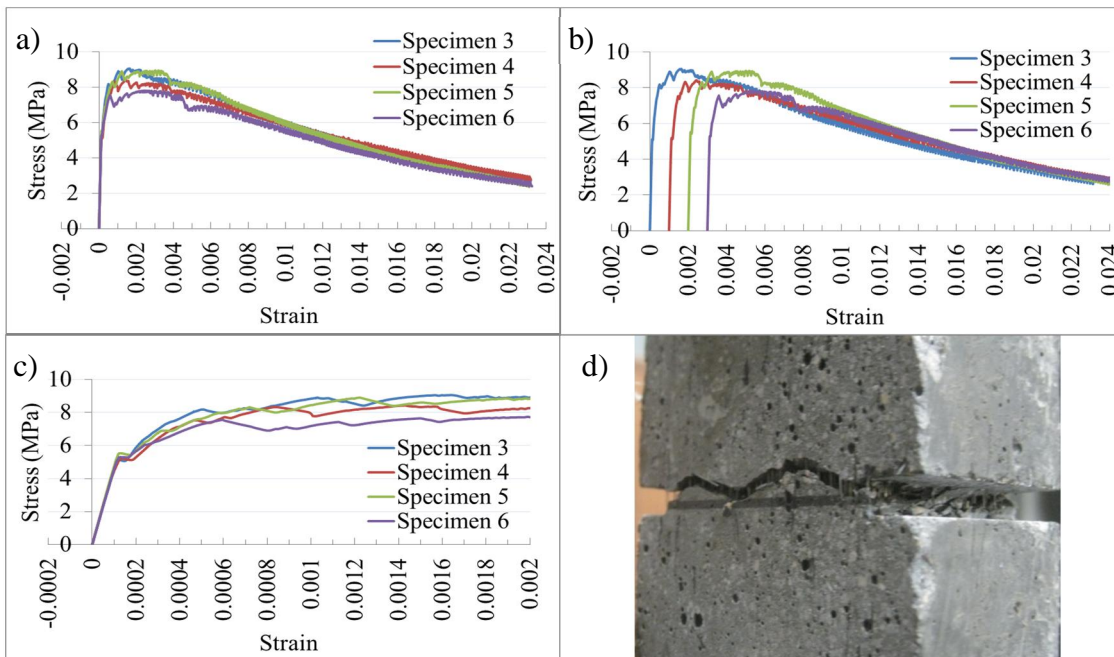
Figure 6-4: Stress-strain curve for 40 mm thick dumbbell shaped specimens, (a) Full stress-strain; (b) Shift axis of 0.001 between each specimen; (c) Stress-strain up to ultimate strength and (d) Crack pattern.

It can be seen from Figure 6-5 that the practical steel fibres are not orientated parallel to the length direction, which differ from the theoretical arrangement of steel fibres. The dispersion of steel fibres reflects the flow of fresh UHPC. Form the face view, fresh UHPC can flow freely along the face of the mould and the fibre orientation represents the flow of fresh UHPC, where the fibres form a certain angle to the length direction. From the side view, it can be seen that the majority of steel fibres are parallel to the length direction, but still a minority of them form an angle to length direction.

The tensile behaviour of Phase I is similar for four specimens according to Table 6-3 and as shown in Figure 6-4. For Phase two and phase three, the variation of fibre orientation, multiple cracks location and embedment of steel fibre across the multiple cracks plan can be postulated to affect post cracking behaviour of DTT and the peak tensile strength. For Phase IV, the tensile behaviour of DTT is mainly influenced by steel fibre in major crack opening plane.
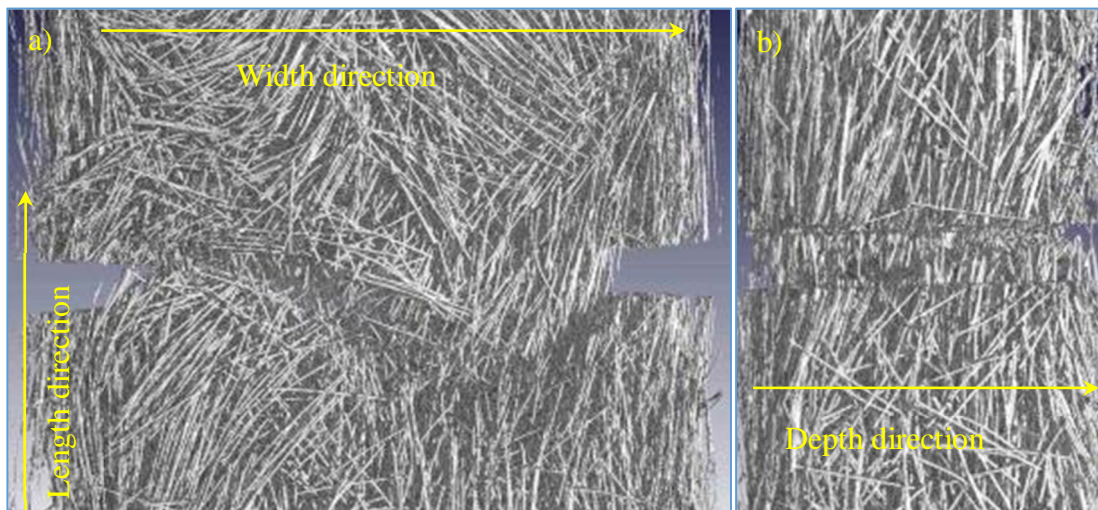
Figure 6-5: 3D image of steel fibre dispersion on specimen 3 through CT scanning: (a) Face view; (b) Side view.

6.2.4.5. Possible solutions to perform un-notched dumbbell specimen tensile test

As a solution for cracks to open at the right location, a steel mesh cast inside the transition

zone of the dumbbell shaped specimen may enhance the transition zone resistance so that the crack occurs in the gauge area. Another way is to add steel plates as shown in Figure 6-6 to strengthen the transition zone (Graybeal & Baby, 2013:177). However, whether the steel mesh or steel plate can help the first crack to open at the right location still needs to be verified in future research.
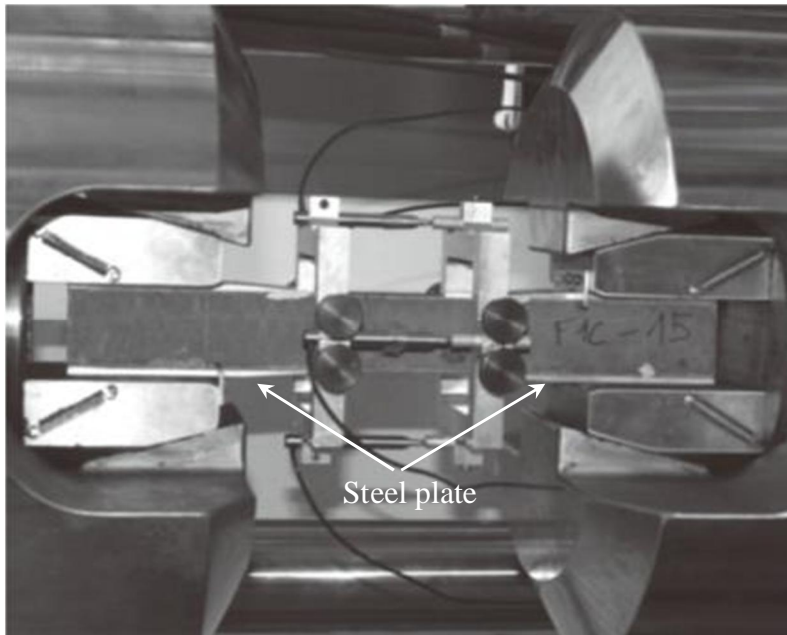
Figure 6-6: The recommended direct tensile test methods (Graybeal & Baby, 2013:177).

6.2.4.6. Conclusive remarks on tensile strength of 40 mm thick dumbbell shaped specimen

Even if notched dumbbell shaped specimens localize the crack opening location, quite a few researchers still used such a setup to obtain concrete tensile behaviour. According to Chuang and Ulm (2002:1314), the tensile strength provided by the Lafarge group is through a notched tensile test with great care to obtain a low standard deviation, of which the resulting data has already been successfully applied in their finite element (FE) model for UHPC bridge analysis.

The 40 mm thick notched dumbbell specimens obtain an average first crack tensile strength of 5.29 MPa and peak tensile strength of 8.56 MPa with a relatively low standard deviation. In

addition, strain hardening behaviour of UHPC can be obtained with only 1.5% of steel fibres by UHPM volume.

6.2.5. Direct tensile test with 16 mm thick un-notched dumbbell shape specimen

6.2.5.1. Introduction

The 16 mm thick dumbbell shaped specimen is also used for DTT as shown in Figure 6-2 (b) to obtain tensile behaviour of UHPC. The introduction of steel mesh enables the un-notched dumbbell shaped specimen used for DTT. Three set of tests were performed in this sub-section.

6.2.5.2. Test preparations for 16 mm thick dumbbell shaped specimens

6.2.5.2.1. Casting method

Since there is no standard casting methods for DTT, the casting methods commonly used for flexural tests, which are the middle casting method or layer casting method as shown in Figure 6-7 (Wille & Parra-Montesinos, 2012:379), are used as a reference. The limited width and the depth of the 16 mm thick dumbbell shaped specimens make it more practical to use the layer casting method with steel mesh.

a) Middle casting
(RILEM TC 162-TDF)

b) Layer casting ASTM (C1609/C1609M) with different chute speeds
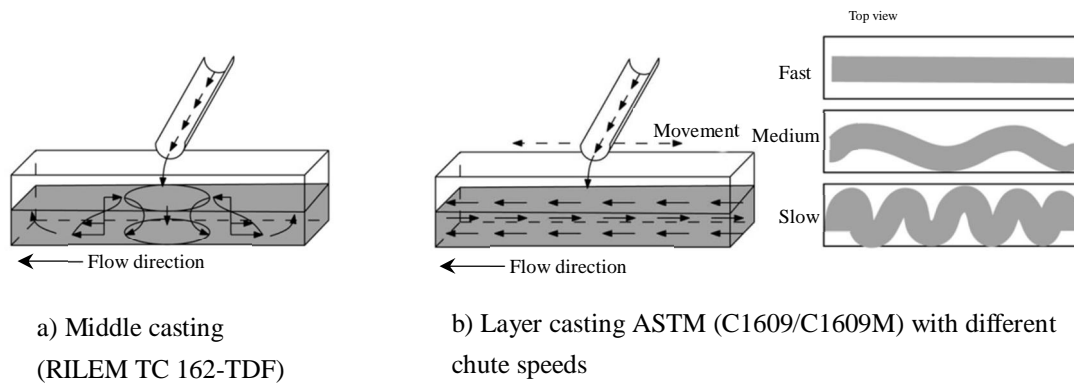
Figure 6-7: Middle casting method and layer casting method (Wille & Parra-Montesinos, 2012:379).

6.2.5.2.2. Test specimens preparation

The mixing procedure and testing equipment are the same as that of 40 mm thick dumbbell shaped specimens. A woven wire stainless steel mesh with the wire spacing of 25 mm and wire diameter of 0.6 mm is cut according to the shape of the mould transition zone as shown in Figure 6-8. Along the thickness direction, the steel mesh is located in the middle. Along the length direction, the steel mesh extends 12 mm after the transition zone towards the middle section in order to shift cracks opened in the gauge area.

In compliance with the layer casting method, half of the mould was filled with fresh UHPC, after which the steel mesh was placed in the transition zone on top of the first UHPC layer and vibrated for 1 minute. Then, the second layer of fresh UHPC was filled and vibrated for another 1 minute. After a total of 2 minutes of vibration, all the specimens were put in the PPC laboratory under the same ambient condition for 2 days and cured into the water tank until the day of testing.

101
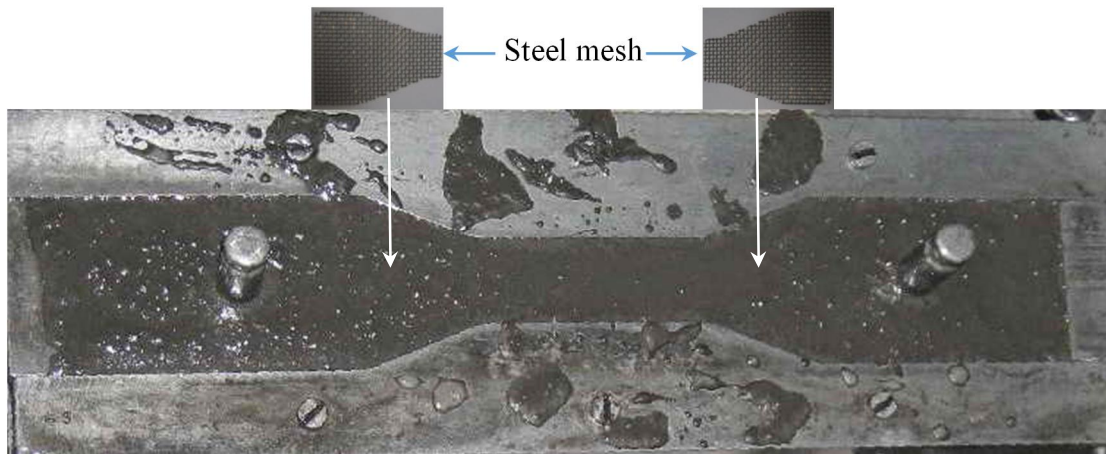
Figure 6-8: Steel mesh for 16 mm thick dumbbell shaped specimen.

6.2.5.3. Tensile results for 16 mm thick un-notched dumbbell shaped specimens

The first crack tensile strength (f_{tc}), peak tensile strength (f_{tp}), E modulus and compressive strength (f_{cu}) for UHPC with Malmesbury #1 sand (M#1) and Malmesbury #2 sand (M#2) are summarized in Table 6-4.

Table 6-4: Tensile strength for 16 mm thick un-notched dumbbell shape specimens.

Batch No.	No.	Sand type	First tensile crack strength (MPa)			Tensile peak strength (MPa)			E modulus (GPa)			f_{cu} (MPa)
			f_{tc}	Mean	Std	f_{tp}	Mean	Std	Single	Mean	Std	
TS4	M1	M#1	5.52	5.43	0.067	8.5	9.05	0.450	X	55.30	0.615	142.9
	M2		5.36			8.9			55.73			
	M4		5.41			9.53			X			
	M6		5.43			9.28			54.86			
	M3	M#1	7.18	7.35	0.333	11	10.45	0.659	58.82	58.82	X	
	M5		7.73			9.72			X			
	M7		7.13			10.63			X			
TS5	M1	M#1	5.91	5.98	0.384	8.63	9.23	0.618	53.5	54.70	1.697	139.06
	M3		6.2			9.43			X			
	M5		5.47			10			X			
	M7		6.34			8.84			55.9			
TS6	M1	M#2	6	6.35	0.783	9.39	9.07	0.372	X	57.50	X	147.6
	M2		7.73			8.83			X			
	M3		6.61			9.06			X			
	M4		5.74			9.22			X			
	M5		6.42			8.46			X			
	M6		5.58			9.44			57.5			

With the help of a steel mesh, cracks for the majority of specimens occurred in the gauge area.

Some specimens experienced first crack and major crack openings in the gauge area, but cracks still occurred in the transition zone during the multi-cracking stage.

6.2.5.3.1. Tensile strength data analysis

● Comparing the tensile strength difference in the same batch of TS4.

It can be seen from Table 6-4 that there are two sets of data in set one for TS4 specimens. One set has a lower value of the average first crack tensile strength and peak tensile strength of 5.43 MPa and 9.05 MPa respectively, which is a strain-hardening increase of 66.7%. The other set has a higher value of first crack tensile strength and peak tensile strength of 7.35 MPa and 10.45 MPa respectively, with the increment rate of 42.2% in tensile strength. The fibre number and orientation may lead to such a difference. One typical specimen from each set was chosen to compare the steel fibre orientation and number of steel fibres through major crack opening plane through CT scanning as shown in Figure 6-9 and Figure 6-10.

Based on the CT scanning images in Figure 6-9, the steel fibre dispersion is similar under the layer casting method for 16 mm thick dumbbell shaped specimen. The steel fibre forms a certain angle based on the face view as shown in Figure 6-9 (b) and (e). From the side view, it can be seen that the set with higher value of tensile strength has more steel fibre content which may be the main reason why such a difference occurred. The number of steel fibre can be compared through the major crack opening plane.
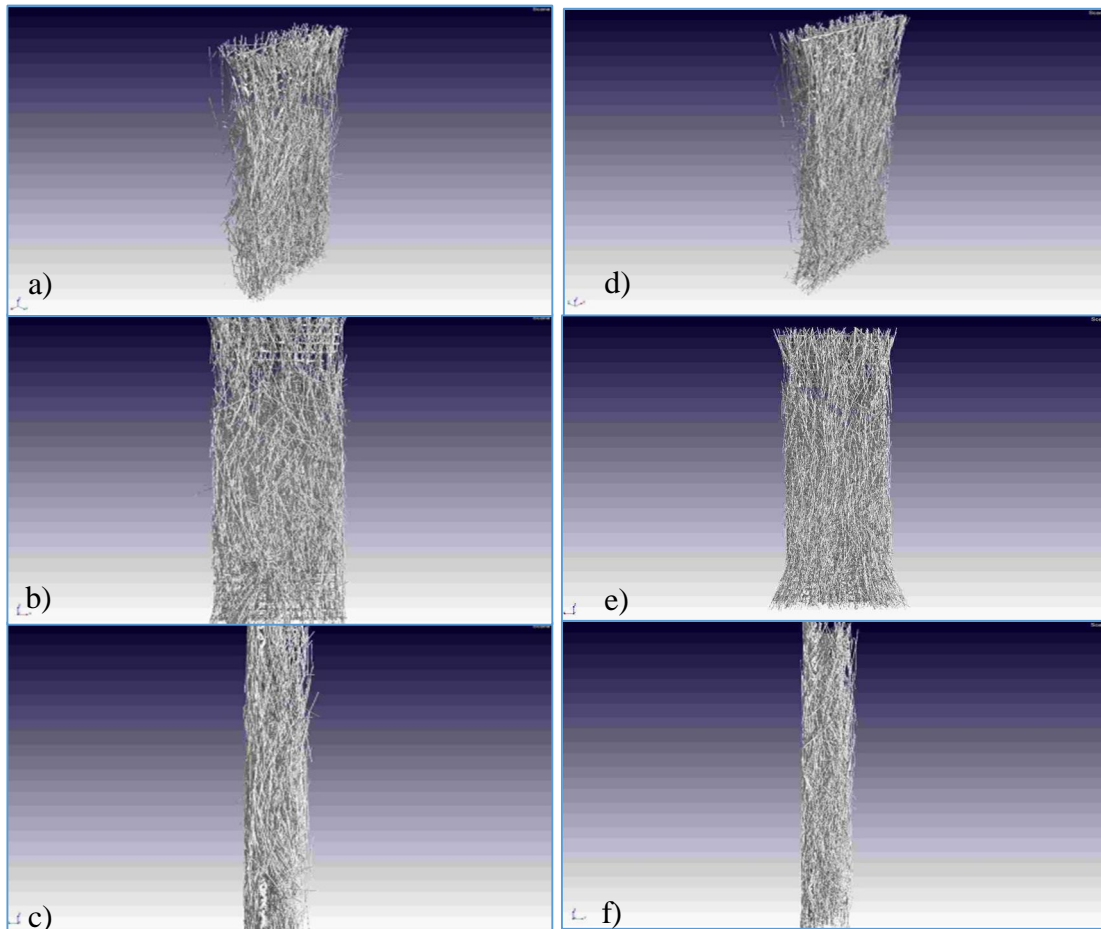
Figure 6-9: Overall steel fibre dispersion on: (a) TS4 M2 3D view; (b) TS4 M2 face view; (c) TS4 M2 side view; (d) TS4 M3 3D view; (e) TS4 M3 face view; (f) TS4 M3 side view.

The steel fibre dispersion in the top view of the specimen at the major crack opening plane is shown in Figure 6-10. On the cross-section, the total numbers of steel fibres are 216 in TS4 M2 while 286 in TS4 M3. The 40 mm thick notched dumbbell shaped specimen contains 1012 steel fibres on its major crack opening plane, which is equivalent to 211 steel fibres on the plane of 16 mm thick un-notched dumbbell specimens. The lower value set of similar steel fibre numbers of 216 in TS4 M2 and 211 in converted steel fibre from 40 mm thick notched dumbbell shaped specimen, shows that the lower value set of tensile strength in TS4 is more representative, while the higher value set tensile strength in TS4 is caused by higher steel fibre content.

For the first crack tensile strength, the increment of 32.4% steel fibre content in TS4 M3 results in a 35.3% higher strength than that of TS4 M2, where the increment rate between the

number of steel fibres and first crack tensile strength is similar. Such a finding differs from most researchers that steel fibre does not help to improve UHPC first crack tensile strength. Here, it is postulated that the steel fibres are already involved in resisting the shrinking and are pre-stressed before testing, which corresponds to the mix design philosophy in this research. The peak tensile strength reflects the steel fibre number and orientation together with the bond between steel fibre and matrix across the major crack plane.

The higher volume of steel fibres in TS4 M3 is mainly caused by the second layer of casting. After the second layer of filling, there may still be a gap between the top surface of fresh UHPC and the top surface of the mould. A trowel is then used to push fresh UHPC from the scoop to fill this gap, which may introduce more volume of steel fibres. All above phenomena further indicate that the dimension of the 16 mm dumbbell shaped specimen is most likely too small to be representative of UHPC in structural elements.
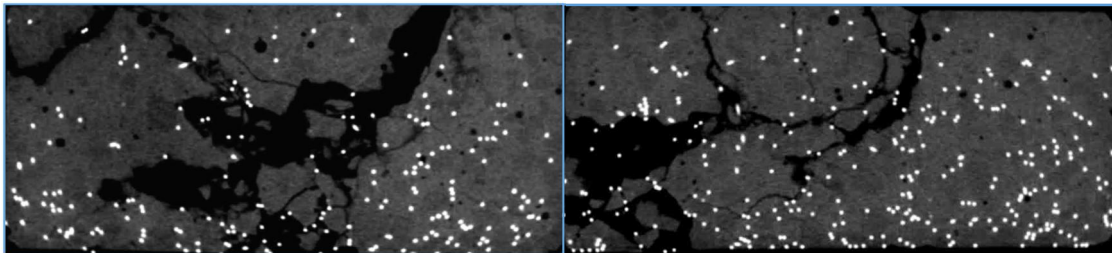
Figure 6-10: Steel fibre dispersion in crack opening location: (a) TS4 M2; and (b) TS4 M3.

● Comparison of the tensile strength between different batches

As introduced in compressive test, TS4 is de-moulded in 24 hours while TS5 is de-moulded in 48 hours and both of them use M#1. The sand in TS6 is M#2 but under the same mix design as that of TS4 and TS4 as shown in in Table 6-4.

Compared with TS6 and the lower tensile value in TS4, it can be seen that the peak tensile strengths are similar but that the tensile crack strength in TS6 is much higher. The peak tensile strength is mainly determined by the number of steel fibres across the major crack opening plane, which shows that the number of steel fibres in TS6 is similar to that of the lower set in

TS4. The higher first crack tensile strength in TS6 can be postulated to be the fine sand particles causing less differential stress in UHPP, which both increase tensile crack strength and compressive strength.

A slightly higher first crack tensile strength and tensile peak strength are found in TS5 than that of lower value set in TS4. The higher peak tensile strength in TS5 shows that the number of steel fibre is higher than that of the lower value set in TS4, which may be caused by the second layer of casting. The higher first crack tensile strength may also be caused by the relatively longer moulded period of 48 hours besides the higher steel fibre content.

6.2.5.3.2. The tensile behaviour for 16 mm thick dumbbell shaped specimen

The tensile behaviour for 16 mm thick dumbbell shaped specimen is similar to that of 40 mm dumbbell shaped specimen. It can be seen from Figure 6-11 (a) that the tensile behaviour for 16 mm thick dumbbell shaped specimen also experienced four phases as indicated by Graybeal and Baby (2013:177) with the multiple cracks shown in Figure 6-11 (b). This phenomenon further shows that only 1.5% of steel fibre by UHPM volume can still achieve strain hardening behaviour of UHPC.
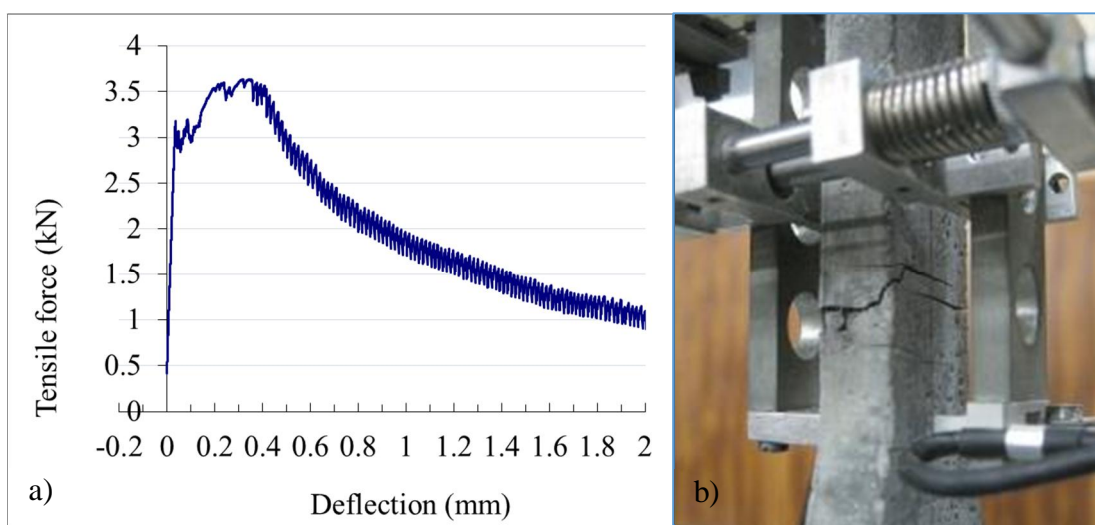
Figure 6-11: Tensile behaviour for 16 mm thick dumbbell shaped specimens: (a) Typical force-deflection curve; and (b) Crack pattern.

The wiggles for the descending of force deflection curve can be postulated to be caused by the steel fibre pull-out. The steel fibre orientation, steel fibre embedment, length of steel fibre in the major crack opening plane and the bond between steel fibre and matrix, all contribute to such phenomenon. When a single steel fibre pulls out, which can be heard during the test with a sound, the tensile resistance shows a sudden drop. The rest of the steel fibres still have not reached the de-bonding stage as shown in Figure 2-14 and are still able to provide higher tensile resistance with larger slip. Under the constant strain control of loading rate, the tensile resistance increases until the next single fibre pull-out occurs where the following sudden drop in tensile resistance occurs. Because the 16 mm thick dumbbell shaped specimen contains much fewer steel fibres than that of 40 mm thick dumbbell shaped specimen, the amplitude of wiggle appears larger than that of larger sized specimen as shown in Figure 6-4 because of its relatively low overall tensile resistance caused by relatively lower number of steel fibres.

6.2.5.4. Concluding remarks on tensile behaviour of 16 mm thick un-notched dumbbell shaped specimens

Through the comparison of tensile data, it can be seen that the difference in tensile strength is mainly caused by the higher steel fibre content. By counting the steel fibre across the plane where the major crack opens, the lower value set of TS4, with an average first crack tensile strength of 5.43 MPa and peak tensile strength of 9.05 MPa, appears to be more representative for local UHPC with M#1 sand. The M#2 sand can help to improve the first crack tensile strength but the tensile peaks strength is mainly determined by the steel fibre content under the same casting methods.

A higher steel fibre content results in a higher tensile crack strength and tensile peak strength as shown in Table 6-4 (TS4). The higher first crack tensile strength shows that the number of steel fibre does help to improve the first crack tensile strength which reflects the mix design philosophy in this research that the steel fibre is already pre-stressed before the test started.

Even if great care is taken, the casting of the second layer can still cause the changing in steel fibre content in 16 mm thick dumbbell specimens. The steel mesh can provide a solution for un-notched dumbbell shaped specimen DTT, but the crack can still be observed in the transition zone in some specimens. All the above evidence shows that 16 mm thick dumbbell specimen is not ideal for UHPC DTT.

6.2.6. Comparison of direct tensile test results with other researchers

In order to better understand the UHPC tensile behaviour, the UHPC results from this research is used to compare with other researchers as shown in Table 6-5. It can be seen from Table 6-5 that the UHPC in this research, with only 1.5% of steel fibre by UHPM volume, provides a much higher tensile strength increment between first crack tensile strength and peak tensile strength, while first crack tensile strength is lower than the results obtained by other researchers.

The relatively lower first crack tensile strength reflects the non-ideal materials used in this research as elaborated on in Chapter 3, which cause the lack of UHPP strength as elaborated on in Chapter 5. Even if the steel fibre follows the mix design philosophy in this research that is already pre-stressed before the test, the resistance between steel fibre and matrix is driven by the shrinkage. The shrinkage increases first, then the clamping pressure starts to increase the bond between steel fibre and matrix to confine further shrinkage increment. Therefore, lower first crack tensile strength is obtained in local UHPC even with the help of steel fibre.

The higher increment between first tensile crack strength and peak tensile strength for UHPC in this research also reflects a high clamping pressure. It can be seen that the 1.5% of steel fibre by UHPM content in this research achieves a higher tensile increment rate than other researchers even if their UHPC contains 2% of steel fibre by UHPM volume.

By comparing the tensile strength differences between 40 mm thick notched dumbbell shaped

specimens and 16 mm thick un-notched dumbbell shaped specimens, it can be seen that the 16 mm thick dumbbell shapes achieve slightly higher tensile strength. The main reason for this higher increment in tensile strength is the orientation of steel fibres. It can be seen from Figure 6-5 and Figure 6-9 that the random casting of 40 mm thick dumbbell shaped specimen makes the alignment of steel fibre not as ideal as that of layer casting of the 16 mm thick dumbbell shaped specimen.

As for the elastic modulus, it is difficult to establish the relationship between compressive strength, tensile strength and elastic modulus with limited tests. However, the un-sealed cube specimen caused much lower compressive strength as well as elastic modulus, but retained similar tensile strength as the dumbbell specimen was covered with plastic sheeting during the moulded period.

The above analyses provide the evidence that the mix design philosophy in this research makes better use of steel fibre in tension. In addition, it can be seen that the UHPC tensile strength is not really proportional to UHPC compressive strength, but more related to the mix design, material property, steel fibre volume, and casting methods.

Table 6-5: The DTT results from different researchers.

Tensile strength (MPa)				Steel fibre		Compressive strength (MPa)	Filling methods	Reference
First crack	Peak	Increased rate (%)	E modulus (GPa)	Content (%)	Length (mm)			
6.67	9.18	37.6	62.8	2	13	192	Single-point cast allow UHPC flow along the length of moulds	(Graybeal & Baby, 2013:177)
6.18	10.53	70.4	63.9	2.5	20	213		(Graybeal & Baby, 2013:177)
9.13	11.49	25.8	X	1	13	X	X	(Park *et al*. 2012:172)
				0.5	30			
7.95	9.07	14.1	45.55	2	13	150.56	X	(Hassan *et al*. 2012:874)
10.93	16.05	46.8	X	2	13	X	X	(Kang & Kim, 2011:1001)
5.29	8.56	61.6	34.5	1.5	13	124.3	Random casting	This research t = 40 mm
5.43	9.05	66.7	55.3	1.5	13	142.9	Layer casting	This research t = 16 mm

6.3. FLEXURAL TEST OF UHPC

6.3.1. Introduction

Besides the tensile behaviour obtained DTT from previous sub-section, the UHPC bending behaviour was also studied. Two batches of UHPC mixes with and without 6.7 mm aggregate were used to obtain flexural strength under two loading rates. The standard four point flexural tests were implemented.

6.3.2. Test preparation.

6.3.2.1. The loading rate

The flexural tests were performed according to ASTM C1609. The loading rate recommended in this standard was 0.05 to 0.10 mm/min. But in this research, a much lower loading rate of 7.5 times lower was chosen to simulate a more quasi-static test environment. Therefore, two loading rates of 0.10 mm/min and 0.013 mm/min were selected.

6.3.2.2. Test equipment and specimens

A Zwick Materials testing machine (MTM) with the capacity of 250 kN is used for flexural tests. The test setup is based on ASTM C1609 with the deflection control from an LVDT shown in Figure 6-12. The Zwick used can be controlled by only one LVDT signal. Two LVDTs should be used, one on each side of the specimen, but only one LVDT was eventually used to measure the deflection. For the compressive test, a Contest compressive materials testing machine is used as introduced in the previous chapter.

The flexural test beams with dimensions of 100×100×500 mm, and 50 mm cubes were used

for compressive testing as before. A 50 L pan mixer with lid was used, since a large volume of UHPC is needed.

Figure 6-12: Test setup for four point flexural test.

6.3.2.3. Specimen preparation

After vibrating the beam for two minutes and the cube for one minute, a plastic cover was used to prevent moisture losses as most researchers did. The specimens were stored in the laboratory and de- moulded 48 hours after casting. The specimens were then stored in water tank with the temperature of 23 ± 2 ℃ until the test at an age of 28 days.

Two minutes of vibration may cause settlement of steel fibres in beams. The beam element was rotated 90 degrees with the casting direction. This means that if fibres settled downward during casting and vibration, the rotated orientation in the flexural test would prevent a biased response. In Figure 6-12, the formed face (bottom of mould) is indicated to illustrate the test orientation of the beam. Therefore, the settlement of steel fibre will not have a big influence

on the UHPC flexural behaviour.

6.3.3.   The UHPC flexural behaviour under two loading rates

The flexural strength for four point flexural tests were calculated according to Equation 6-1 from ASTM C1609 and summarized in Table 6-6, with the corresponding force deflection curve as shown in Figure 6-13. It can be seen that the different loading rate does have an effect on first crack flexural strength and peak flexural strength for UHPC with and without 6.7 mm aggregate. Both two batches of UHPC show deflection hardening behaviour with 1.5% of steel fibre by UHPM content. The multiple cracks can be observed on the bottom surface of the beam during the test as shown in Figure 6-14.

When comparing the tensile strength between the flexural test and DTT, it can be seen that a significant overestimation is obtained from the flexural test, which was also found by most researchers. Except the size effect, the casting methods and support conditions also influence flexural strength (Wille & Parra-Montesinos, 2012:379). Therefore, the flexural test is not recommended to obtain tensile behaviour of UHPC.

The cement used for flexural test is the same as the UHPC strength of 168 MPa was achieved. For UHPC without stone (BFT1) the average UHPC strength of 150 MPa was achieved, which is lower than that of 168 MPa. For UHPC with stone (BFT2), the average strength is 164 MPa which is similar to the previous test of 161 MPa. The spillage is the main reason that causes reduction in UHPC strength in BFT1, which can be observed during the dry mix period. The slump flow also reflects the spillage of dry powder. The slump flow for UHPP without stone (BFT1) achieves a slump flow of 357.5 mm, while the slump flow for UHPP with stone (BFT2) achieves 336 mm, which is same as that of T(20HE)1 as shown in Table 5-2.

112

Table 6-6: The flexural test results under two loading rate.

Batch No.	Beam No.	6.7 mm Agg (vol %)	Loading rate (mm/min)	First crack flexural strength (MPa)				Peak flexural strength (MPa)				Compressive strength (MPa)		
				f_{cf}	Avg	No.	Std	f_{pf}	Avg	No.	Std	f_{cu}	No.	Std
BFT1	#1		0.1	14.2	13.8	2	0.49	14.5	14.3	2	0.30	149.5	3	5.9
	#2			13.5				14.0						
	#3		0.013	12.7	12.6	2	0.05	16.1	15.5	2	0.77			
	#4			12.6				15.0						
BFT2	#1	12	0.1	11.7	11.4	2	0.36	15.8	15.7	2	0.12	164.4	3	5
	#2			11.2				15.7						
	#3		0.013	11.7	11.8	2	0.14	16.6	17.2	2	0.82			
	#4			11.9				17.8						

The formula for calculation of first cracking strength according to ASTM C1609 is as follows:

$$f_{cf} = \frac{PL}{bd^2}$$ (6-1)

Where:

f $_{cf}$= the first crack flexural strength, MPa;

P = the load at first crack formation, N;

L = the span length, mm;

b = the average width of the specimen at the fracture, mm;

d = the average depth of the specimen at the fracture, mm;
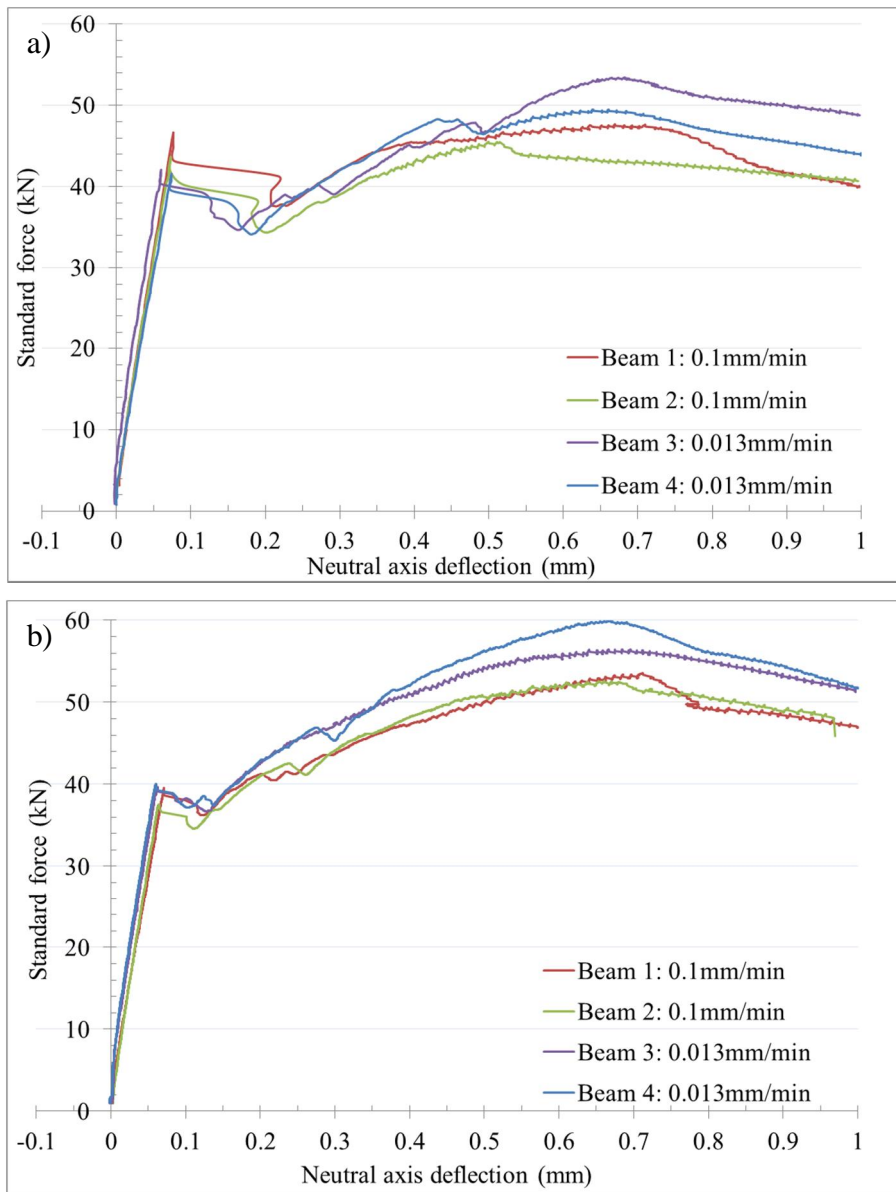
Figure 6-13: Force deflection curve for four point flexural test: (a) BFT1; and (b) BFT2
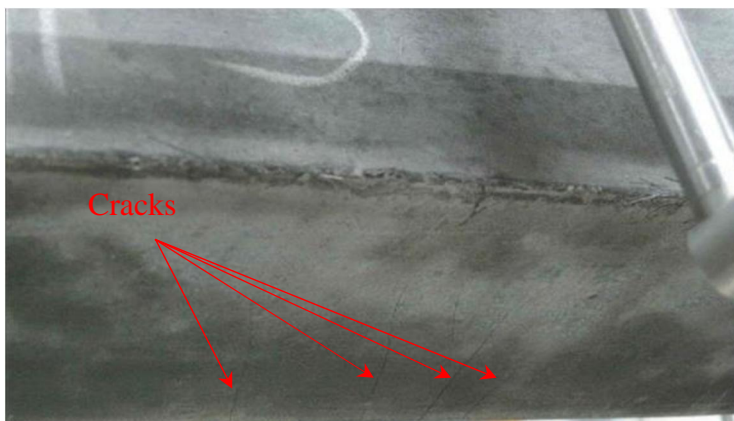
Figure 6-14: Multi-cracks of the beam during the flexural test.

6.4. CONCLUSIONS

This chapter compared the tensile behaviour of UHPC from DTT and the flexural test. Due to the overestimation of flexural test, the DTT (with great care) is recommended to obtain UHPC tensile behaviour. In this research, with only 1.5% of steel fibre by UHPM volume, the tensile strain hardening behaviour of UHPC is achieved.

For DTT, the dumbbell shaped specimen with the thickness of 40 mm was found to achieve more reliable tensile strength with a low standard deviation compared with that of 16 mm thickness. The first crack tensile strength of 5.29 MPa and the peak tensile strength of 8.56 MPa are obtained for 40 mm thick dumbbell shaped specimens that can better represent the tensile behaviour for real application. The small size of the 16 mm thick dumbbell specimen is difficult to control and causes higher steel fibre content in some specimens that results in high tensile strength, which is not recommended for DTT for UHPC.

But the higher first crack tensile strength in a higher set of TS4 shows that the number of steel fibre also helps to improve the first crack tensile strength that further reflects the UHPC mix design philosophy that steel fibre is pre-stressed before the test started. The relatively higher peak tensile strength, compared with the first crack tensile strength, shows that steel fibre is better used under the mix design philosophy developed for this research.

115

Chapter 7: Post tensioned box girder test and analysis

7.1. INTRODUCTION

Once the compressive strength and tensile strength of UHPC are characterised, a large scale physical experiment is executed as verification of structural element behaviour. A post tensioned box girder is manufactured and tested to examine its flexural behaviour on a structural level. This chapter will introduce the design, casting, testing and data analysis of this post tensioned box girder.

7.2. POST TENSIONED BOX GIRDER PREPARATION

Even if the cross-section and span length of bridge girders can vary according to the design request, the calculation of fundamental design parameters, such as bending moment and shear resistance must be larger than the applied load. The AASHTO box girders are typically used for short to medium span highway bridges up to a span length of 38 meters according to Hassoun and Al-Manasee (2012). Since there has been no design code available for UHPC until now, a rough check is applied with current design codes. SANS10100-1, TMH7 and AASHTO LRFD are used by assuming UHPC follows the general concrete design assumptions, for the purpose of initial dimensioning.

7.2.1. Preliminary design of post tensioned box girder

In order to test bending behaviour of a post tensioned box girder, the dimension of the box girder is selected through preliminary calculation, considering the laboratory equipment capacity as well as reference from standard girder types. The cross-section dimension of the box girder is selected according to AASHTO Standard Beam BI-48 box girder, which can accommodate a span length of 28 meters for normal concrete that meets the span requirement

for a general highway bridge. Based on the available moulds in the laboratory, the cross sectional width and height are reduced by a ratio of approximately 2.5 from that of the BI-48 box girder. The flange and web of the box girder require a certain thickness of UHPC cover to protect post tensioning tendons and stirrups, which cannot be simply proportioned. The cross-sectional dimensions are then determined as shown in Figure 7-1 and the length is limited to be less than 2400 mm due to available steel moulds.
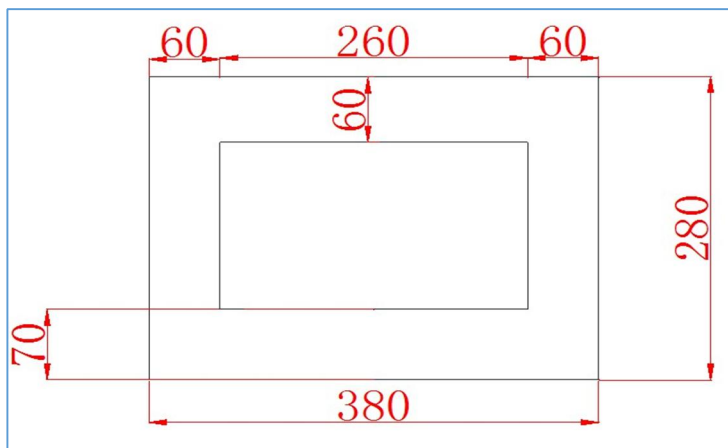
Figure 7-1: Cross-sectional dimension for post tensioned box girder in mm.

Once the cross-sectional dimensions and the span length of the box girder have been determined, the preliminary check on bending resistance and shear consideration are calculated as shown in Appendix D. Three 12.7 mm diameter post tensioning tendons are used to apply a 180 kN post tensioning force. The stirrups are chosen to be 10 mm diameter mild steel bars at a spacing of 90 mm. No other tension steel was included apart from the post tensioning tendon, implying that a special technique was required to keep the stirrups in position.

7.2.2. Design and casting and curing for post tensioned box girder

Based on the preliminary design of the post tensioned box girder, the end timber plate and the inner timber box mould are designed and the dimensions are shown in Figure 7-2. The post tensioned box girder was successfully manufactured through the following two steps:

Step 1: The stirrups were fixed and the post tensioned tendon was fixed to the Section I of the end plate as shown in Figure 7-3 (a). Fresh UHPC was cast to fill the mould up to a level of 70 mm high and a poker vibrator was used to vibrate fresh UHPC for compaction. Similarly, 50 mm cubes and 40 mm thick dumbbell shaped tensile specimens were prepared from the UHPC batch and vibrated on the materials laboratory vibrating table.

Step 2: The inner timber box mould was located and the end plate Section II was fixed in position as shown in Figure 7-2. Then the rest of the UHPC was cast up to the top surface and poker vibrated right after the casting was finished.
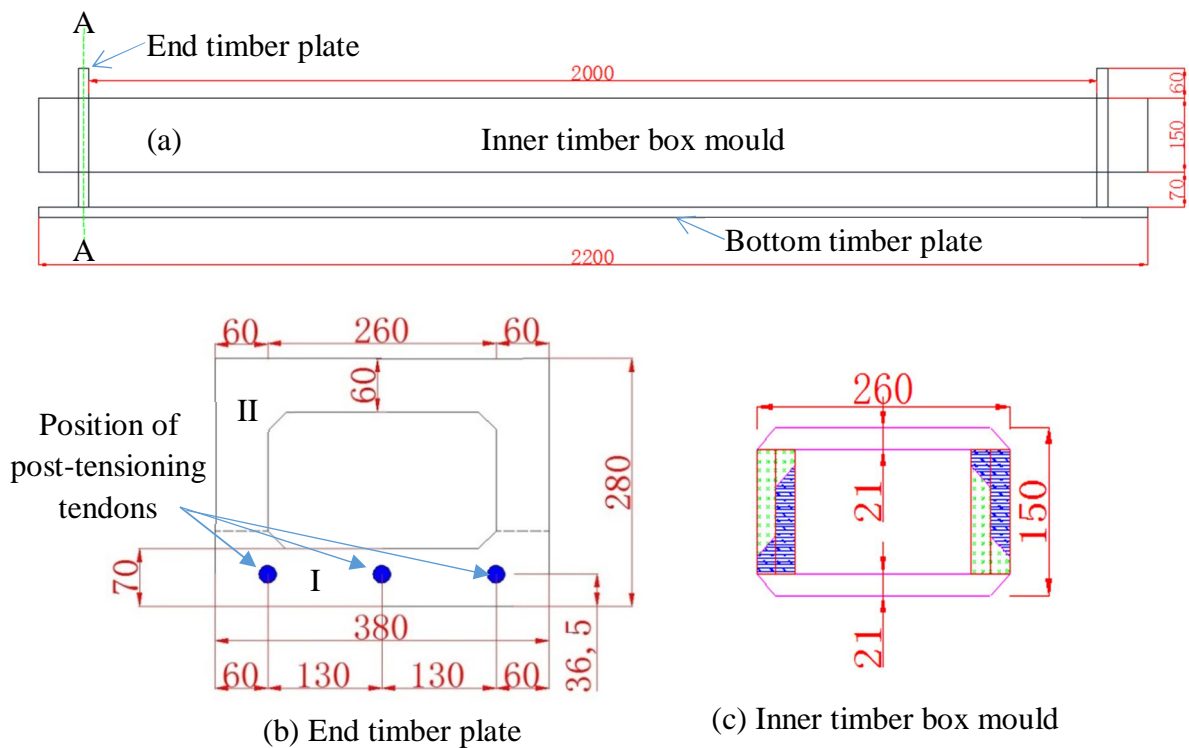
Section A-A

Figure 7-2: Illustration of the post tensioned box girder mould.

After casting the post tensioned box girder, no top cover was applied, because of the stirrups being held in position by the timber bar as in Figure 7-3. The steel moulds were stripped two days after casting and wet blankets were used to cover the girders for moisture curing.

118

Figure 7-3: Post tensioned box girder: (a) before casting; and (b) after de-moulding.

7.2.3. Applying the post tensioning force

The post tensioning force was applied one day before the box girder flexural test, i.e. at the age of 27 days, to avoid tendon relaxation and to enable UHPC to obtain sufficient strength. It is acknowledged that this might not be practical in all cases in construction projects. Similar to the general post-tensioning anchors, the anchoring system used included a bearing plate, anchor head and wedge as shown in Figure 7-4 with the tendon location as shown in Figure 7-2 (b). The post tensioning procedure followed the following steps.

Step1: The tendon surface was cleaned from grease where the anchorage was located. Then the bearing plate, anchor head and wedge were placed in position.

Step2: The hydraulic jack was clamped to the tendon and the jack head attached to the wedge. Then a post tensioning force of 60 kN was applied. The jack was then released so that the anchor head could lock the wedge by post tensioning force.

119
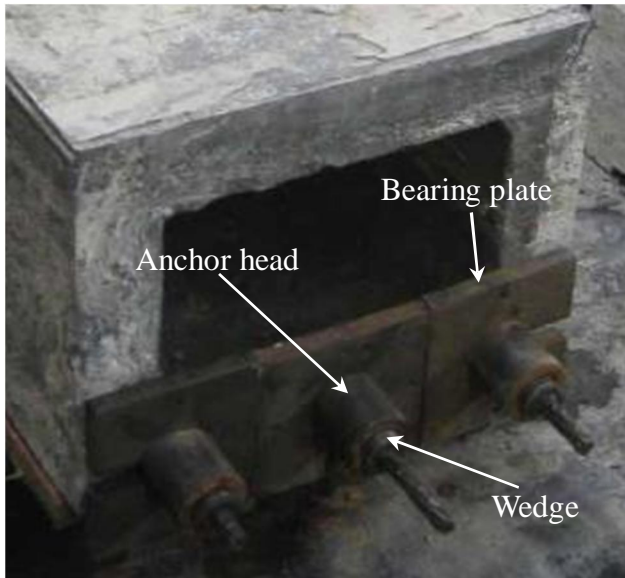
Figure 7-4: Sketch for post-tensioning anchors.

The above mentioned two steps are generally applied in local industry for long span post tensioned elements of say 24 m. The slip is approximately 4 mm due to the locking of the anchor wedge so that the post tensioning force loss can be roughly controlled. However, it was difficult to control the exact post tensioning force due to the limited post tensioning force and limited span length of the laboratory specimen in this case. So, one more step was applied by attaching the jack head to the wedge through a load cell and applying a 60 kN post tensioning force. The load cell reading started at approximately 40 kN and slowly reached 60 kN within approximately 1 minute. After applying post tensioning force, the tendons are not grouted.

7.2.4. Test setup for post tensioned box girder

Two post tensioned box girders were manufactured with nearly the same geometry as shown in Appendix E. The slight difference in dimensions is due to the imperfection of the moulds. The post tensioned tendons were of the same batch and the post tensioning force was applied with the same procedure. Therefore, the post tensioning force was supposed to be the same for two post tensioned box girders.

A four point bending setup as shown in Figure 7-5 was used. The Instron materials testing machine with the capacity of 500 kN was used to apply the load. Through a spreader beam and two square steel bars, the jack force was transferred into two line loads on the box girder. Four LVDTs were located at the line loads and end supports to track the displacements into a Spider8 data acquisition device. The steel box support with roller was used to minimize the friction between the post tensioned box girder and support.
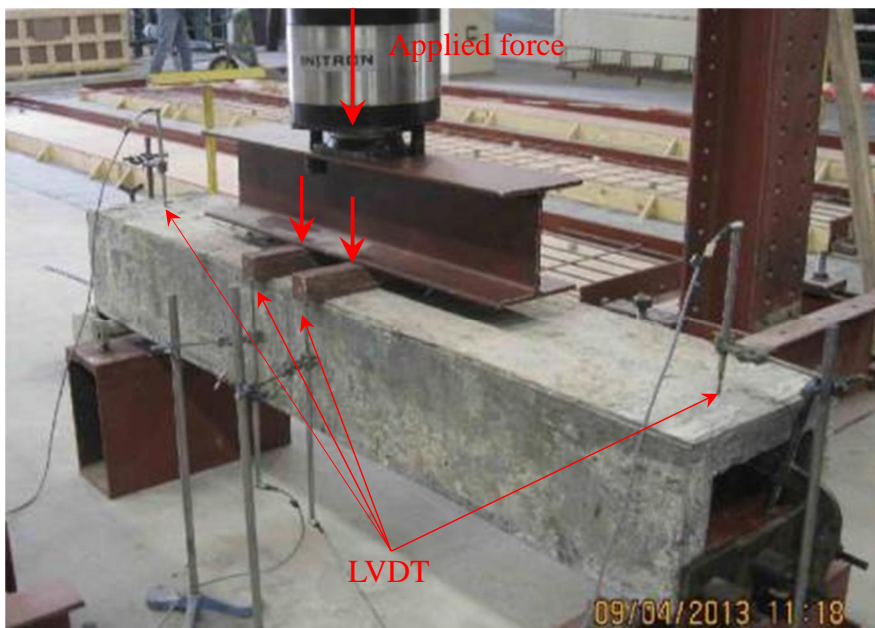
Figure 7-5: Test setup for post tensioned box girder.

The UHPC bursting/splitting failure at the post tensioning force transfer was considered before testing. The bearing plate is thicker than the web thickness so that the post tensioning force is supposed to be uniformly transferred to the bottom flange of the post tensioned box girder. Even though a theoretical calculation could confirm that the bursting/splitting would not occur, clamps were still used at each end of post tensioned box girder for safety.

In order to complete the test within approximately 30 minutes, the deflection loading rate was set as follows: a loading rate of 0.5 mm/min from 0 to 3 mm central deflection, followed by a loading rate of 2 mm/min up to 30 mm deflection, and finally a loading rate of 4 mm/min was set up to 80 mm when the test stopped, where the total testing time was 32 min.

121

7.3.   FLEXURAL BEHAVIOUR OF POST TENSIONED BOX GIRDER

The force displacement curve for post tensioned box girder 1 and 2 is shown in Figure 7-6 and Figure 7-7 respectively. Besides a sudden drop seen in the force deflection curve, a sound could also be heard during the test, indicating when the first crack occurred. The corresponding first crack force is 122.8 kN for box girder 1 and 121.75 kN for box girder 2 as shown in Table 7-1.
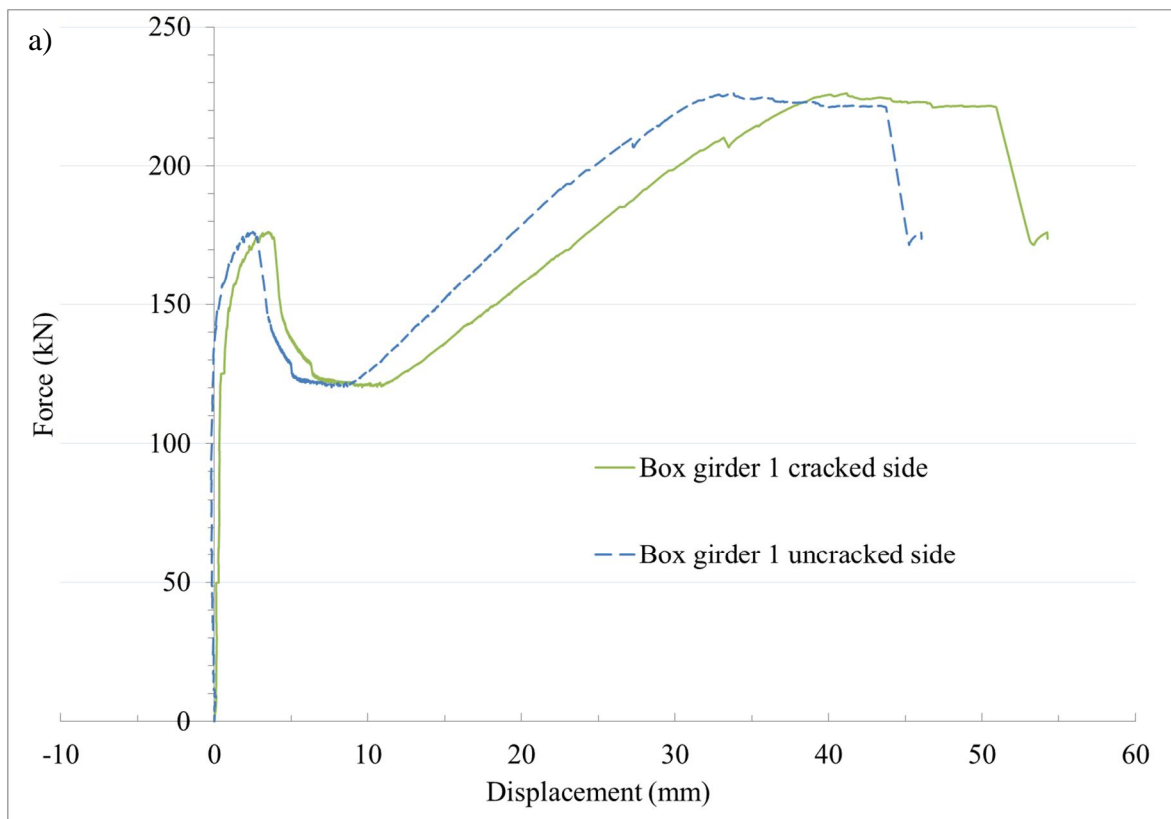
Figure 7-6: Box girder 1: (a) Force deflection curve; and (b) Crack opening photo.

122
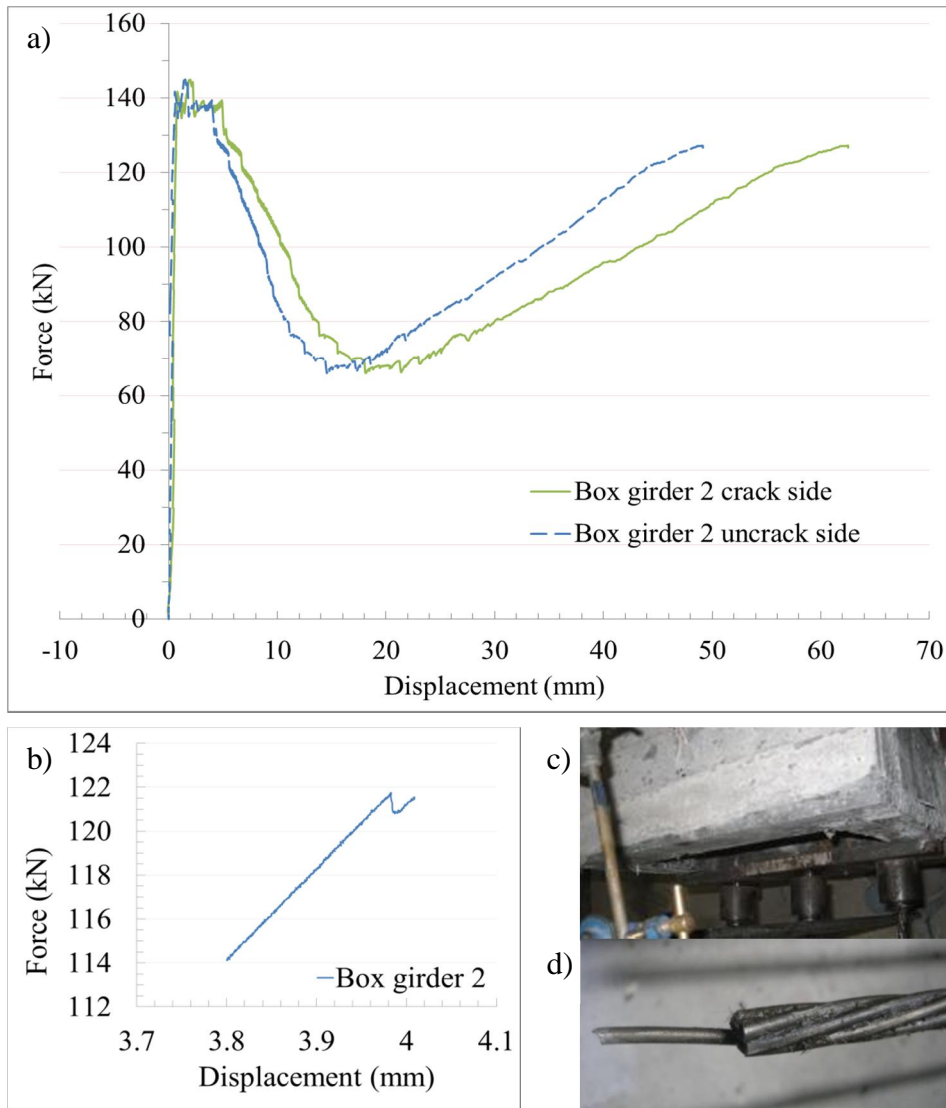
Figure 7-7: Box girder 2: (a) Force deflection curve; (b) Zoomed curve in order to view first crack; (c) End anchor after the applied force was released; and (d) Single wire pull-out.

Table 7-1: Post tensioned box girder first crack force and bending moment.

Girder No.	Cracking force (kN)	Bending moment (kNm)			Theoretical calculation of post tensioning force (kN)	Assumed first crack tensile strength	
		Applied load	Dead load	Total		Value (MPa)	Reference
Box girder 1	122.8	49.4	0.675	50.08	139.54	5.13	40 mm thick DTT min
					128.2	5.53	40 mm thick DTT max
					134.9	5.29	40 mm thick DTT average
					-66.3	12.6	Flexural test in Table 6-6
Box girder 2	121.75	48.7	0.675	49.38	135.3	5.13	40 mm thick DTT min
					124	5.53	40 mm thick DTT max
					130.8	5.29	40 mm thick DTT average
					-51.9	11.8	Flexural test in Table 6-6

It can be seen that the post cracking behaviour is different for the two post tensioned box girders, which is caused by the slipping of post tensioning tendon. For post tensioned box girder 1, a sudden drop in force when the displacement is approximately 60 mm is caused by a sudden slip of the post tensioning anchor. It can be seen from Figure 7-6 (a) that there is a slight change in displacement when the force is approximately 50 kN, which was caused by the uneven top surface of the box girder. The force deflection curve and the slipping of anchor are shown in Figure 7-7.

The first crack for box girder 2 can be observed in Figure 7-7 (b) with a sound during the test. The major crack in box girder 2 is similar to that of box girder 1 in that the crack develops along the stirrup right beneath one load point.

The slipping of the end anchor is postulated to be the grease around the tendon not having been cleaned properly, which could have been avoided. Limited post tensioned force may cause further slipping of the end anchor due to the lack of friction force. A single wire fracture is not supposed to happen because the tendon is still far from its limit. However, the post tensioning industry needs to follow standard operational procedures for the quality control.

7.4.   POST TENSIONED BOX GIRDER DATA ANALYSIS

7.4.1.   The compressive and tensile strength of post tensioned box girder

The compressive strength of the post tensioned box girder is determined to be 124.3 MPa from cube tests on specimens prepared from the same batch and cured in similar conditions as the beams. Such reduction of compressive strength from the UHPC developed earlier in the research is considered to be caused mainly by the unsealed condition during the moulded period based on the following reasoning: The trial mix for the post tensioned box girder achieved 163.4 MPa under similar lab temperature during the moulded period, as elaborated on in

Section 5.5.1. Secondly, after two days of de-moulding, the curing condition only has a slight effect on UHPC strength as elaborated on in Section 5.5.3.

The tensile behaviour is characterised from 40 mm thick dumbbell shaped specimens as elaborated on in Chapter 6. The first crack tensile strength and peak tensile strength is 5.3 MPa and 8.6 MPa respectively.

7.4.2. Post tensioned box girder linear elastic stage analysis

In order to estimate the actual post tensioning force that was applied to the post tensioned box girder, elastic theory is used to calculate the behaviour up to the first crack. This is required, as no strain gauge or other monitoring of actual strain in the tendon was applied. By assuming UHPC as homogeneous material and applying the Euler-Bernoulli beam theory, the bending and axial stress need to be balanced. Spread sheet calculation is applied to adjust the tendon force so that two equilibrium conditions are met: a) compression force is equal to tensile force; b) the corresponding bending moment is equal to the bending moment caused by the applied load and self-weight. In this way, for the given first crack tensile stress at the bottom extreme fibre of the box girder, the corresponding post tensioning force can be calculated. The calculation results are listed in Table 7-1 based on the actual measured post tensioned box girder dimensions from Appendix E and the detailed procedure was listed in Appendix F.

It can be seen from Table 7-1 that the first crack tensile strength from DTT results in a possible post tensioning force in the range between 120 kN and 180 kN, which is a reasonable value as described in Section 7.2.3. However, when applying the flexural strength value from the 100×100×500 mm beam bending test as shown in Table 6-6, the post tensioning force is negative. This further indicates the overestimation first crack tensile strength calculated from the flexural test as elaborated on in Chapter 6.

The calculated post tensioning force in the two box girders differs by approximately 4 kN for the assumed first crack tensile strength as shown in Table 7-1. Such a difference can be postulated to be the imperfection of the post tensioned box girder dimension and the anchor of the post tension tendon.

7.4.3. Post tensioned box girder nonlinear analysis

Once the first crack occurs, the linear theory cannot be applied for flexural analysis and the nonlinear analysis is required. According to, for instance Menin *et al*. (2009:166), a smeared crack model provides an efficient way to analyse bending behaviour of reinforced beams. The FE software Diana is used for analysing the bending behaviour of the box girder. 2D plane conditions are considered to be sufficiently representative of the girder and the linear softening smeared, and a rotating cracking model is used, which fits the data obtained from this research well. The stress-strain relationship in the crack is defined in Equation 7-1. With the mesh size set to be 20 mm, the input parameters for FE analysis are listed in Table 7-2. The fracture energy is calculated through numerical integration of the stress-inelastic deformation response from DTT results as shown in Figure 7-8. The input parameters in Table 7-2 use mean values of the four tested dumbbell shaped specimens. The FE model is shown in Figure 7-9 using 2D plane stress model with Quadratic 8 element where symmetry is used with corresponding boundary conditions, post tensioned force and applied load

Table 7-2: Value of post tensioned UHPC box girder input parameters.

Input model parameter	Value	Unit
Fracture energy	15.646	mJ/mm^2
Tensile strength	8.56	MPa
E modulus	34500	MPa
Poisson's ratio	0.2	
UHPC density	2.39E-09	T/mm^3
Post tensioned force	134900	N

$$\frac{\sigma_{cr}(\varepsilon_{cr})}{f_t} = \begin{cases} 1 - \dfrac{\varepsilon_{cr}}{\varepsilon_{ult}} & \to \mathbf{0} < \varepsilon_{cr} < \varepsilon_{ult} \\ 0 & \to \varepsilon_{ult} < \varepsilon_{cr} < \infty \end{cases} \tag{7-1}$$

Where:

ε_{cr}:   Crack strain;

ε_{ult}:   Ultimate strain;

σ_{cr}:   Crack stress, MPa;

f_t :   Tensile strength, MPa.
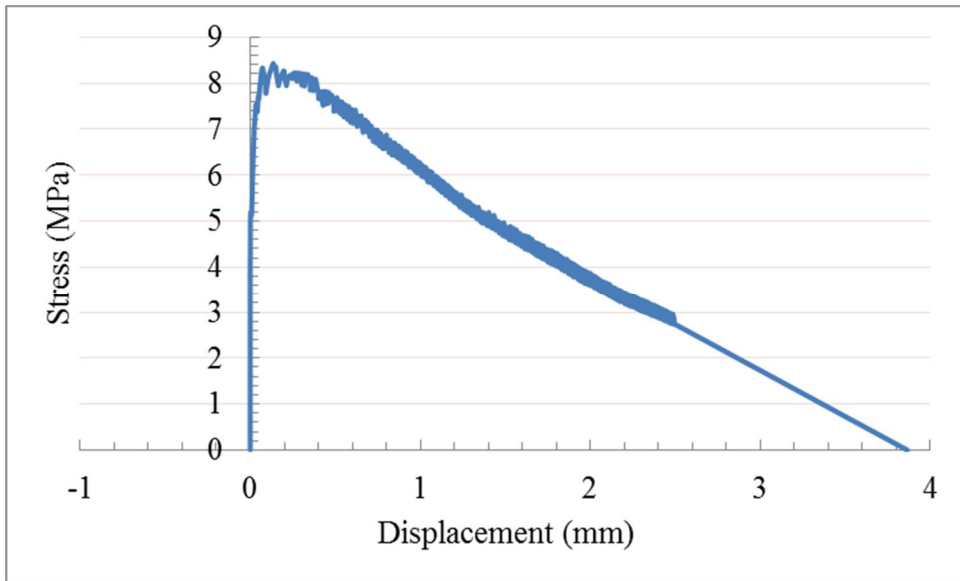
Figure 7-8: Stress displacement curve for fracture energy calculation.

Applied load   Post tensioning force   Boundary conditions
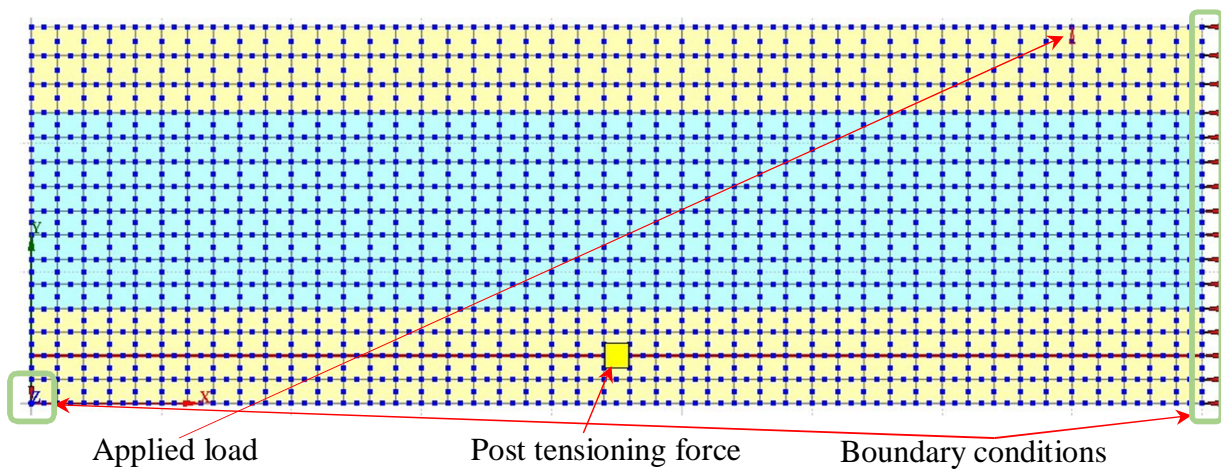
Figure 7-9: FE mesh with boundary conditions.

The FE results based on the various mesh sizes were used to compare with the experimental result as shown in Figure 7-10. The gradient of FE force-deflection result is larger than that of the experimental result after a deflection of approximately 10 mm, while the force deflection curves are quite similar up to the peak tensile strength of UHPC, reached at the deflection of approximately 4 mm. Two possible reasons could cause such differences: the first reason could be attributed to different deflections under the two load points, which caused reduced resistance during the box girder test; the second reason could be that the gradual slip of the tendon in the experiment had led to reduced post tensioning force (as found in box girder 2).

In order to investigate mesh objectivity, different mesh sizes of 5 mm, 10 mm 20 mm and 25 mm element side lengths (more or less square in all cases) were compared. Except for the softening stage immediately after the first peak, the force deflection curves under various mesh sizes are similar.

The softening of flexural resistance shown in Figure 7-10 was caused by the relatively low post tensioning force used for the laboratory tests for safety purposes. In order to simulate higher post tensioning force for the box girder, which is limited by crack formation on the top surface before onset of the downward flexural load, the post tensioning force is determined to be 595.2 kN. Such a force matches a total of four 12.7 mm tendons with each tendon loaded 80% of the maximum post tensioning force. The location of tendons remains the same as shown in Figure 7-2 (b). When fixing the post tensioning forces, the number of tendons is increased to compare the effect of total tendon area on the box girder flexural behaviour. The same FE analysis is performed based on 20 mm mesh size; the FE results are listed in Table 7-3 and shown in Figure 7-11.

128
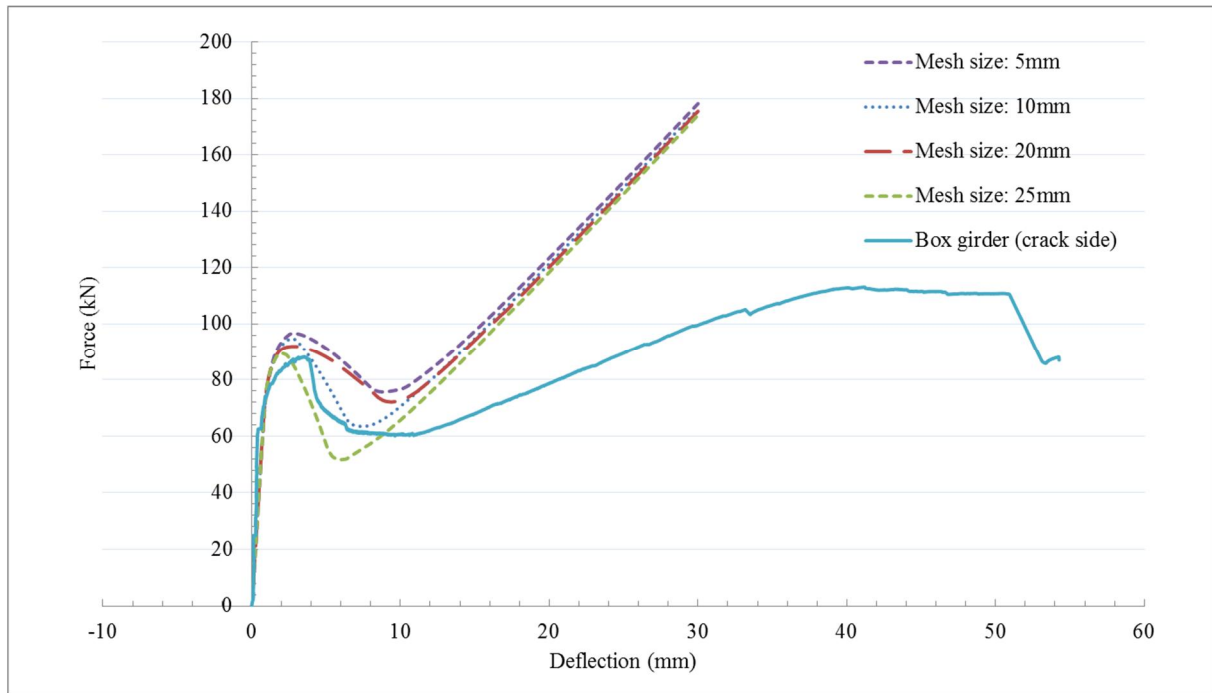
Figure 7-10: Force deflection curve between experimental results and FE analysis.

It can be seen from Figure 7-11 that an increase in the post tensioning force only has a limited increment in bending resistance, but the deflection hardening behaviour can be achieved. Increase in the total area of tendon provides a more efficient way to increase flexural resistance, which can be explained to be increased tendon area caused by a higher tensile force under the same elongation.

Besides the enlarged tendon area, the larger lever arm is also supposed to increase the total bending resistance. It can be seen from Table 7-3 that large tensile force results in higher compressive strength. But limited height confines better use of high compressive strength of UHPC. The real size girder is able to provide a higher lever arm and enough tendons, which help to better utilize the compressive strength of UHPC and the tensile strength of the tendon.

Table 7-3: Effect of post tensioning force and tendon number on flexural behaviour.

Test No.	Post tensioning tendon		Load point extreme top fibre of box girder		Tendon force (kN)	
	Applied force (kN)	Total No.	Deflection (mm)	Compressive strength (MPa)	Total	Each
1	595.2	4	30	56	621.02	155.26
2	595.2	12	30	85	1040.7	117.06
3	595.2	24	30	97.5	2180.94	87.87

The crack width from the FE analysis that corresponds to Figure 7-11 is shown in Table 7-4. The higher post tensioning force shifts the crack localization position from the load point to the middle section of the beam, which can be explained to be the improved box girder stiffness due to higher post tensioning force. However, the increased post tensioning force does not contribute to the crack opening width under the same deflection at load point. In addition, the increased post tensioning force has limited contribution to the flexural resistance, especially at relatively low deflection. Under the same post tensioning force, it can be seen that the increased tendon number both limits the crack opening width and increases the flexural resistance, which was caused by the enlarged tendon area. Although the crack widths are approximated from the smeared cracking computational results obtained in this dissertation, they are of significant importance for structural durability. Here, the maximum crack widths were approximated by multiplying the maximum smeared cracking strain with the crack band, which is the FE 'size', or square root of the element area.
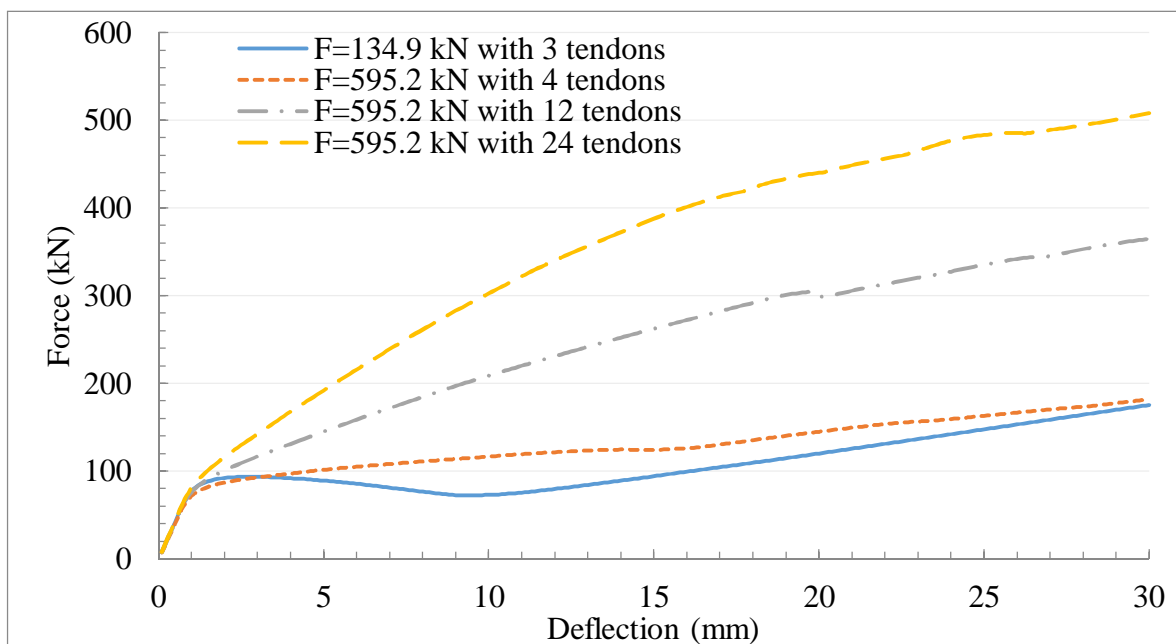
Figure 7-11: Force deflection curve from FE analysis between two post tensioned force.

Table 7-4: Crack width at the load point deflection of 1, 2, 5 and 10 mm for the post tensioned box girder from FE analysis.

Post tension force and tendon numbers	Deflection at load point	Crack width (mm) at		Corresponding reaction force (kN)
		Load point	Middle section of girder	
134.9 kN 3 tendons	1 mm	0.01	0.004	77.66
	2 mm	0.15	0.004	92.24
	5 mm	0.9	0.001	89.08
	10 mm	2.22	0	72.82
595.2 kN 4 tendons	1 mm	0.002	0.04	71.73
	2 mm	0.002	0.32	86.84
	5 mm	0.001	1.25	101.42
	10 mm	0	2.61	116.54
595.2 kN 12 tendons	1 mm	0.002	0.04	76.04
	2 mm	0.002	0.3	100.71
	5 mm	0.001	1.17	144.89
	10 mm	0.001	2.46	208.65
595.2 kN 24 tendons	1 mm	0.002	0.03	80.91
	2 mm	0.002	0.27	115.98
	5 mm	0.001	1.08	191.86
	10 mm	0.001	2.27	302.47

According to Park (2003), the AASHTO Type II UHPC girder under the four point flexural test with a height of 910 mm and with 24 pre-stressed tendons, with a distance between the applied load point and support of 11.05 m as shown in Figure 7-12, can resist approximately 800 kN of applied load which corresponds to 4520 kNm of bending resistance at a deflection of 500 mm. Using this beam geometry and reinforcement together with the material parameters from the smaller girder tested in this research, the load resistance of approximately 438 kN is achieved under the same deflection of 500 mm from the FE analysis. The different in resistance is mainly caused by the UHPC property differences shown in Table 7-5.

It can be seen from Table 7-5 that under the deflection of 50cm, the compressive stress reached 170 MPa for Park (2003), at which point the tendons yield. For the material of this research, the compressive stress reaches 121.4 MPa which is close to its ultimate strength, while the tendon force is at approximately 37% of the tendon ultimate strength. However, this is at the ultimate resistance. The serviceability limit state may dominate for slender post-tensioned bridge design. Crack width limitation will be required according to durability requirements especially for post-tensioning, and more UHPC parameters are required to be tested in future research to provide the database for reliable UHPC structural design.
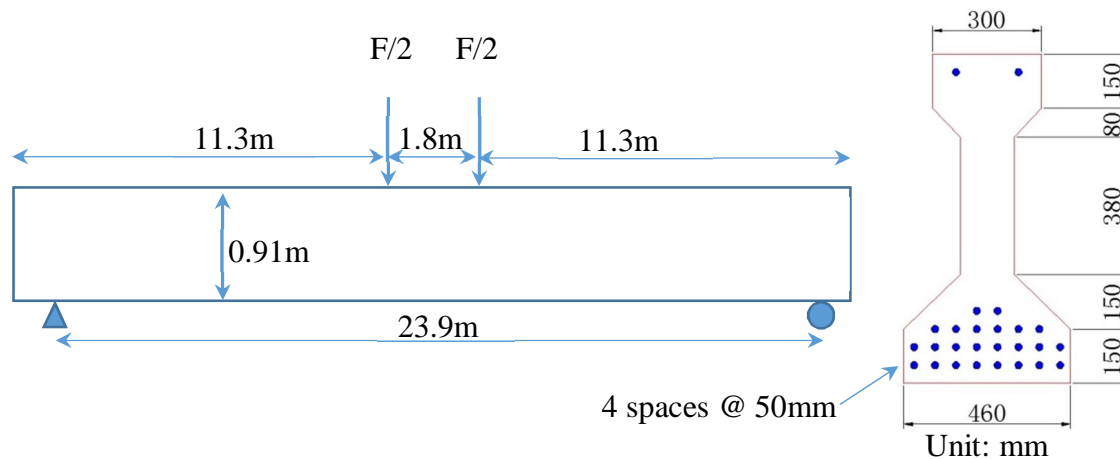
Figure 7-12: Sketch for AASHTO type II girder (Park, 2003).

Table 7-5: The main parameters of Park (2003) and this research for AASHTO type II girder FE analysis.

Parameters	Park (2003)	This research
Ultimate Compressive strength (MPa)	190	124.3
Tensile strength (MPa)	11	8.56
E-modulus (GPa)	53.9	34.5
Tendon tensile strength (MPa)	1860	1860
Bottom tendon total area (mm^2)	2368.8	2368.8
Ultimate resistance (kN)	800	438
UHPC strength (MPa)	170	121.6
Tendon force (kN)	Yield	68.64 (37% of ultimate resistance)
Deflection (mm)	500	500

7.5. CONCLUSIONS

This chapter presents the preliminary design and implementation of a post tensioned box girder under laboratory conditions. The limited size of a post tensioned box girder, post tension loss and local post tensioned application, result in uncertainties pertaining to the actual post tensioning forces. Through applying elastic theory, the calculated post tensioning forces are found to be similar, based on the various first crack tensile strength obtained from DTT. In addition, the calculation shows that using the tensile force calculated from the four point flexural test to estimate the tendon force in the inverse analysis exercise, leads to an unrealistic, negative tendon force, indicating that the flexural strength overestimates the actual tensile strength.

132

The FE analysis is performed for the limited tests in this research. From these analyses, it appears that the rotating smeared cracking model is quite applicable for bending behaviour of the UHPC post tensioned box girder and that the tensile and stiffness material parameters have been reasonably accurately characterised. The selected mesh size results in similar bending behaviour, except in the deflection softening section, which is not expected for industrial applications.

From FE analysis, it can be seen that an increased lever arm and enlarged total tendon area contribute significantly to the ultimate bending resistance at large deflection, while the higher post tensioning force has limited contribution to the bending resistance for the box girder with limited depth.

The nonlinear FE analysis and post tensioned box girder test are not the main focus of this research, but serves to present that the data obtained from the compressive test and DTT can provide fundamental parameters for structural design and FE analysis. Future research is recommended to obtain and calibrate UHPC fracture energy that fits for different smeared crack models. Through the analysis in this chapter, the tensile behaviour dominates the behaviour, while UHPC should be exploited for its ultra-high compressive resistance in actual bridge girders. Full sized bridge girders of appropriate geometry to exploit the compressive resistance, are recommended for tests in future research.

Chapter 8: Conclusions and future research

8.1. CONCLUSIONS

The main contribution of this research was to develop a new mix design philosophy for UHPC. The general UHPC development methods fail to achieve the designated strength based on the local non-ideal materials. The UHPC mix design philosophy was developed through the mechanisms of shrinkage induced clamping pressure, bridging effect of steel fibre with adequate lap length and uniform steel fibre dispersion as elaborated on in Chapter 4. The UHPC under such mix design methods have the following characteristics:

- The steel fibre does not only enhance the UHPC ductility but also increases the compressive strength;

- The steel fibres are pre-stressed inside UHPC so that the fibre content can also help to increase apparent first crack tensile strength as characterised from 16 mm thick dumbbell shaped specimens in direct tension tests;

- The UHPC has the ability to resist shrinkage in later days and no special treatment is needed such as SAP or SRA to reduce future shrinkage. The reduction of UHPP strength under very low W/C ratio is postulated to be caused by the higher shrinkage in later days. With the help of steel fibre, the 56 days UHPC strength is approximately 8% higher than that at 28 days as shown in Table 5-6.

Under such a mix design philosophy, the UHPC finally achieves a compressive strength of 168 MPa, first crack tensile strength of 5.29 MPa and peak tensile strength of 8.56 MPa with the help of only 1.5% steel fibres by UHPM volume.

During the UHPC development, the following findings and decisions contributed to the successful development of UHPC with local non-ideal materials:

134

- The threshold of 300 mm in slump flow indicated by Wille *et al.* (2011:46) is also an indication for UHPP with local materials to retain appropriate packing density and therefore the strength;

- Both reduced W/C ratio and increased addition of SF content up to a threshold level of 30% by cement weight help to improve UHPP strength. Reduced W/C ratio is a primary mechanism for UHPP mix design rather than increasing the SF content;

- The skeleton of UHPC is built up from hardened paste, sand and steel fibre that grows stronger with the increase in UHPP strength at early age. The improved skeleton strength resists further shrinkage caused by cement hydration and SF pozzolanic reaction. In this process, as elaborated on in Chapter 4, the skeleton grows stronger and UHPP contributes both to the skeleton formation and the bridging effect of steel fibres;

- UHPP early age strength development is of key importance to provide UHPC strength. Even with the reduction of the UHPP strength after 14 days as found in this research, the UHPP mix can still be used to develop UHPC by applying the mix design philosophy of this research. It is found that the UHPC strength continues to increase, as tested in this research up to an age of 56 days.

Once UHPC was successfully developed in this research, additional test series illuminated the following factors that influence UHPC strength:

- The environmental temperature where UHPC is kept during moulded period significantly affects UHPC strength. Under room temperature, an increase of 15 ℃ in ambient temperature results in an approximately 20% increase in UHPC strength for the UHPC developed in this work;

- The cement chemical composition, especially C_3S content according to the Bogue analysis, significantly affects UHPC strength. For the same mix design and similar environmental temperature during moulded period, the batch of cement with C_3S content of 2.4% higher causes an approximately 24% improvement in UHPC strength;

- Curing in sealed conditions significantly affects UHPC strength. The specimen without top cover causes a 24% reduction in UHPC strength under similar room temperature for the UHPC developed in this study;

- After two days of moulded period, the UHPC strength is only slightly affected by the subsequent environment, whether cured in water or exposed in the air. However, the UHPC is more affected by the subsequent curing environment after only one day of moulded period.

For UHPC tensile behaviour, the UHPC with only 1.5% of steel fibre by UHPM volume (1.478% by UHPC volume) obtained both deflection hardening and strain hardening behaviour. The multiple cracks can be obtained from both the direct tensile test (DTT) and four-point flexural test. The DTT is recommended to obtain UHPC tensile strength rather than a flexural test and a larger dimension of DTT specimen is recommended to provide more reliable results.

The UHPC can flow into the moulds due to its self-compacting property to make the manufacturing easier. The purpose of slight vibration is only to accelerate air bubbles coming out of fresh UHPC, which can be avoided in future application.

The bending behaviour of the post tensioned box girder highlights that the various UHPC properties, such as tensile strength, fracture energy, E-modulus obtained from average values of laboratory tests, match well between FE analysis and laboratory post tensioned box girder tests, which indicate that the smeared cracking model is quite applicable for bending behaviour of the UHPC post tensioned box girder.

The FE analysis shows that the increased lever arm and the enlarged total tendon area contribute to the ultimate bending resistance at large deflection, which is helpful to the ultimate limit state of the box girder. The higher post tensioning force has a limited contribution to the bending resistance. For the same post-tensioning force, a larger total

136

tendon cross-section area provides additional resistance at larger deflections, whereby the bending resistance is enhanced. The high compressive strength of UHPC can be exploited to an extent in an AASHTO Type II UHPC girder. However, the modified material behaviour of UHPC demands girder section and post-tensioning optimisation to fully benefit from the particular compressive and tensile strength of UHPC as developed here.

8.2.   RECOMMENDATIONS FOR FUTURE RESEARCH WORK

After developing UHPC in South Africa in this research, the following recommendations will help to better understand UHPC technology:

- Special sand shape and size are recommended for future research that can improve the aggregate packing density, increase UHPM slump flow and enable more sand content to be used in UHPC to make it economical;
- The research on steel fibre orientation and dispersion is recommended in the future for UHPC research with optimised sand;
- The characterization of shrinkage of locally developed UHPC is recommended for future research, which may help to provide data for future improvement in UHPC mix design and application;
- Systematic testing of UHPC properties towards a larger database and statistical base is recommended for future research;
- The FE analysis shows that smeared crack model can be applied to UHPC girder to simulate its bending behaviour. However, in order to aid in structural design, extensive research is recommended to calibrate the parameters input into different types of smeared cracking models;
- It is recommended that the industry uses more consistent materials for UHPC mix in order to assist in controlling composite behaviour and make the tested data valuable;

- Once the systematic testing of UHPC properties is finished, design standards are recommended to incorporate UHPC to current concrete design codes, such as safety factors for UHPC strength through structural reliability analysis.

Reference list

Books and Publications

Aitcin, P. & Neville, A. 1993. High-Performance Concrete Demystified. *Concrete International,* 15(1). 30 September 2013

Aitcin, P., Neville, A.M. & Acker, P. 1997. Integrated View of Shrinkage Deformation. *Concrete International,* 19(9). 7 October 2013

Alwan, J.M., Naaman, A.E. & Hansen, W. 1991. Pull-Out Work of Steel Fibers from Cementitious Composites: Analytical Investigation. *Cement and Concrete Composites,* 13(4).

Artelt, C. & Garcia, E. 2008. Impact of Superplasticizer Concentration and of Ultra-Fine Particles on the Rheological Behaviour of Dense Mortar Suspensions. *Cement and Concrete Research,* 38(5).

Bažant, Z.P. 2001. Prediction of Concrete Creep and Shrinkage: Past, Present and Future. *Nuclear Engineering and Design,* 203(1).

Bonen, D. & Sarkar, S.L. 1995. The Superplasticizer Adsorption Capacity of Cement Pastes, Pore Solution Composition, and Parameters Affecting Flow Loss. *Cement and Concrete Research,* 25(7).

Brouwer, G. 2001. Bridge to the Future. *Civil Engineering Magazine,* 71(11).

Chan, Y. & Chu, S. 2004. Effect of Silica Fume on Steel Fiber Bond Characteristics in Reactive Powder Concrete. *Cement and Concrete Research,* 34(7).

Chatterji, S., Thaulow, N. & Christensen, P. 1982. Puzzolanic Activity of Byproduct Silica-Fume from Ferro-Silicon Production. *Cement Concrete Research,* 12(6).

Chuang, E.Y. & Ulm, F. 2002. Two-Phase Composite Model for High Performance Cementitous Composites. *Journal of Engineering Mechanics,* 128(12).

de Larrard, F. 1988. *Mix-design and properties of very-high performance concrete. Unpublished thesis.* Rapport de Recherche des LPC N°149: Doctoral Thesis of Ecole Nationale des Ponts et Chaussees.PhD thesis

de Larrard, F. & Sedran, T. 1994. Optimization of Ultra-High-Performance Concrete by the use of a Packing Model. *Cement and Concrete Research,* 24(6).

de Larrard, F. & Tondat, P. 1993. Sur La Contribution De La Topologie Du Squelette Granulaire À La Résistance En Compression Du Béton [on the Contribution of the Topology of the Aggregate Skeleton to the Compressive Strength of Concrete]. *Materials and Structures/Materiaux et Constructions,* 26(9).

Detwiler, R.J. & Mehta, P.K. 1989. Chemical and Physical Effects of Silica Fume on the Mechanical Behavior of Concrete. *ACI Materials Journal,* 86(6). 4 June 2014

Dudziak, L. and Mechtcherine, V. 2008. Mitigation of Volume Changes of Ultra-High Performance Concrete (UHPC) by using Super Absorbent Polymers. Paper presented at Second International Symposium on Ultra High Performance Concrete, Kassel, Germany. March 05-07.

Edward, G. & P.E. Nawy(eds.) 2008. *Concrete construction engineering handbook.* U.S.A.: CRC Press

Esping, O. 2007. *Early-age properties of self-compacting concrete - effects of fine aggregate and limestone filler. Unpublished thesis.* Sweden: Chalmers University of Technology.PhD Thesis

Feylessoufi, A., Tenoudji, F.C., Morin, V. & Richard, P. 2001. Early Ages Shrinkage Mechanisms of Ultra-High-Performance Cement-Based Materials. *Cement and Concrete Research,* 31(11).

Głodkowska, W. & Kobaka, J. 2013. Modelling of Properties and Distribution of Steel Fibres within a Fine Aggregate Concrete. *Construction and Building Materials,* 44(0).

Graybeal, A. 2009. UHPC Making Strides. *Public Roads Magazine,* 72(4).

Graybeal, B. 2006. Material Property Characterization of Ultra-High Performance Concrete.

Graybeal, B.,A. & Baby, F. 2013. Development of Direct Tension Test Method for Ultra-High- Performance Fiber-Reinforced Concrete. *Materials Journal,* 110(2).

Grünewald, S. 2004. Performance-Based Design of Self-Compacting Fiber Reinforced Concrete. PhD thesis.

Habel, K., Charron, J., Braike, S., Hooton, R.D., Gauvreau, P. & Massicotte, B. 2008. Ultra-High Performance Fibre Reinforced Concrete Mix Design in Central Canada. *Canadian Journal of Civil Engineering,* 35(2).

Habel, K., Viviani, M., Denarié, E. & Brühwiler, E. 2006. Development of the Mechanical Properties of an Ultra-High Performance Fiber Reinforced Concrete (UHPFRC). *Cement and Concrete Research,* 36(7).

Hassan, A.M.T., Jones, S.W. & Mahmud, G.H. 2012. Experimental Test Methods to Determine the Uniaxial Tensile and Compressive Behaviour of Ultra High Performance Fibre Reinforced Concrete (UHPFRC). *Construction and Building Materials,* 37(0).

Hassoun, M.N. & Al-Manasee, A. 2012. *Structural concrete: Theory and design.* New Jersey: John Wiley and Sons

Hegger, J. & Bertram, G. 2008. Shear carrying capacity of ultra-high performance concrete beams, in Joost C. Walraven, Dick Stoelhorst(ed.). *Tailor made concrete structures: New solutions for our society.* London: CRC Press.Pages 341-347 in

Holt, E. 2001. *Early-age autogenous shrinkage of concrete. Unpublished thesis.* United States: University of Washington.PhD Thesis

Kang, S.H., Kim, J.J., Kim, D.J. & Chung, Y. 2013. Effect of Sand Grain Size and Sand-to-Cement Ratio on the Interfacial Bond Strength of Steel Fibers Embedded in Mortars. *Construction and Building Materials,* 47(0).

Kang, S. & Kim, J. 2011. The Relation between Fiber Orientation and Tensile Behavior in an Ultra High Performance Fiber Reinforced Cementitious Composites (UHPFRCC). *Cement and Concrete Research,* 41(10).

Kim, D.j., El-Tawil, S. & Naaman, A.E. 2009. Rate-Dependent Tensile Behavior of High Performance Fiber Reinforced Cementitious Composites. *Materials and Structures,* 42(3).

Kovler, K. & Zhutovsky, S. 2006. Overview and Future Trends of Shrinkage Research. *Materials and Structures/Materiaux et Constructions,* 39(293). 2 July 2014

Ma, J., Dehn, F. and Koenig, G. 2003. Autogenous Shrinkage of Self-Compacting Ultra-High Performance Concrete (UHPC). Paper presented at International Conference on Advances in Concrete and Structures. 17-19 September 2003.

Markovic, I. 2006. *High-performance hybrid-fibre concrete- development and utilisation . Unpublished thesis.* Netherlands: Delft University.PhD thesis

McKee, D.C. 1969. The Properties of Expansive Cement Mortar Reinforced with Random Wire Fibers. PhD Thesis.

Menin, R.C.G., Trautwein, L.M. & Bittencourt, T.N. 2009. Smeared Crack Models for Reinforced Concrete Beams by Finite Element Method. *Ibracon structures and materials journal,* 2(2).

Mihashi, H. & Leite, J.P. 2004. State-of-the-Art Report on Control of Cracking in Early Age Concrete. *Journal of Advanced Concrete Technology,* 2(2).

Mindess, S. & J.F. Young(eds.) 1981. *Concrete.* U.S.A.: Prentice Hall

142

Mindess, S., J.F. Young & D. Darwin(eds.) 2002. *Concrete.* U.S.A.: Prentice Hall

Mooney, M. 1951. The Viscosity of a Concentrated Suspension of Spherical Particles. *Journal of colloid science,* 6(2). 11 September 2013

Morin, V., Cohen Tenoudji, F., Feylessoufi, A. & Richard, P. 2001. Superplasticizer Effects on Setting and Structuration Mechanisms of Ultrahigh-Performance Concrete. *Cement and Concrete Research,* 31(1).

Naaman, A.E. & Najm, H. 1991. Bond-Slip Mechanisms of Steel Fibers in Concrete. *ACI Materials Journal,* 88(2).

Park, H. 2003. *Model-based optimization of ultra high performance concrete highway bridge girders. Unpublished thesis.* Massachusetts Institute of Technology.

Park, J.J., Kang, S.T., Koh, K.T. and Kim, S.W. 2008. Influence of the Ingredients on the Compressive Strength of UHPC as a Fundamental Study to Optimize the Mixing Proportion. Paper presented at Second International Symposium on Ultra High Performance Concrete. Kassel, Germany. March 05-07.

Park, S.H., Kim, D.J., Ryu, G.S. & Koh, K.T. 2012. Tensile Behavior of Ultra High Performance Hybrid Fiber Reinforced Concrete. *Cement and Concrete Composites,* 34(2).

Plank, J., Schroefl, C., Gruber, M., Lesti, M. & Sieber, R. 2009. Effectiveness of Polycarboxylate Superplasticizers in Ultra-High Strength Concrete: The Importance of PCE Compatibility with Silica Fume. *Journal of Advanced Concrete Technology,* 7(1). 24 September 2013

Romualdi, J.P. & Mandel, J.A. 1964. Tensile Strength of Concrete Affected by Uniformly Distributed Closely Spaced Short Lengths of Wire Reinforcement. *Journal of the American Concrete Institute,* 61(4).

Sakai, E., Akinori, N., Daimon, M., Aizawa, K. & and Kato, H. 2008. Influence of Superplasticizer on the Fluidity of Cements with Different Amount of Aluminate Phase. *Second International Symposium on Ultra High Performance Concrete,*

Schachinger, I., Schmidt, K., Heinz, D. and Schießl, P. 2002. Early Age Cracking Risk and Relaxation by Restrained Autogenous Deformations of Ultra-High Performance Concrete. Paper presented at 6th International Symposium on High Strength / High Performance Concrete.

Schroefl, C., Gruber, M. and and Plank, J. 2008. Structure Performance Relationship of Polycarboxylate Superplasticizers Based on Methacrylic Acid Esters in Ultra High Performance Concrete. Paper presented at Second International Symposium on Ultra High Performance Concrete. Kassel, Germany.

Schröfl, C., Gruber, M. & Plank, J. 2012. Preferential Adsorption of Polycarboxylate Superplasticizers on Cement and Silica Fume in Ultra-High Performance Concrete (UHPC). *Cement and Concrete Research,* 42(11).

Soliman, A.M. 2011. *Early-age shrinkage of ultra high-performance concrete: Mitigation and compensating mechanisms. Unpublished thesis.* Canada: The University of Western Ontario.PhD thesis

Soliman, A.M. & Nehdi, M.L. 2014. Effects of Shrinkage Reducing Admixture and Wollastonite Microfiber on Early-Age Behavior of Ultra-High Performance Concrete. *Cement and Concrete Composites,* 46(0).

Soliman, A.M. & Nehdi, M.L. 2011. Effect of Drying Conditions on Autogenous Shrinkage in Ultra-High Performance Concrete at Early-Age. *Materials and Structures/Materiaux et Constructions,* 44(5). 23 June 2013

Stang, H. 1996. Significance of Shrinkage-Induced Clamping Pressure in Fiber-Matrix Bonding in Cementitious Composite Materials. *Advanced Cement Based Materials,* 4(3–4).

Tam, C.M., Tam, V.W.Y. & Ng, K.M. 2012. Assessing Drying Shrinkage and Water Permeability of Reactive Powder Concrete Produced in Hong Kong. *Construction and Building Materials,* 26(1).

Tazawa, E., Miyazawa, S. & Kasai, T. 1995. Chemical Shrinkage and Autogenous Shrinkage of Hydrating Cement Paste. *Cement and Concrete Research,* 25(2).

Tazawa, E., Sato, R., Sakai, E. & Miyazawa, S. 2000. Work of JCI on Autogenous Shrinkage. *International RILEM Workshop on Shrinkage of Concrete (Shrinkage 2000),* 21-40.

Tue, N.V., Ma, J. and Orgass, M.；. 2008. Influence of Addition Method of Superplasticizer on the Properties of Fresh UHPC. Paper presented at Second International Symposium on Ultra High Performance Concrete.

Wille, K., Naaman, A.E., El-Tawil, S. & Parra-Montesinos, G.J. 2012. Ultra-High Performance Concrete and Fiber Reinforced Concrete: Achieving Strength and Ductility without Heat Curing. *Materials and Structures,* 45(3).

Wille, K. & Naaman, A.E. 2013. Effect of Ultra-High-Performance Concrete on Pullout Behavior of High-Strength Brass-Coated Straight Steel Fibers. *ACI Materials Journal,* 110(4).

Wille, K., Naaman, A.E. & Parra-Montesinos, G.J. 2011. Ultra-High Performance Concrete with Compressive Strength Exceeding 150 MPa (22 Ksi): A Simpler Way. *ACI Materials Journal,* 108(1). 23 June 2013

Wille, K. & Parra-Montesinos, G.J. 2012. Effect of Beam Size, Casting Method, and Support Conditions on Flexural Behavior of Ultra-High-Performance Fiber-Reinforced Concrete. 109(3).

Yogendran, V., Langan, B.W. & Ward, M.A. 1991. Hydration of Cement and Silica Fume Paste. *Cement and Concrete Research,* 21(5).

Zhang, M.H., Tam, C.T. & Leow, M.P. 2003. Effect of Water-to-Cementitious Materials Ratio and Silica Fume on the Autogenous Shrinkage of Concrete. *Cement and Concrete Research,* 33(10).

Zingg, A. 2009. Interaction of Polycarboxylate-Based Superplasticizers with Cements Containing Different C3A Amounts. *Cement and Concrete Composites,* 31(3).

National Standards

"AASHTO LRFD Bridge Design Specifications", 6th Edition. American Association of State Highway and Transportation Official; Washington, DC; 2012.

AASHTO LRFD Bridge Design Specifications Prestressed Concrete

ASTM C109. Standard test method for compressive strength of hydraulic cement mortars (using 2-in. or [50-mm] cube specimens); 2011.

ASTM C230. Standard specification for flow table for use in tests of hydraulic cement. Annual book of ASTM standards, vol. 4.01, American Society for Testing and Materials, Conshohocken, PA; 2008.

ASTM. ASTM C 1437-07 Standard test method for flow of hydraulic cement mortar. West Conshohocken, USA; 2007.

ASTM C1609/C1609M-07. Standard test method for flexural performance of fiber-reinforced concrete (using beam with third-point loading). American Society of Testing and Materials; 2007. p. 1–8.

"EN 14487-1: Sprayed concrete, definition, specification and conformity". BSI, 2006.

RILEM TC-162 TDF, "Final Recommendation of RILEM TC 162-TDF: Test and Design Methods for Steel Fibre Reinforced Concrete". Materials and Structures, V. 36, No. 262, 2003, pp. 560-567.

"SANS 10100-1: The structural use of concrete. Part 1: Design". Pretoria: South African Bureau of Standards, 2000.

"TMH7 Part 3: Code of practice for the design of highway bridges and culverts in South Africa". Pretoria, South Africa; 1989.

Appendix A: Cement chemical composition and Bogue analysis

Table A1: Characteristic of CEM I 42.5N in 2011 (provided by PPC)

Chemical composition	Percentage (%)	Bogue analysis for Clinker produced for the corresponding period	Percentage (%)
Silica (SiO_2)	21.2		
Alumina (Al_2O_3)	4.0	C_3S	59
Iron Oxide (Fe_2O_3)	3.1	C_2S	19.5
Lime (CaO)	64.5	C_3A	7.26
Magnesia (MgO)	0.9	C_4AF	10.16
Sulphate content (as SO_3)	2.2	Compressive Strength (MPa)	
Chloride content	0.01		
Potassium (K_2O)	0.7		
Sodium (Na_2O)	0.1	2-days	19.8
Loss on Ignition	2.7	7-days	-
Insoluble Residue	1.1	28-days	50.0

Table A2: Characteristic of CEM I 52.5N in 2012 (provided by PPC)

Chemical composition	Percentage (%)	Bogue analysis for Clinker produced for the corresponding period	Percentage (%)
Silica (SiO_2)	21.1		
Alumina (Al_2O_3)	4.0	Free CaO	1.33
Iron Oxide (Fe_2O_3)	3.35	C_3S	61.61
Lime (CaO)	65.8	C_2S	17.22
Magnesia (MgO)	0.87	C_3A	6.77
Sulphate content (as SO_3)	2.3	C_4AF	10.63
Chloride content	0.01	Compressive Strength (MPa)	
Potassium (K_2O)	0.7		
Sodium (Na_2O)	0.1	2-days	29.5
Loss on Ignition	2.79	7-days	44.5
Insoluble Residue	1.0	28-days	55.5

The grading of CEM I 52.5N in 2012 (Provided by PPC)

Size	Retained
90 μm	4%
45 μm	20%
32 μm	32.4%
25 μm	39.5%

148

Table A3: Characteristic of CEM I 52.5N in 2013 (provided by PPC)

Chemical composition	Percentage (%)	Bogue analysis for Clinker produced for the corresponding period	Percentage (%)
Silica (SiO$_2$)	21.1		
Alumina (Al$_2$O$_3$)	4.0	C$_3$S	59.2
Iron Oxide (Fe$_2$O$_3$)	3.1	C$_2$S	19
Lime (CaO)	64.8	C$_3$A	6.7
Magnesia (MgO)	1	C$_4$AF	10.5
Sulphate content (as SO$_3$)	2.3	Compressive Strength (MPa)	
Chloride content	0.01		
Potassium (K$_2$O)	0.7		
Sodium (Na$_2$O)	0.1	2-days	30.0
Loss on Ignition	2.7	7-days	45.8
Insoluble Residue	1.1	28-days	58.0

The grading of CEM I 52.5 in 2013 (Provided by PPC)

Size	Retained
90 μm	3%
45 μm	19%
32 μm	31.5%
25 μm	52.5%

Appendix B: Preliminary design of post tensioned box girder

Typical UHPC mix design in this research

Table B1: Input data.

W/C	0.2
SF/C	0.16
SP content (as % of cement weight)	2.8
S/C	0.6
Steel fibre volume content (%)	1.5

Table B2: Calculated value.

	Mass (kg)	Volume (Litre)
Water	217	217
Cement	**1190**	379
Silica fume	190	84
Superplasticizer	33	30
Sand	714	275
Steel fibre	116	15
Total volume		**1000**

Note that the water in superplasticizer is included in the total water content.

150

Appendix C: Compressive strength of UHPC development

Table C1: Average UHPC strength development with CEMI 42.5N.

Batch No.	Compressive strength (MPa)												Type
	7 days			14 days			21 days			28 days			
	No.	f_{cu}	Std.	No.	f_{cu}	Std.	No.	f_{cu}	Std.	No.	f_{cu}	Std.	
T1	2	95.7	2.7	2	107.4	6.2				3	109.2	5.2	UHPP
T2	2	94.3	9.1				2	118.1	1.7	3	112.6	5.8	
T3	2	111.9	1.4				2	123.3	8.0	4	125.2	4.4	
T4	2	98.6	1.9				2	112.8	7.4	4	113.1	7.7	
T5	2	104.4	7.0				2	118.9	0.8	4	124.1	4.7	
T6	2	91.3	5.5				2	113.0	1.0	4	111.1	6.1	
T7	4	91.1	7.2	4	138.6	6.9	4	112.3	3.1	4	107.5	8.5	UHPP
T8	4	109.8	5.7	4	143.9	2.3	4	121.0	5.9	4	131.6	3.4	
T9	4	115.4	5.0	4	148.4	5.9	4	120.0	6.1	4	130.6	6.7	
T10	1	102.1		1	110.2		1	74.3		3	119.5	3.5	UHPM
T11	1	83.6		1	61.3		1	96.2		3	117.2	2.2	
T12	1	101.8		1	114.8		1	122.5		3	116.1	9.2	
T13	1	110.8		1	98.3		1	128.3		3	119.4	2.6	
T14	1	88.4		1	89.6		1	123.8		2	65.3	0.4	UHPM
T15	1	86.1		1	96.8		1	49.5		3	76.1	11.5	
T16	1	90.2		1	103.1		1	92.7		3	85.2	6.5	
T17	1	88.8		1	99.9		1	100.7		3	98.9	5.1	
T18	1	97.9		1	111.3		1	110.9		2	128.6	5.9	UHPM+6.7 mm aggregate
T19	1	90.5		1	95.4		1	96.1		3	118.9	4.2	
T20	1	84.4		1	45.0		1	97.5		3	115.4	4.9	
T21	1	105.9		1	74.3		1	100.0		3	112	12.6	

Table C2: Average UHPC strength development with CEMI 52.5N.

Batch No.	Compressive strength (MPa)												Type
	7 days			14 days			21 days			28 days			
	No.	f_{cu}	Std.	No.	f_{cu}	Std.	No.	f_{cu}	Std.	No.	f_{cu}	Std.	
T(20HE)1	1	109.6		1	152.8		1	148.6		3	108	4.2	UHPP
T(20HE)2	1	103.2		1	130.7		1	144.3		3	141.3	6.2	UHPM
T(20HE)3	1	91.3		1	129.1		1	106.4		3	135.3	4.7	
T(20HE)4	1	96.7		1	72.7		1	88.0		3	99.3	6.5	
T(SP1)1	1	107.5		1	122.2		1	127.2		3	133.5	3.1	UHPP
T(SP1)2	1	101.9		1	91.3		1	112.5		3	100.4	4.2	UHPM
T(20HE)5	1	130.1		1	120.5		1	131.3		3	89.8	4.0	UHPMC+6.7 mm aggregate
T(20HE)6	1	123.0		1	144.1		1	159.0		3	168.7	3.5	UHPC
T(20HE)7	1	135.1		1	141.8		1	161.4		3	161.2	1.5	UHPC+6.7 mm aggregate

Appendix D: Preliminary design of post tensioned box girder
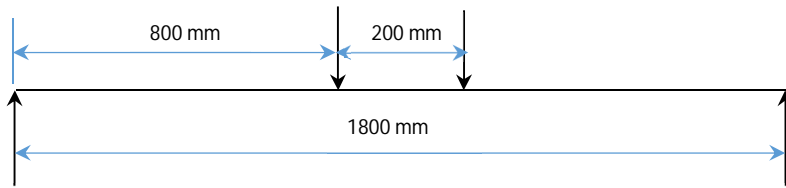
1. Material property

1.1 Box section dimensions

B_{ft}	=380	mm
B_{fb}	=380	mm
h_{ft}	=50	mm
h_{fb}	=70	mm
t_{wl}	=60	mm
t_{wr}	=60	mm
H_{ave}	=270	mm
I	=543878491	mm^4
f_{cu}	=160	MPa
d_{tendon}	=234.65	mm
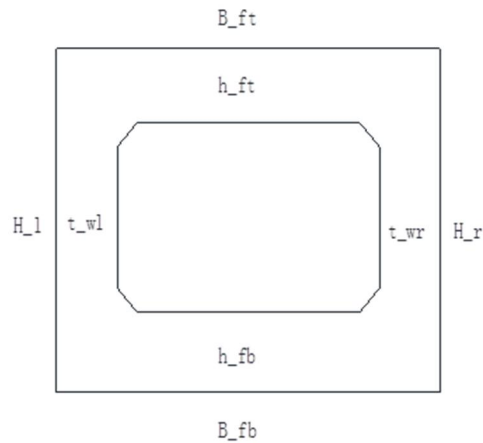
1.2 Post tensioning tendons

diameter	=12.7	mm
N	=186	kN
A	=98.7	mm^2
f	=1884.5	MPa

2. Flange flexural resistance

2.1 According to SANS 0100-1:

$$M_u = 0.45 f_{cu} b h_f (d - \frac{h_f}{2})$$

M_u=286.8 kNm, which can resist reaction force F=318.7 kN

2.2 According to TMH7 part 3:

$$M_u = 0.4 f_{cu} b h_f (d - \frac{h_f}{2})$$

M_u= 254.9 kNm, which can resist reaction force F=358.5 kN

3. Shear resistance

Most design codes regard web as the only element for shear resistance. The traditional shear formula has the limitation of concrete strength, which may not applicable for UHPC. The traditional shear formula is still used as a preliminary check to deploy stirrups.

3.1 According to SANS 0100-1:

$$V_c = \frac{0.75}{\gamma_m} \left(\frac{f_{cu}}{25}\right)^{\frac{1}{3}} \left(\frac{100 A_s}{b_v d}\right)^{\frac{1}{3}} \left(\frac{400}{d}\right)^{\frac{1}{4}}$$

V_c=1.569 MPa

3.2 According to AASHTO LRFD Bridge Design Specifications Pre-stressed Concrete:

$$V_c = 2\sqrt{f_c'} b_w d$$

V_c=2.099 MPa

Assume reaction force F=150 kN, therefore, the shear force is 150 kN.

Based on SANS 0100-1

$$\frac{A_{sv}}{S_v} \geq \frac{b(v - v_c)}{0.87 f_{yv}} = 1.903$$

Based on AASHTO LRFD

$$\frac{A_{sv}}{S_v} \geq \frac{b(v - v_c)}{0.87 f_{yv}} = 1.741$$

Choose R10@90 stirrups, where $\frac{A_{sv}}{S_v} = 1.744 > 1.741$, OK

The actual shear resistance may be high. It is found that UHPC with 0.9% volume steel fibre results 80% higher shear resistance and with 2.5% volume lead to a 177% higher shear resistance (Hegger & Bertram, 2008:341).

154

Appendix E: Measured post tensioned box girder cross-sectional dimensions
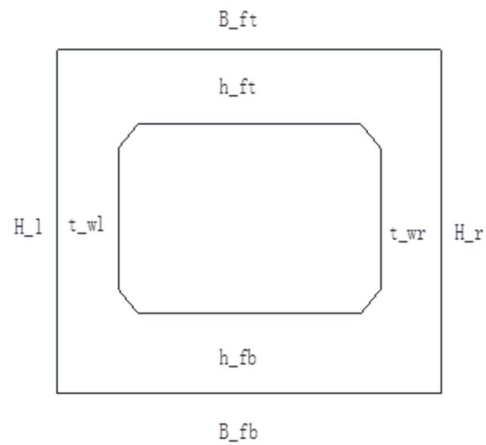
For box girder 1

B_{ft} =383 mm

B_{fb} =383 mm

h_{ft} =66 mm

h_{fb} =72 mm

t_{wl} =63 mm

t_{wr} =62 mm

H_{ave} =289 mm

For box girder 2

B_{ft} =383 mm

B_{fb} =383 mm

h_{ft} =67 mm

h_{fb} =72 mm

t_{wl} =62 mm

t_{wr} =63 mm

H_{ave} =290 mm

Appendix F: Detailed procedure in calculating post tensioning force

Based on Euler-Bernoulli beam theory, the following conditions are met:

- Compressive force equals to tensile force;
- the corresponding bending moment is equal to the bending moment caused by the applied load and self-weight;
- Plane section remains plane;
- Stress distribution is linear as shown in the figure.
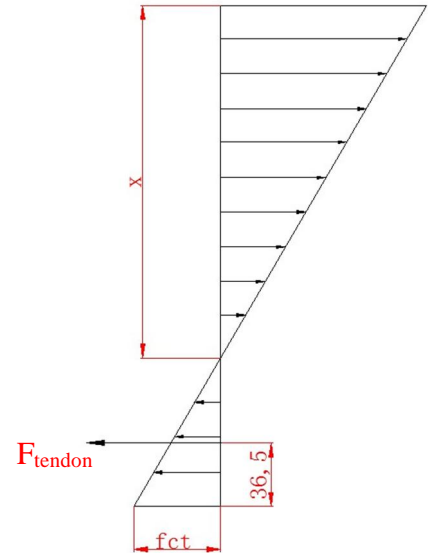
Step 1: Determine unknowns:

Tendon force (F_{tendon}) and neutral location x are unknown;

Step 2: Input parameters:

The first crack tensile strength (f_{ct}) is obtained from DTT;

The force in each section of the box girder can be calculated by the given stress;

The tendon elongation can be calculated by the distance from neutral axis;

The additional tendon force is calculated based on the tendon elongation when the first crack of box girder occurs;

Step 3: Calculation:

Two equations are used to solve two unknowns as mentioned above. Use trial and error methods through spreadsheet to obtain the post tensioning force and corresponding neutral axis location for the given first crack tensile strength.

$$\sum \delta_{c,i} A_{c,i} = \sum f_{t,i} A_{t,i} \tag{F-1}$$

$$M_t = \sum \delta_{c,i} A_{c,i} d_{c,i} + \sum f_{t,i} A_{t,i} d_{t,i} \tag{F-2}$$

Where:

$\delta_{c,i}$:   Average compressive stress of section i in compression zone;

$A_{c,i}$:   Section i area in compression zone;

$d_{c,i}$:   The distance from centroid of section i in compression zone to neutral axis;

$f_{t,i}$:   Average tensile stress of section i in tension zone;

$A_{t,i}$:   Section i area in tension zone;

$d_{t,i}$:   The distance from centroid of section i in tension zone to neutral axis;

M_t: The total applied bending moment.